12

SENSITIVITY OF INR SHIELDING ANALYSES TO SOURCE AND STRUCTURAL VARIATIONS

FINAL REPORT

CONTRACT DCPA01-76-C-0326
WORK UNIT 1118E

DECEMBER 31, 1977

SCIENCE APPLICATIONS, INC.

APPROVED FOR PUBLIC RELEASE;
DISTRIBUTION UNLIMITED.

SAI-77-867-LJ

SENSITIVITY OF INR SHIELDING ANALYSES TO SOURCE AND STRUCTURAL VARIATIONS

FINAL

CONTRACT DCPA01-76-C-0326 new

WORK UNIT 1118E

BY

T. E. ALBERT
L. HUSZAR
G. L. SIMMONS

FOR

DEFENSE CIVIL PREPAREDNESS AGENCY
WASHINGTON D. C. 20301

DCPA REVIEW NOTICE

THIS REPORT HAS BEEN REVIEWED IN THE DEFENSE CIVIL PREPAREDNESS AGENCY AND APPROVED FOR PUBLICATION. APPROVAL DOES NOT SIGNIFY THAT THE CONTENTS NECESSARILY REFLECT THE VIEWS AND POLICIES OF THE DEFENSE CIVIL PREPAREDNESS AGENCY.

DECEMBER 31, 1977

SCIENCE APPLICATIONS, LA JOLLA, CALIFORNIA
ALBUQUERQUE • ANN ARBOR • ARLINGTON • ATLANTA • BOSTON • CHICAGO • HUNTSVILLE
LOS ANGELES • McLEAN • PALO ALTO • SANTA BARBARA • SUNNYVALE • TUCSON

P.O. Box 2351, 1200 Prospect Street, La Jolla, California 92037

UNCLASSIFIED

SECURITY CLASSIFICATION OF THIS PAGE (When Data Entered)

REPORT DOCUMENTATION PAGE

READ INSTRUCTIONS BEFORE COMPLETING FORM

1. REPORT NUMBER: SAI-77-867-LJ	2. GOVT ACCESSION NO.
3. RECIPIENT'S CATALOG NUMBER	Final rept. 23 Aug 76 - 31 Dec 77
4. TITLE (and Subtitle): SENSITIVITY OF INR SHIELDING ANALYSES TO SOURCE AND STRUCTURAL VARIATIONS.	5. TYPE OF REPORT & PERIOD COVERED: Final, August 23, 1976 to December 31, 1977
	6. PERFORMING ORG. REPORT NUMBER
7. AUTHOR(s): T. E./Albert, L./Huszar, G. L./Simmons	8. CONTRACT OR GRANT NUMBER(s): DCPA01-76-C-0326
9. PERFORMING ORGANIZATION NAME AND ADDRESS: Science Applications, Inc., P. O. Box 2351, La Jolla, CA 92038	10. PROGRAM ELEMENT, PROJECT, TASK AREA & WORK UNIT NUMBERS: Work Unit 1118E
11. CONTROLLING OFFICE NAME AND ADDRESS: Defense Civil Preparedness Agency, Washington, D.C. 20301	12. REPORT DATE: December 31, 1977 (31 Dec 77)
	13. NUMBER OF PAGES: 82 (86p.)
14. MONITORING AGENCY NAME & ADDRESS (if different from Controlling Office)	15. SECURITY CLASS. (of this report): Unclassified
	15a. DECLASSIFICATION/DOWNGRADING SCHEDULE

16. DISTRIBUTION STATEMENT (of this Report)

Approved for public release; distribution unlimited.

17. DISTRIBUTION STATEMENT (of the abstract entered in Block 20, if different from Report)

18. SUPPLEMENTARY NOTES

19. KEY WORDS (Continue on reverse side if necessary and identify by block number)

Initial Nuclear Radiation, Shielding

20. ABSTRACT (Continue on reverse side if necessary and identify by block number)

Results of a study of three specific items of interest to the development of procedures for estimating initial radiation protection factors for buildings are presented. These include: (1) the effects of new cross section data for nitrogen and oxygen on initial radiation environments are presented, (2) calculations of delayed radiation environments for large yield weapons are presented; the

DD FORM 1473 1 JAN 73 EDITION OF 1 NOV 65 IS OBSOLETE

UNCLASSIFIED

SECURITY CLASSIFICATION OF THIS PAGE (When Data Entered)

388 862

calculations are based on the NUTDEA code; and (3) sensitivity analyses of the effects of composition, thickness, and design characteristics of wall constructions are presented.

CONTENTS

FIGURES

TABLES

1. ABSTRACT

Results of a study of three specific items of interest to the development of procedures for estimating initial radiation protection factors for buildings are presented. These include:

1. The effects of new cross section data for nitrogen and oxygen on initial radiation environments are presented;

2. Calculations of delayed radiation environments for large yield weapons are presented. The calculations are based on the NUIDEA code; and

3. Sensitivity analyses of the effects of composition, thickness, and design characteristics of wall constructions are presented.

2. SUMMARY

This report presents the results of a study conducted for the Defense Civil Preparedness Agency (DCPA) by Science Applications, Inc. (SAI) to provide supplementary data for the development of a methodology to determine initial radiation protection factors (IPF) for civil defense applications. These data involve characterization of free-field radiation environments based on the best available cross section data, determination of the importance of delayed radiations for large yield nuclear weapons, and presentation of procedures which would allow the IPF assessment methodology to include the effects of construction material composition variations and design characteristics. Suggestions are presented for inclusion of the results of this study into procedures for estimating IPF for civilian structures.

3. INTRODUCTION AND BACKGROUND

The Defense Civil Preparedness Agency (DCPA) has for the past few years been in the process of developing procedures to determine the protection which buildings will provide from initial nuclear radiation (INR) other initial ects associated with nuclear weapons explosions. These procedures, which are similar to procedures developed for fallout radiation, are presently being defined. This report addresses three specific items which are necessary to finalize procedures for estimating initial radiation protection factors (IPF):

1. The determiniation of the effect of new cross section data on free field radiation environments and their impact on earlier INR shielding analysis,

2. The evaluation of delayed neutron and gamma ray environments from large yield weapons, and

3. The analysis of the sensitivity of calculated dose to the composition, thickness, and design characteristics of walls in structures.

These three items are addressed respectively in Chapters 4, 5, and 6.

The free field radiation environments presently being used for IPF calculations are based on the work of E. A. Straker and M. L. Gritzner[4]. These air transport results were obtained in 1969 using cross section data from ENDF/B-II. In the last few years, substantial effort has been spent by the Defense Nuclear Agency (DNA) to obtain better evaluations of the nitrogen and oxygen cross sections. The impact of the newer cross section evaluations are reflected in the analysis described in Chapter 4.

PRECEDING PAGE BLANK-NOT FILMED

The development of the NUIDEA Code sponsored by DNA and carried out by SAI provides a new capability for estimating the delayed radiation dose from large yield nuclear weapons. Results obtained from this code are presented in Chapter 5.

For initial nuclear radiation, the transport of neutrons and the production of secondary gamma rays is not only a function of the mass thickness of shielding material, but also a function of the material composition. Previous calculations of barrier factors for neutrons are based on a fixed concrete composition and do not consider variations in protection factors which may arise from variations in concrete composition and construction methods. Chapter 6 describes a series of transport calculations performed for various thicknesses and several concrete compositions of interest. In addition, perturbation calculations are presented which show the effect of specific chemical constituents of concrete on the shielding properties. Transport results are also shown for several wall and roof constructions.

4. FREE FIELD ENVIRONMENT – PROMPT

Previous recommendations specifying the initial radiations from nuclear weapons were made in 1972 by the ad hoc Subcommittee on Radiation Shielding which is part of the National Academy of Sciences Advisory Committee on Civil Defense[1]. These data have been used for civil defense shielding analyses and, in particular, for the determination of radiation protection factors provided by structures. During the late 1960's and early 1970's, considerable effort was expended by the Defense Atomic Support Agency (DASA) and later the DNA to develop methods for calculating radiation transport in air and to improve the basic cross section data required for these calculations. The results of these efforts can now be used to revise the free field radiation environments recommended in Reference 1.

There are basically two revisions considered in this report. The first reported in this chapter is a revision to the prompt neutron and secondary gamma ray environment due to updated nuclear cross sections derived from DNA sponsored research[2]. The calculations reported in this chapter were performed with the one-dimensional discrete ordinates code, ANISN[3]. The cross sections for nitrogen and oxygen used for the air transport calculations were obtained from the DNA few group library referenced in Reference 2. Additional problem data and results of the calculations are described below.

4.1 TRANSPORT PROBLEM DATA

4.1.1 Source Spectra

The air transport calculations were performed using the nominal "typical" thermonuclear source spectra which has been the convention to use in problems of this type[4]. This

source distributions, grouped in the DNA few groups library group structure, is given in Table 1. Only the neutron source has been considered. The omission of th prompt gamma ray source is justifiable because the prompt gamma ray component of the prompt dose is significant only very near the source. At distances of interest for civil defense applications, the prompt total dose is dominated by neutrons and secondary gamma rays.

4.1.2 Cross Sections

The DNA few group library is a coupled neutron and gamma ray multigroup cross sections library. There are 37 neutron groups and 21 gamma ray groups. The scattering angular distributions are approximated by a P_3 Legendre expansion.

The air density was taken to be 0.00111 gm/cm^3. At this density the atomic density of nitrogen and oxygen are 3.635×10^{-5} and 9.620×10^{-6} atoms per barn·cm, respectively. All other constituents of air were considered to be negligible.

4.1.3 Response Functions

In addition to calculations of the neutron and secondary gamma ray fluxes, tabulations have been made of integral response data appropriate for estimating prompt radiation doses to humans. For this purpose the Snyder Neufeld neutron response function and the Henderson tissue gamma ray response function have been used. This choice of response function is consistent with that which has been used previously. These response functions are given in Tables 2 and 3.

4.1.4 Calculational Method

The neutron and secondary gamma ray flux from a point source in air was calculated using the one-dimensional discrete ordinates code, ANISN. An S_{40} angular quadrature was used. The transport was carried to 333 gm/cm^2 in air so that

Table 1. Typical Thermonuclear Source Distribution.

Group Number	Upper Energy Boundary (MeV)	Group Fraction (Neutrons/Source Neutron)
1	19.6	0.
2	16.9	0.
3	14.9	1.89(-2)
4	14.2	9.34(-3)
5	13.8	2.66(-2)
6	12.8	1.67(-2)
7	12.2	1.69(-2)
8	11.1	1.24(-2)
9	10.0	7.48(-2)
10	9.	6.82(-3)
11	8.2	6.78(-3)
12	7.4	1.03(-2)
13	6.4	1.81(-2)
14	5.0	3.62(-3)
15	4.7	1.24(-2)
16	4.1	2.60(-2)
17	3.0	2.37(-2)
18	2.4	3.75(-3)
19	2.3	2.56(-2)
20	1.8	6.44(-2)
21	1.1	8.85(-2)
22	5.5(-1)	9.14(-2)
23	1.5(-1)	1.16(-2)
24	1.1(-1)	1.11(-1)
25	5.2(-2)	5.40(-2)
26	2.5(-2)	5.68(-3)
27	2.2(-2)	9.26(-2)
28	1.0(-2)	1.16(-1)
29	3.4(-3)	7.38(-2)
30	1.2(-3)	7.32(-2)
31	5.8(-4)	2.03(-2)
32	1.0(-4)	1.90(-3)
33	2.9(-5)	0.
34	1.1(-5)	0.
35	3.1(-6)	0.
36	1.1(-6)	0.
37	4.1(-7)	0.
	1.0(-11)	

Table 2. Snyder Neufeld Neutron Response Function.

Group Number	Upper Energy Boundary (MeV)	Response Function (rads/n/cm^2)
1	19.6	7.00558(-9)
2	16.9	7.00558(-9)
3	14.9	7.00558(-9)
4	14.2	7.00558(-9)
5	13.8	7.00558(-9)
6	12.8	7.00558(-9)
7	12.2	7.00558(-9)
8	11.1	7.00558(-9)
9	10.0	7.05279(-9)
10	9.	7.10289(-9)
11	8.2	7.03619(-9)
12	7.4	6.71089(-9)
13	6.4	6.07429(-9)
14	5.0	5.69619(-9)
15	4.7	5.37649(-9)
16	4.1	4.86219(-9)
17	3.0	4.47859(-9)
18	2.4	4.34239(-9)
19	2.3	4.22839(-9)
20	1.8	3.97819(-9)
21	1.1	3.34990(-9)
22	5.5(-1)	1.84200(-9)
23	1.6(-1)	1.23350(-9)
24	1.1(-1)	9.51589(-10)
25	5.2(-2)	6.92769(-10)
26	2.5(-2)	5.90470(-10)
27	2.2(-2)	5.52389(-10)
28	1.0(-2)	5.57940(-10)
29	3.4(-3)	6.00199(-10)
30	1.2(-3)	6.16599(-10)
31	5.8(-4)	6.72759(-10)
32	1.0(-4)	5.34589(-10)
33	2.9(-5)	3.88369(-10)
34	1.1(-5)	3.43049(-10)
35	3.1(-6)	3.27479(-10)
36	1.1(-6)	3.23040(-10)
37	4.1(-7)	3.20529(-10)
	1.0(-11)	

Table 3. Henderson Tissue Gamma Ray Response Function.

Group Number	Upper Energy Boundary (MeV)	Response Function (rads/[illegible] photon/cm^2)
1	14.	3.20810(-9)
2	10.	2.4722(-9)
3	8.	2.08470(-9)
4	7.	1.86510(-9)
5	6.	1.66130(-9)
6	5.	1.44310(-9)
7	4.	1.19710(-9)
8	3.	1.01110(-9)
9	2.5	8.70689(-10)
10	2.0	5.64059(-10)
11	1.5	5.64059(-10)
12	1.0	4.10599(-10)
13	0.7	2.93009(-10)
14	0.45	1.922[illegible]0(-10)
15	0.30	1.10590(-10)
16	0.15	5.48209(-11)
17	0.10	3.71130(-11)
18	0.07	3.67239(-11)
19	0.045	6.32728(-11)
20	0.03	1.41590(-10)
21	0.02	4.40629(-10)
	0.01	

the spectra will be free of boundary leakage effects to at least 250 gm/cm^2 or a distance of 2.25 km.

4.2 FREE FIELD NEUTRON AND SECONDARY GAMMA RAY SPECTRA

Figure 1a-j shows the neutron fluence per unit lethargy per source neutron for several ranges from 0.2 km to 2 km. The spectra can be observed to harden rapidly with increasing penetration in air to about 1 km. Beyond 1 km the shape of the spectrum is changing slowly although the total intensity continues to decrease with increasing penetration.

Figure 1f which shows the fluence per unit lethargy at 1200 m also gives a plot of the energy spectra recommended in Reference 1. To facilitate a comparison with the prompt environments reported in Reference 1, the present results are also presented in the same format. Figures 2a-p show the free field neutron fluence multiplied by the geometry factor $4\pi R^2$ versus range. Only a few of the DNA few group library groups correspond directly with the group structure utilized in Reference 1.

The previous discussion has focused on spectral differences which result by using more recent cross section evaluations. It is also useful to examine the differences in the angular distributions as a function of distance using these newer data. A convenient method of illustrating these differences is to make direct comparison of the expansion coefficients of the angular distributions at various distances from a point source. Using this procedure provides an adequate summary of the important conclusions, yet presents the data in a readily usable form. In Table 4, we present the ratio of the harmonic coefficients, P_0 through P_3, of the angular dose distributions as a function of distance from the source. The dose response functions and source distributions used were described previously. Examination of these results indicate that the changes in these distributions become more pronounced at larger distances, but are still quite small, i.e., less than 30%.

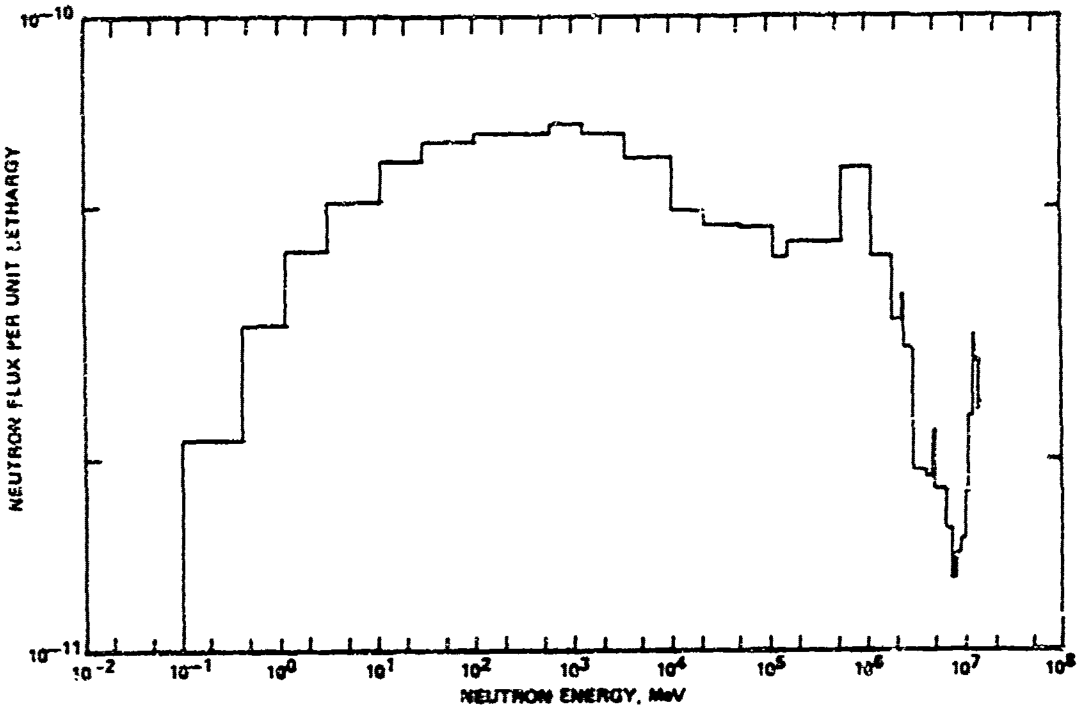

Figure 1a. Free Field Neutron Fluence at 210 M.

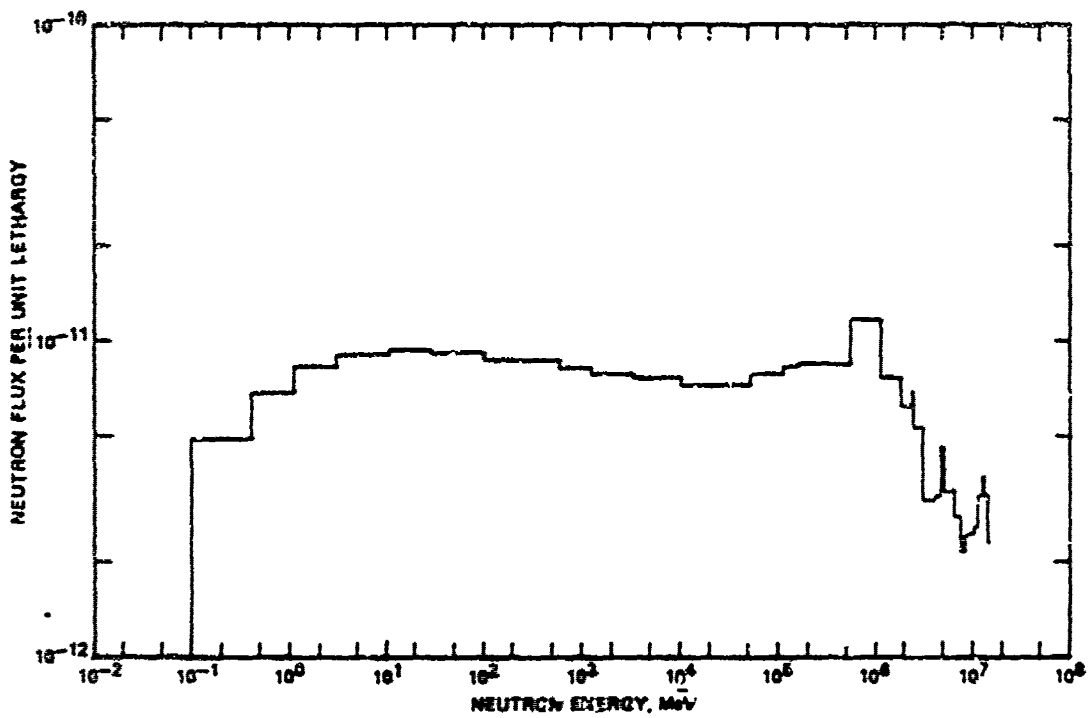

Figure 1b. Free Field Neutron Fluence at 400 M.

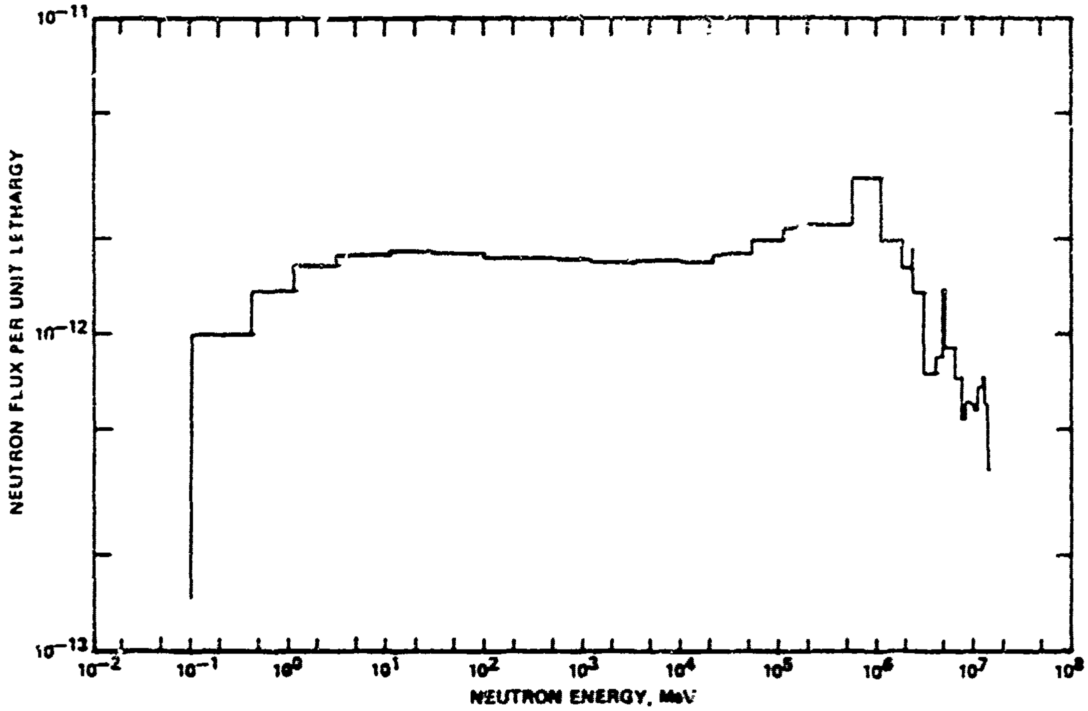

Figure 1c.   Free Field Neutron Fluence at 600 M.

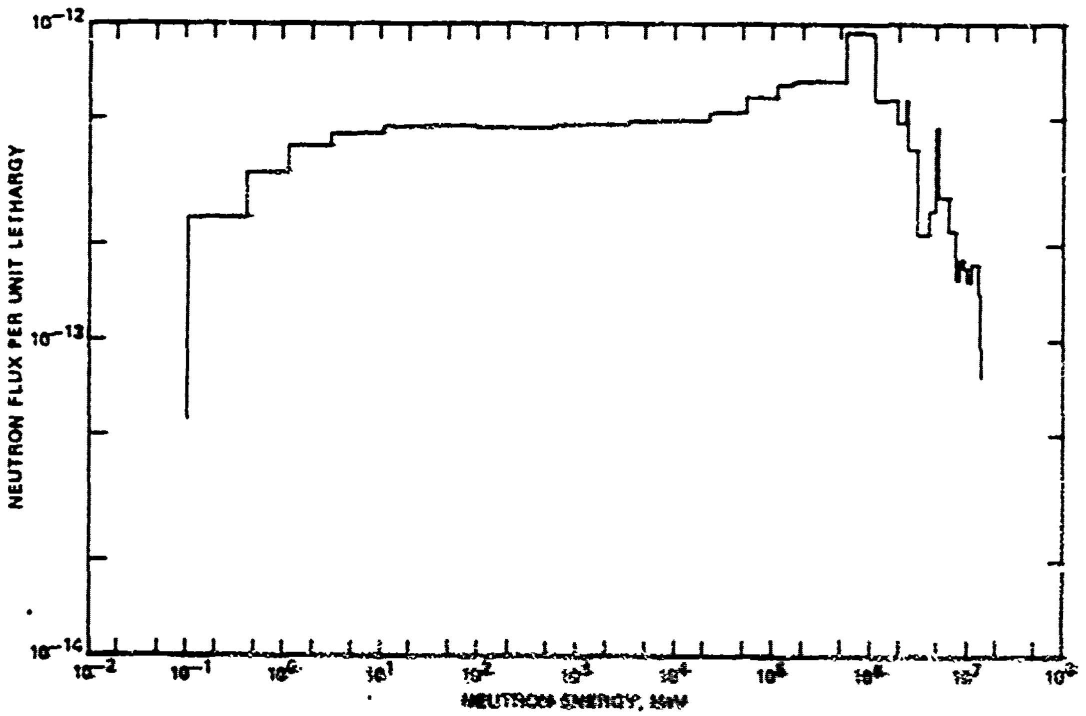

Figure 1d.   Free Field Neutron Fluence at 800 M.

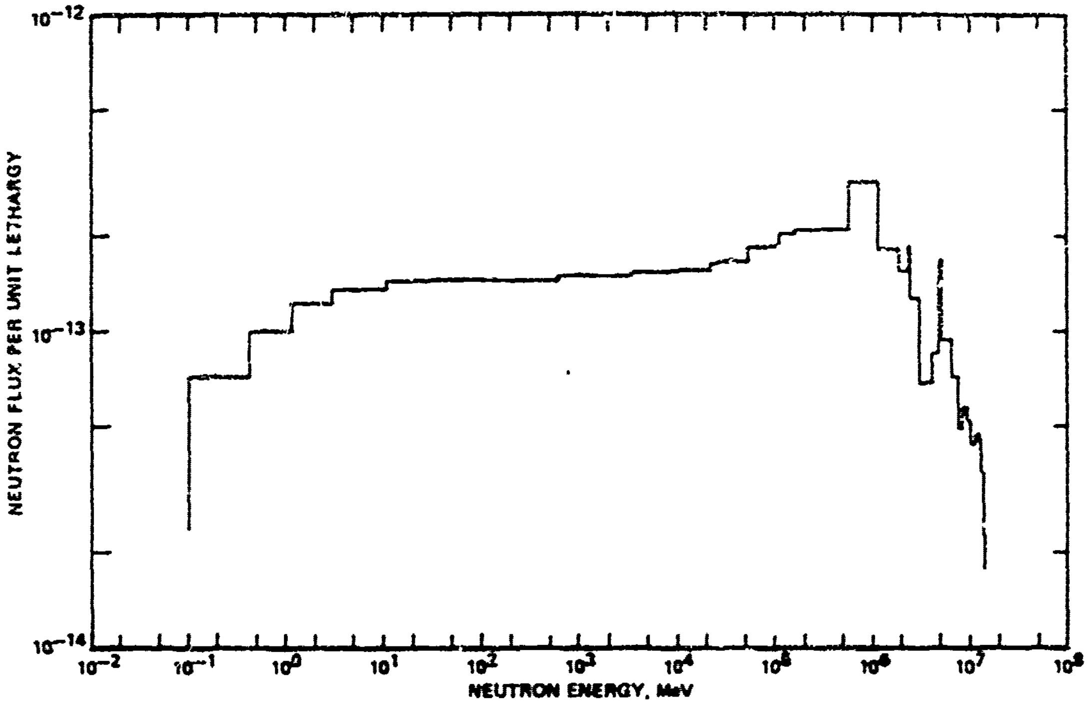

Figure 1e. Free Field Neutron Fluence at 1000 M.

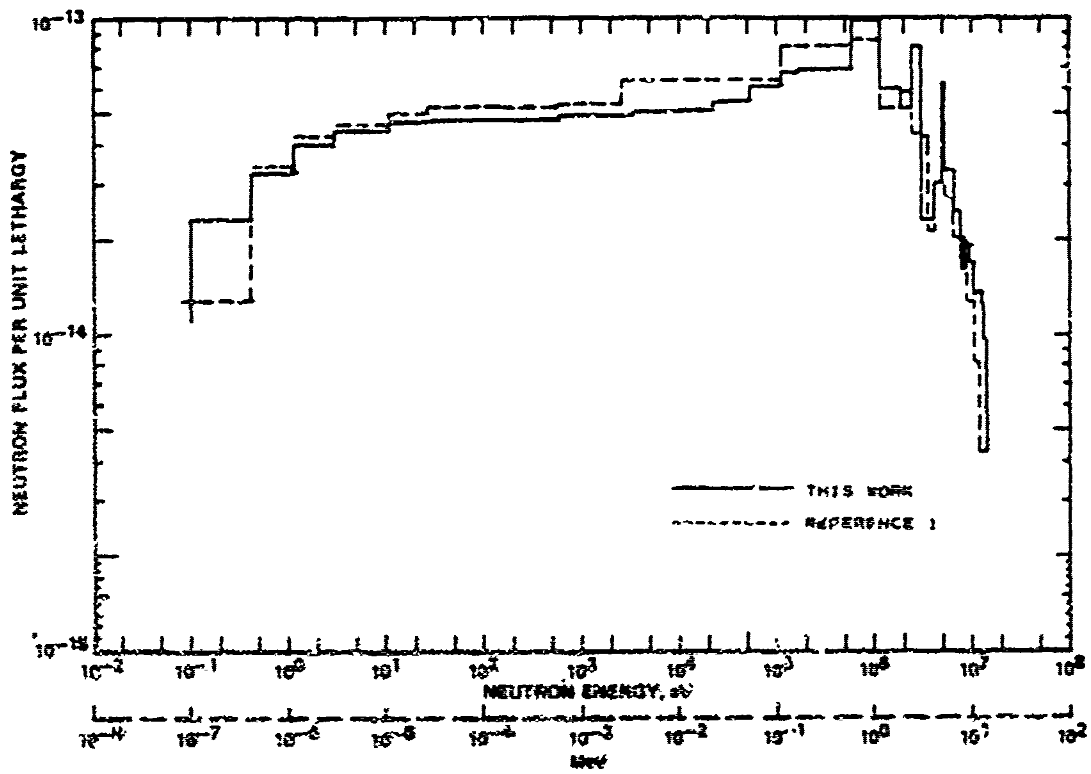

Figure 1f. Free Field Neutron Fluence at 1200 M.

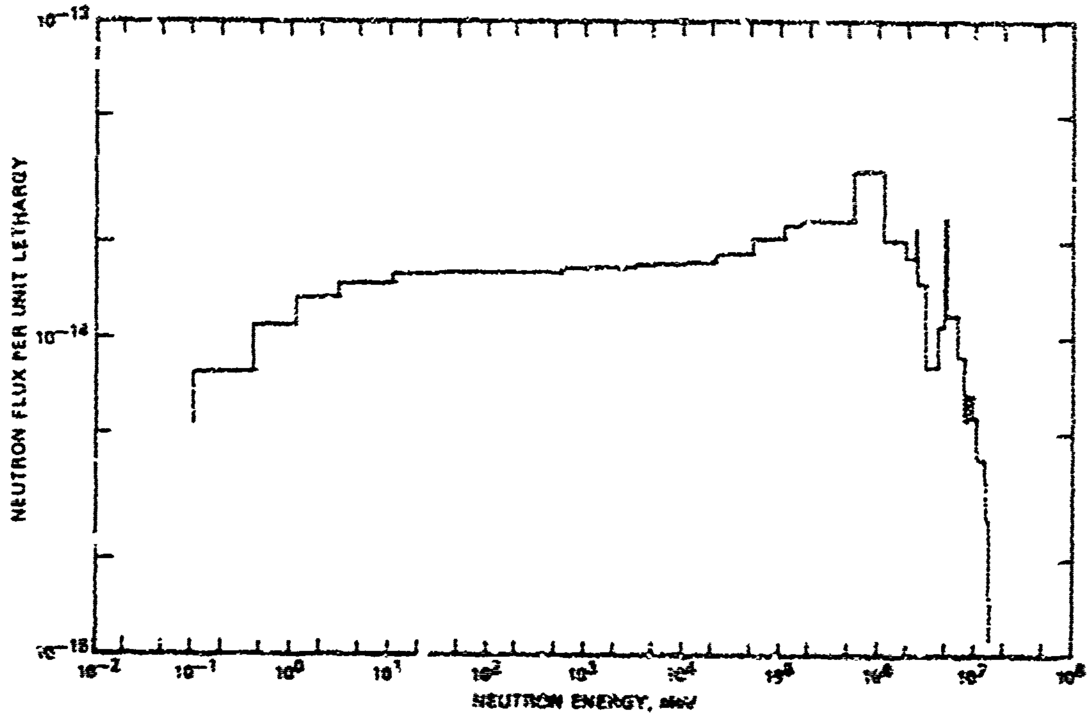

Figure 1g. Free Field Neutron Fluence at 1400 M.

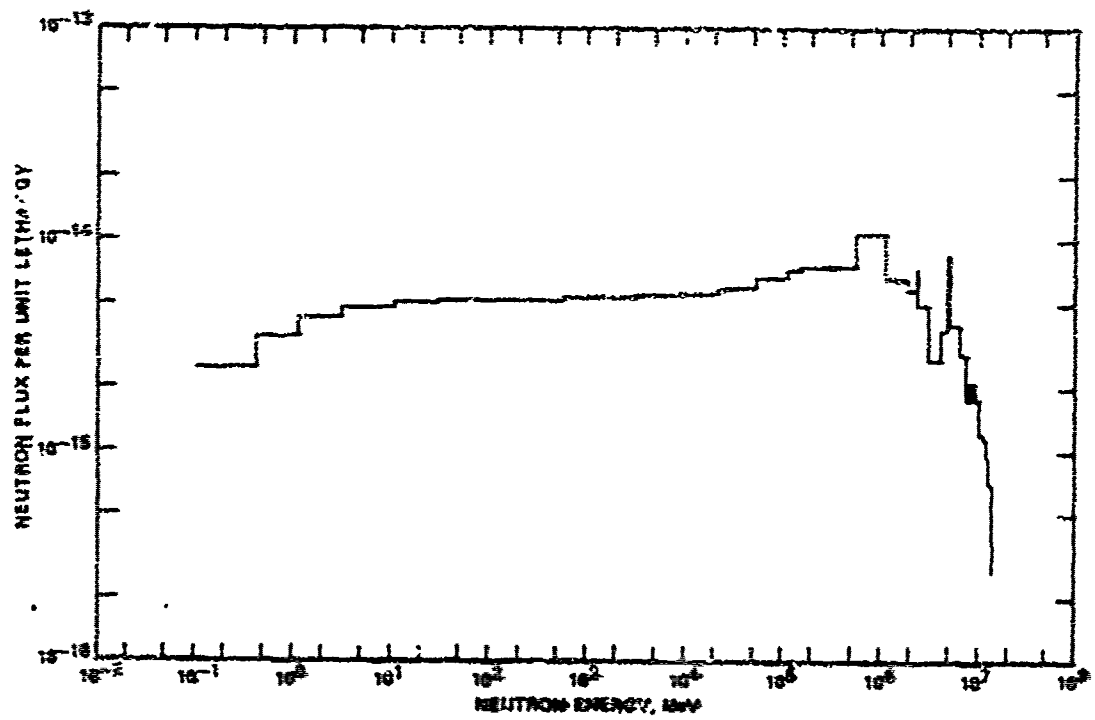

Figure 1h. Free Field Neutron Fluence at 1600 M.

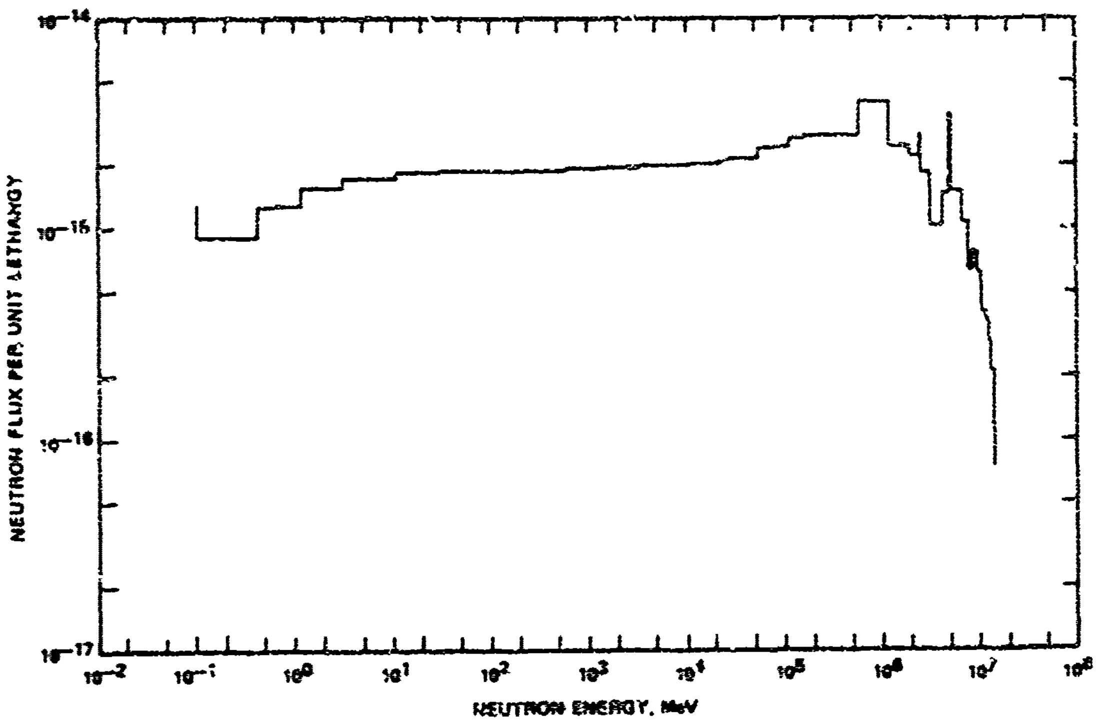

Figure 1i. Free Field Neutron Fluence at 1800 M.

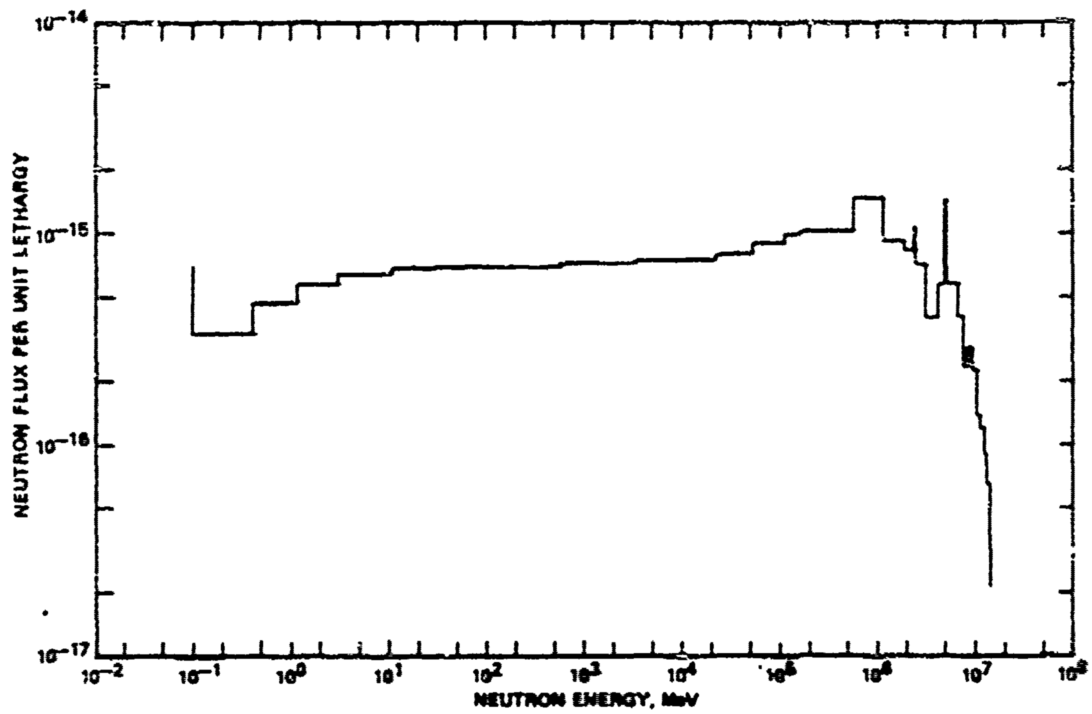

Figure 1j. Free Field Neutron Fluence at 2000 M.

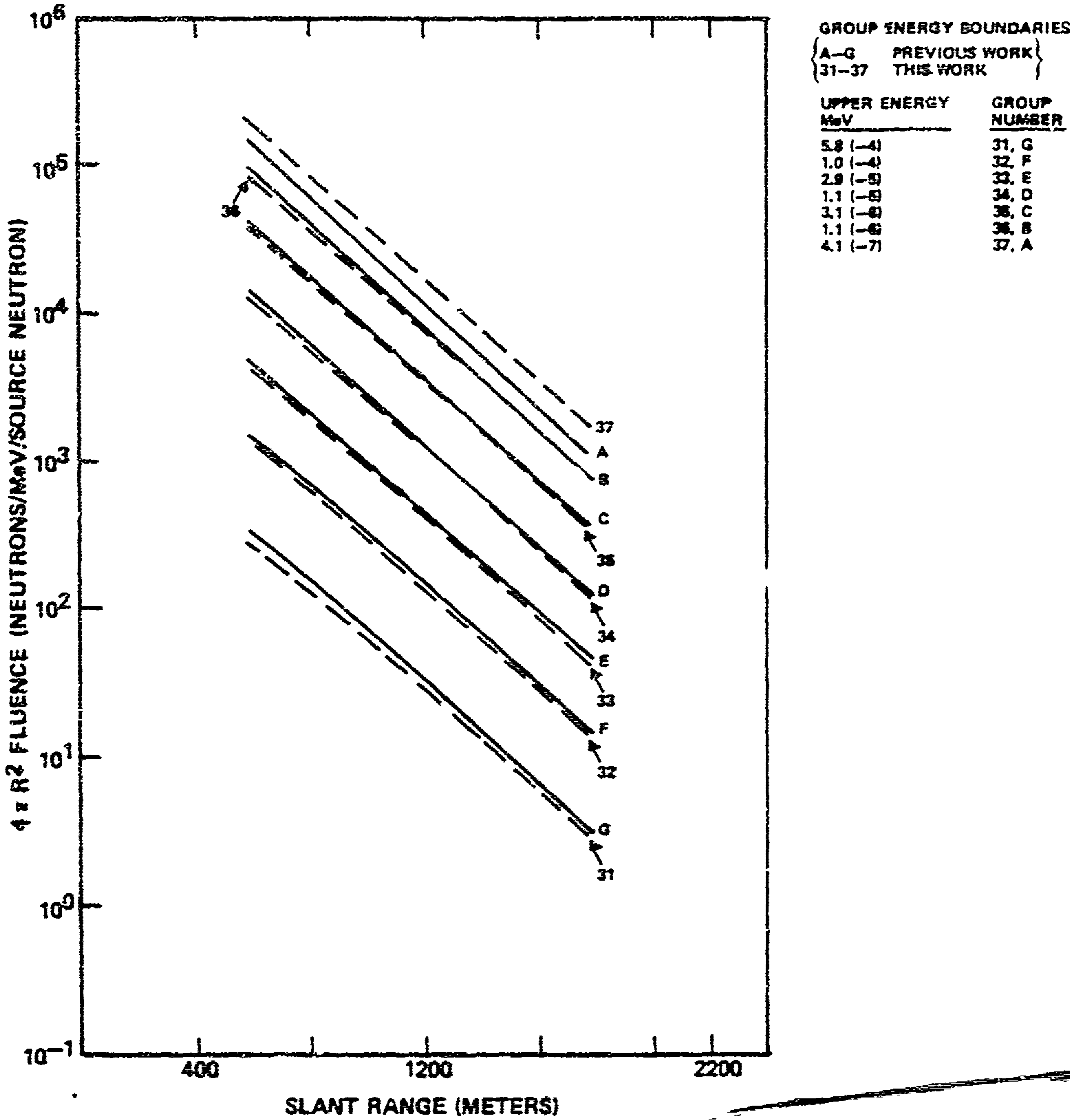

PRECEDING PAGE BLANK-NOT FILMED

Figure 2a. Free Field Neutron Group Fluxes vs Range.

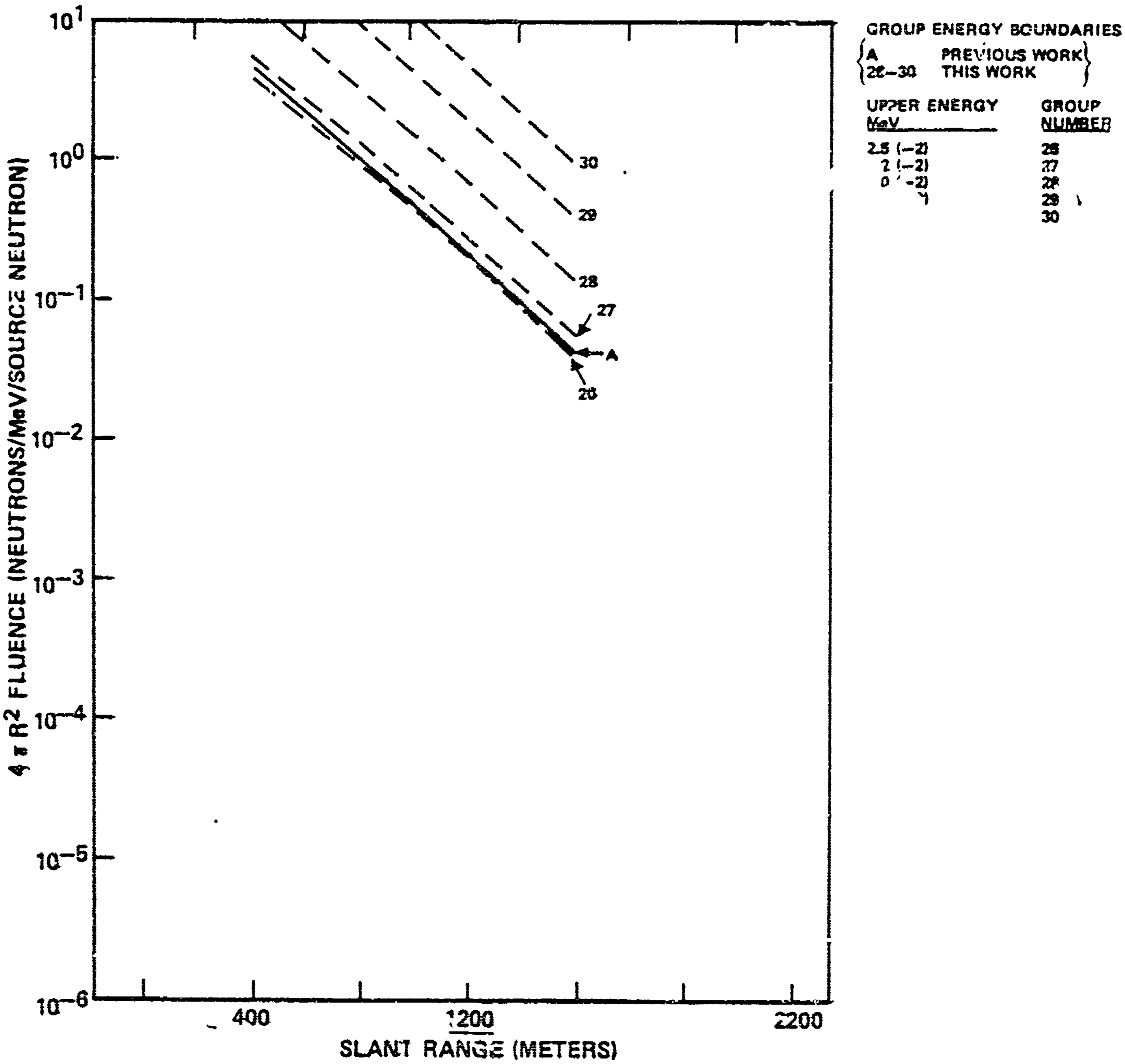

Figure 2b. Free Field Neutron Group Fluxes vs Range.

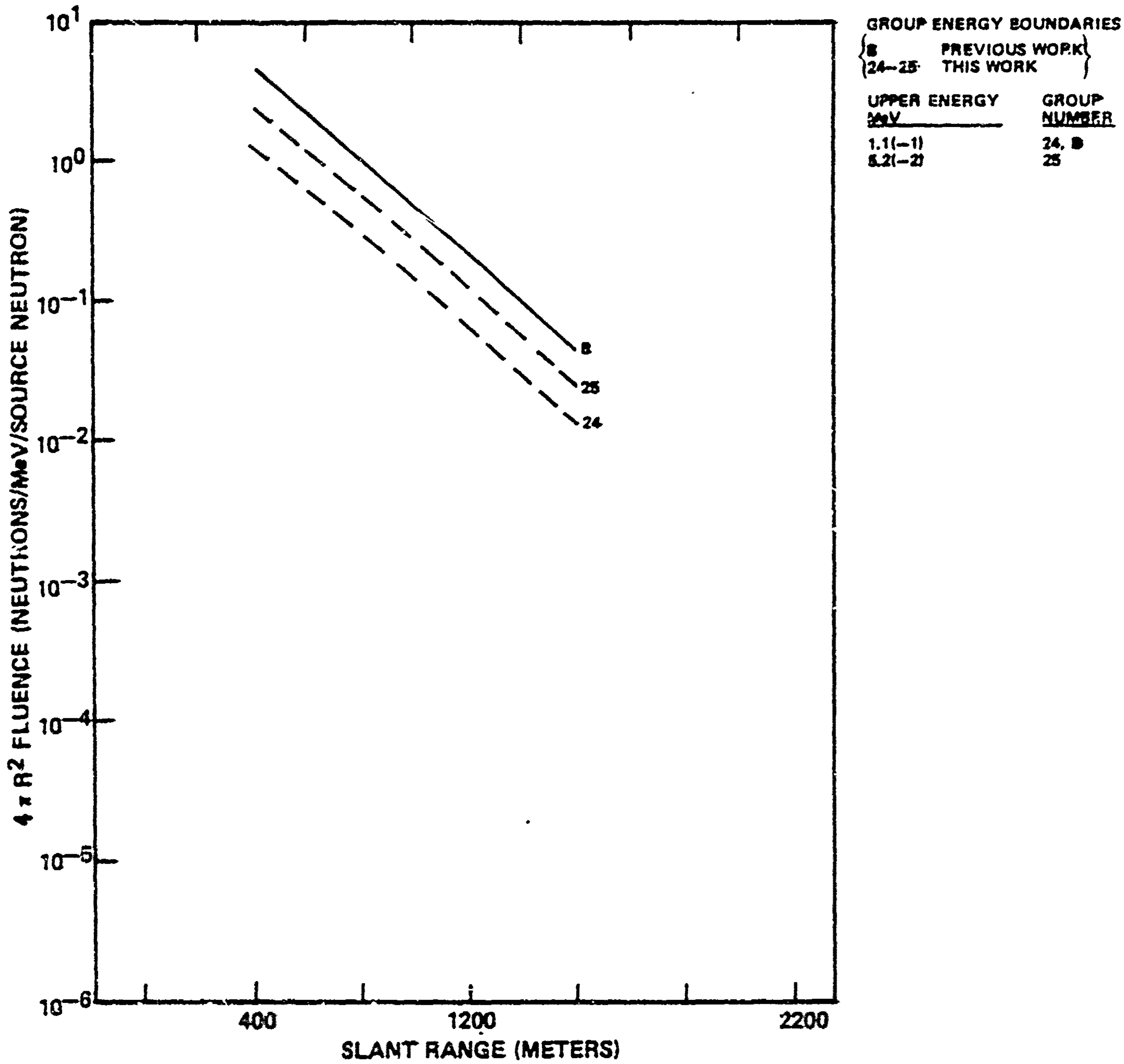

Figure 2c. Free Field Neutron Group Fluxes vs Range.

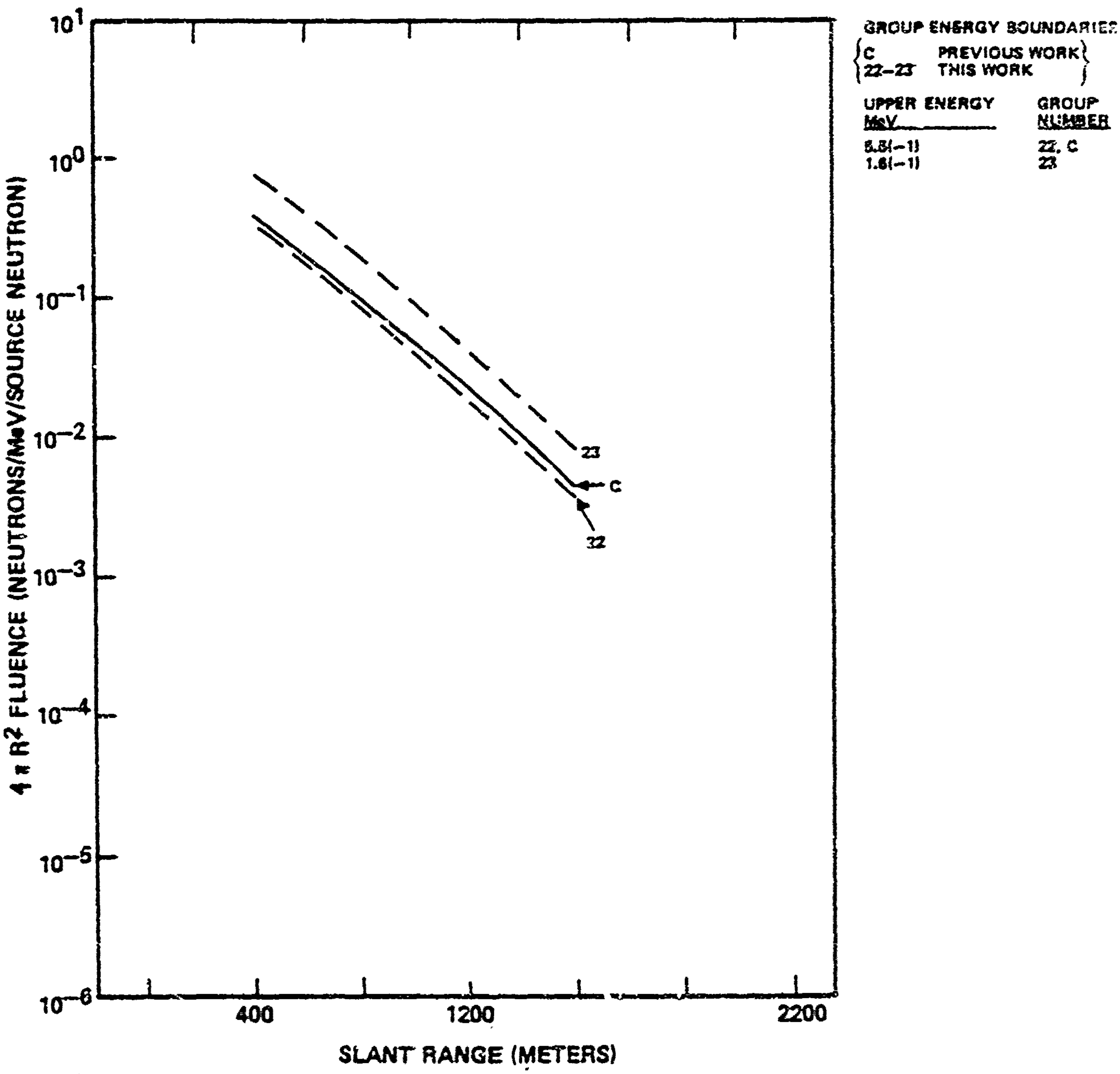

Figure 2d. Free Field Neutron Group Fluxes vs Range.

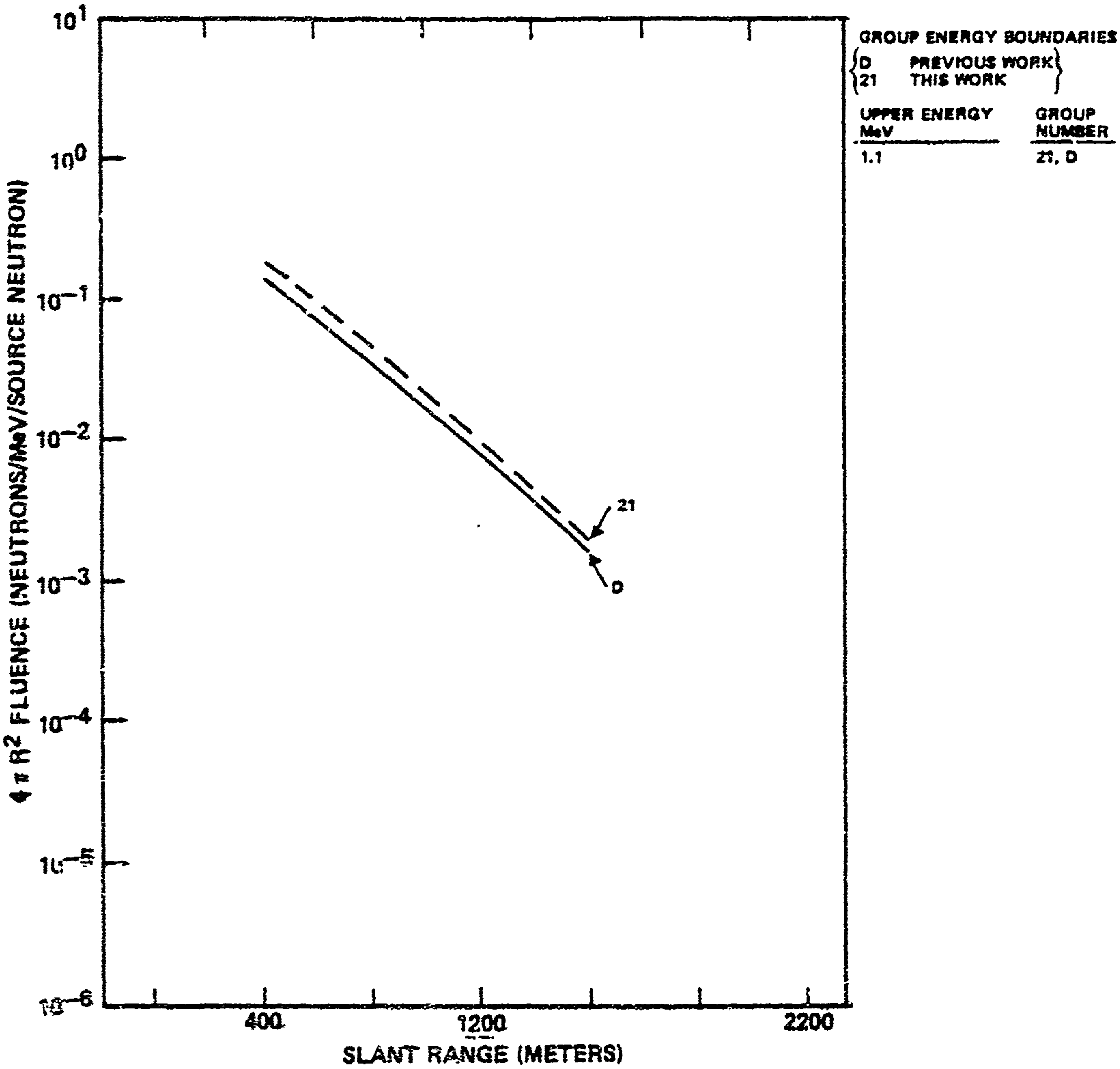

Figure 2e. Free Field Neutron Group Fluxes vs Range.

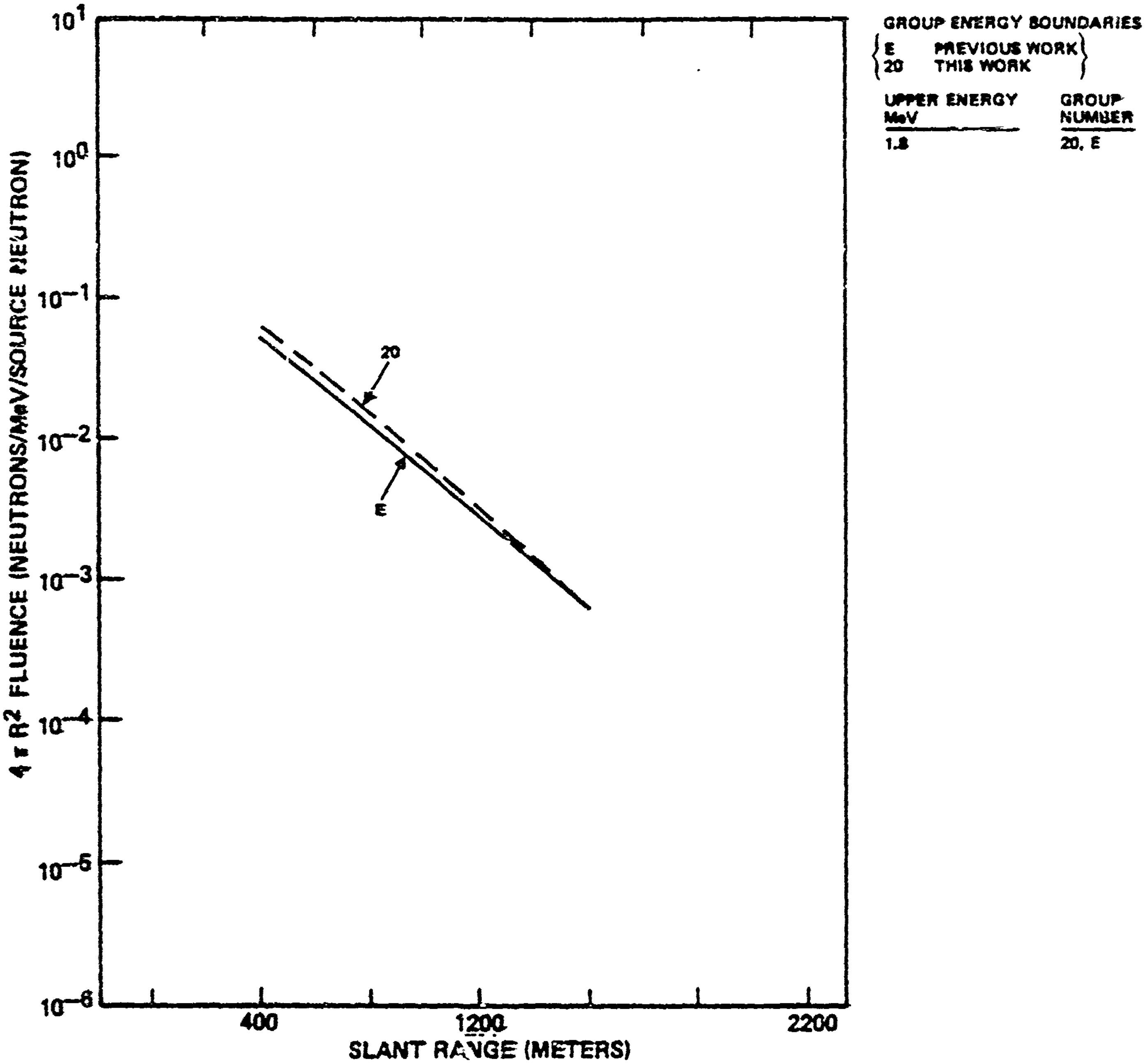

Figure 2f. Free Field Neutron Group Fluxes vs Range.

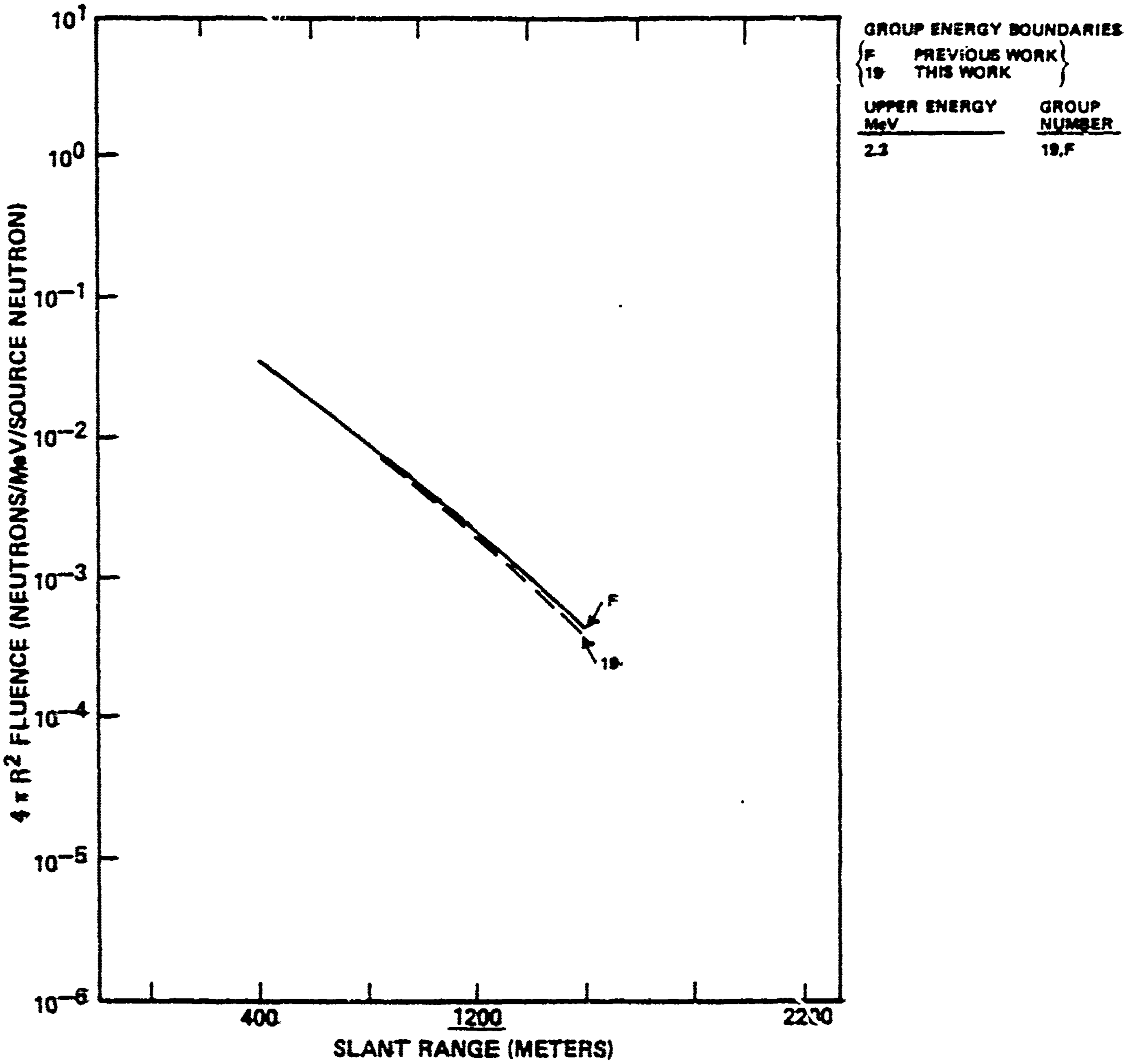

Figure 2g. Free Field Neutron Group Fluxes vs Range.

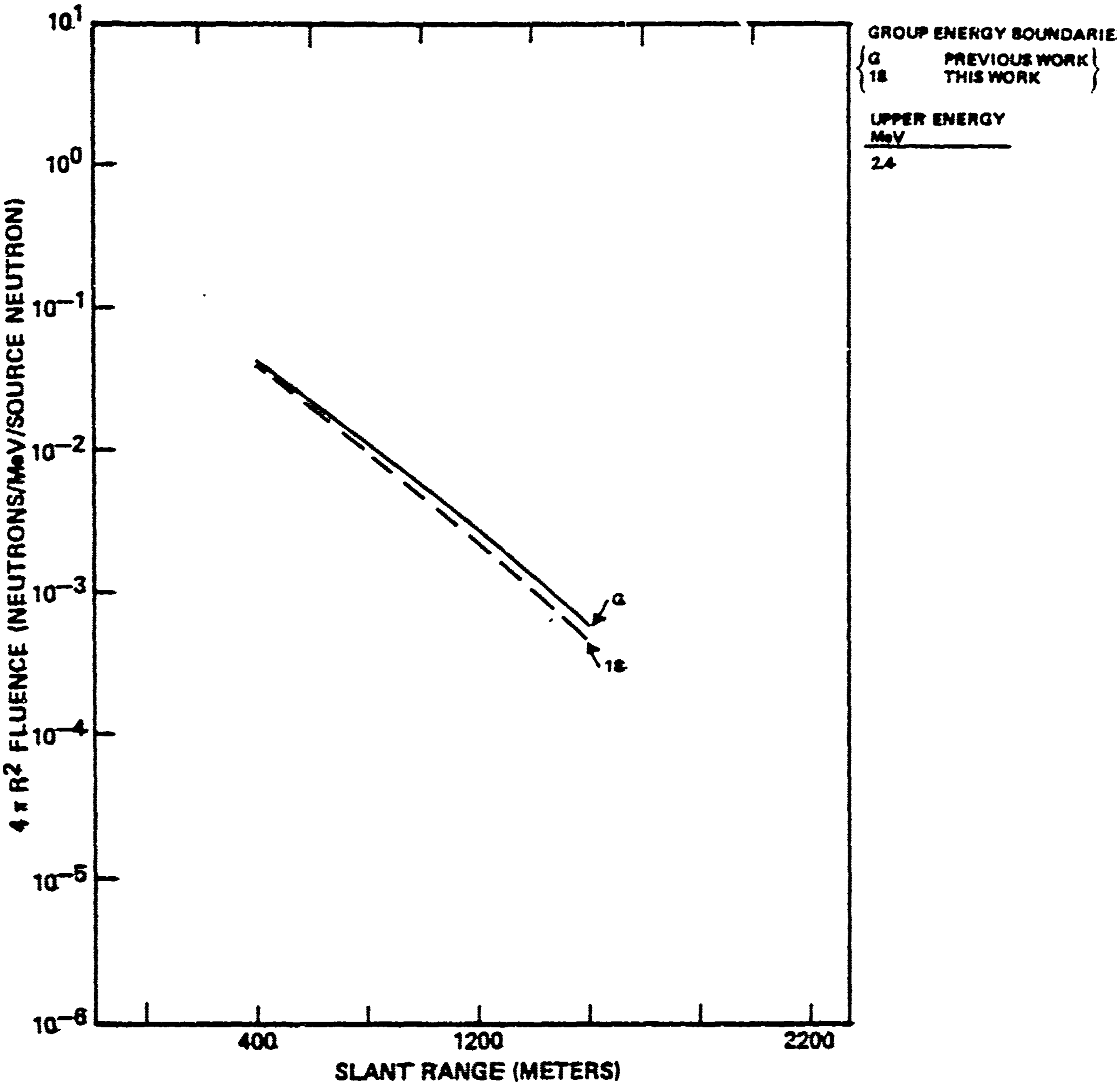

Figure 2h. Free Field Neutron Group Fluxes vs Range.

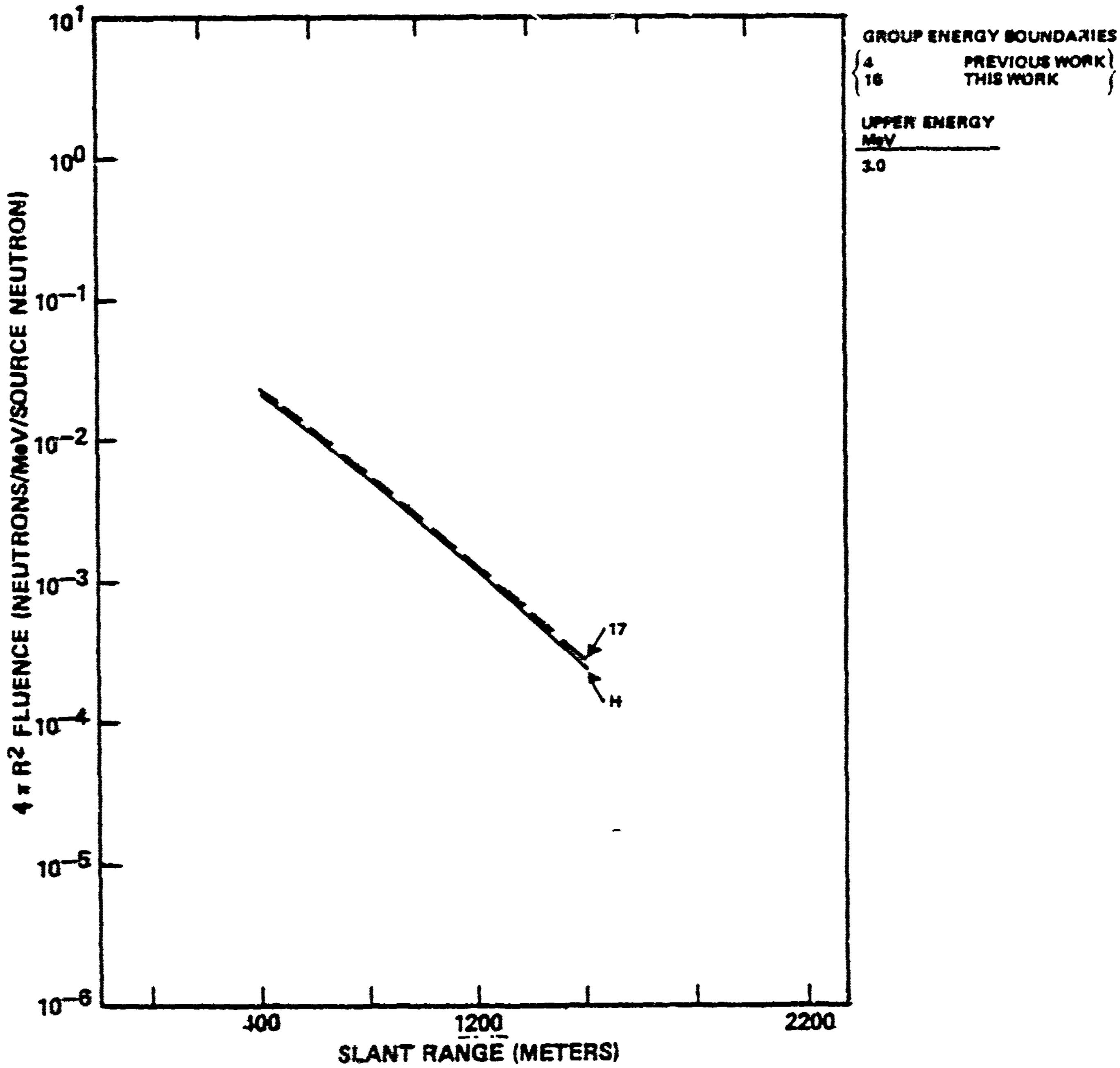

Figure 21. Free Field Neutron Group Fluxes vs Range.

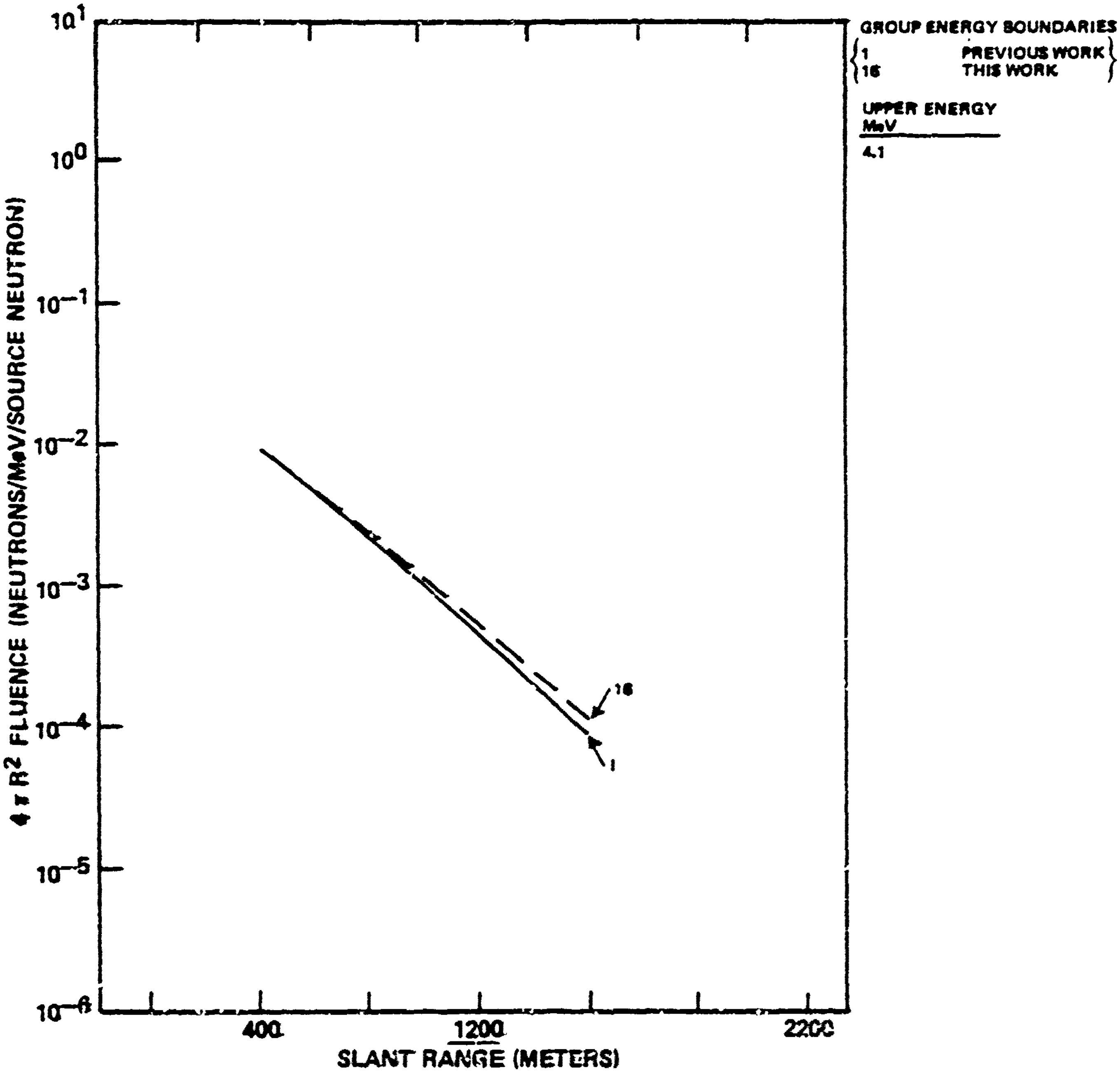

Figure 2j. Free Field Neutron Group Fluxes vs Range.

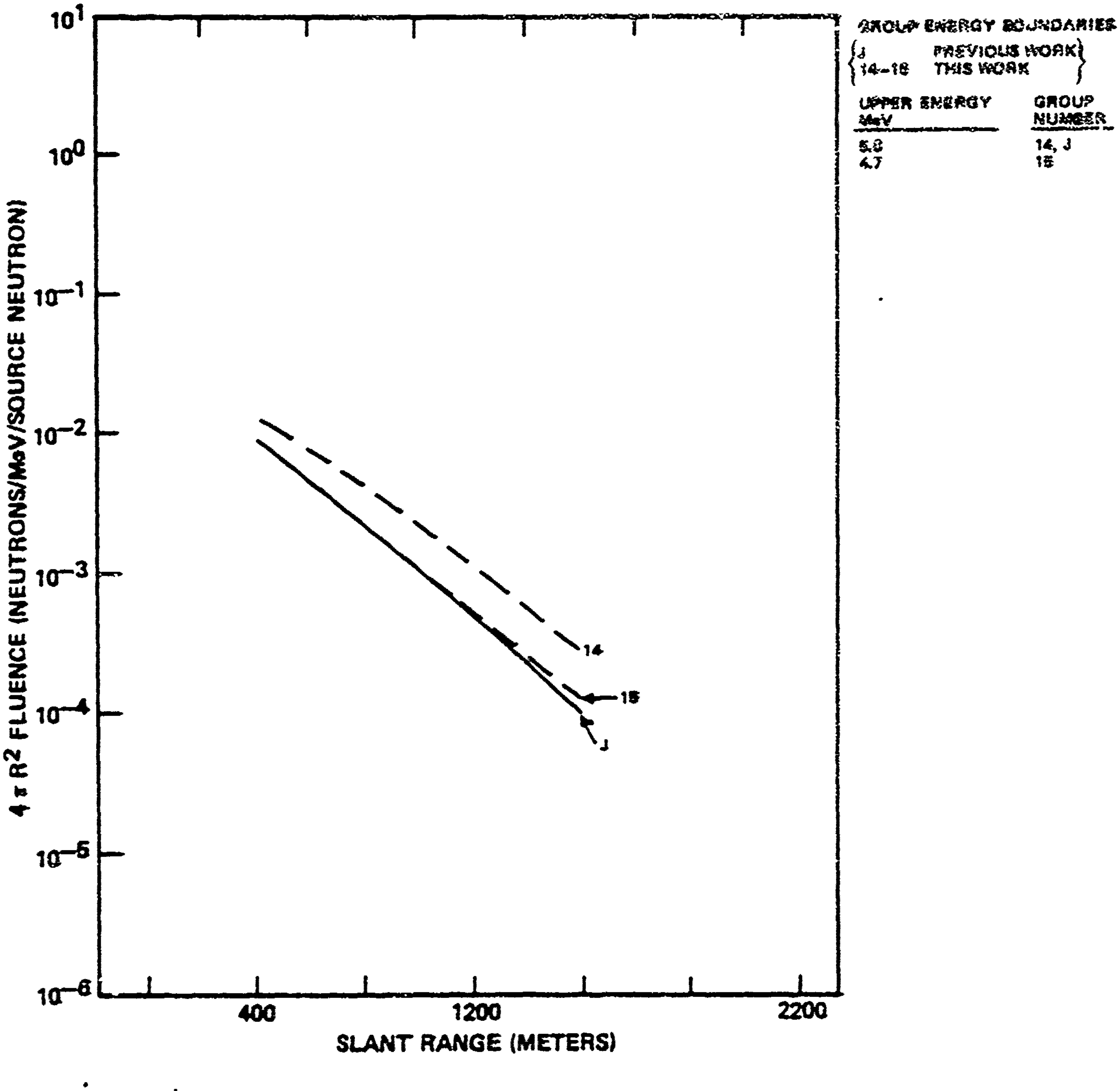

Figure 2k. Free Field Neutron Group Fluxes vs Range.

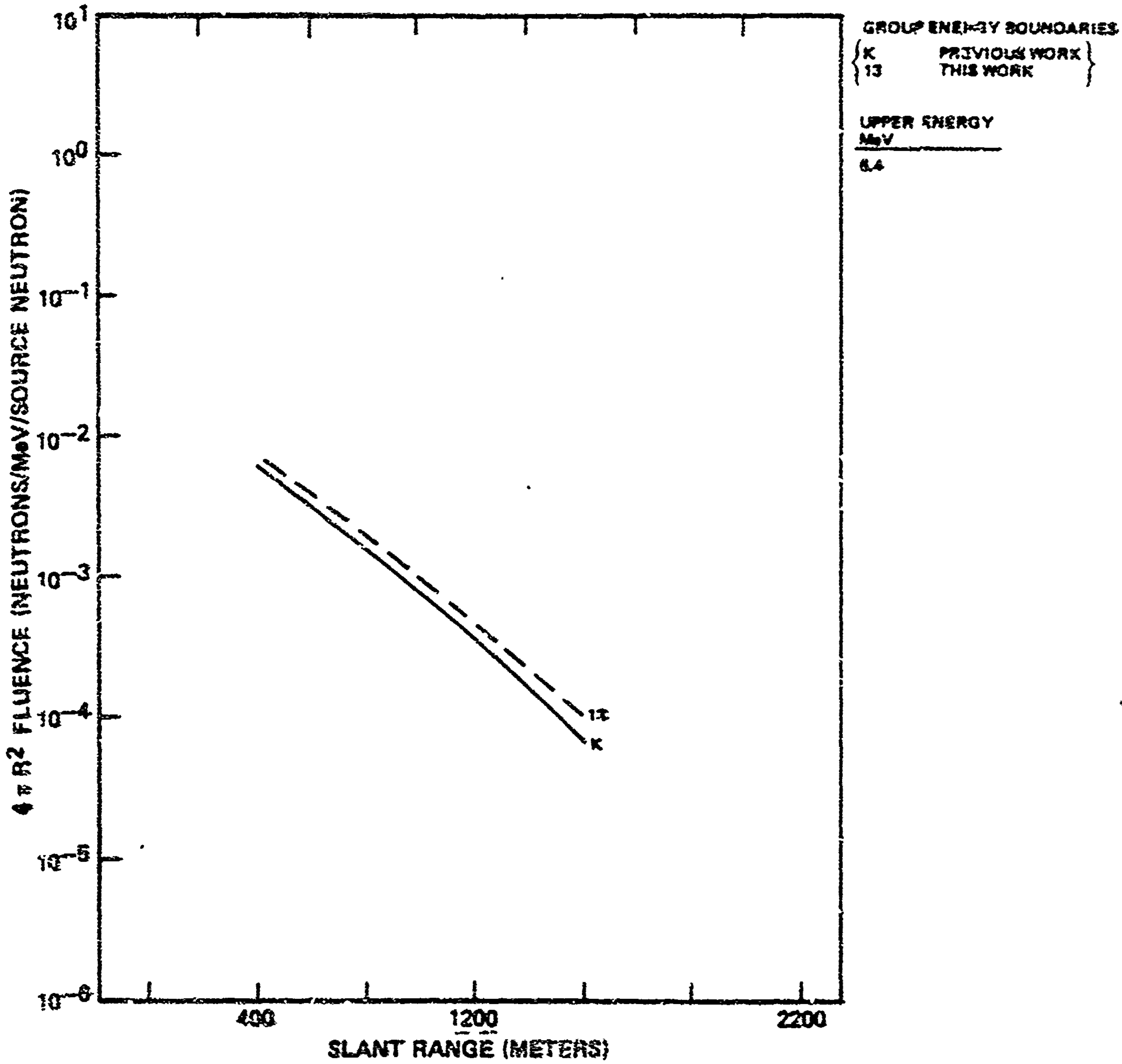

Figure 21. Free Field Neutron Group Fluxes vs Range.

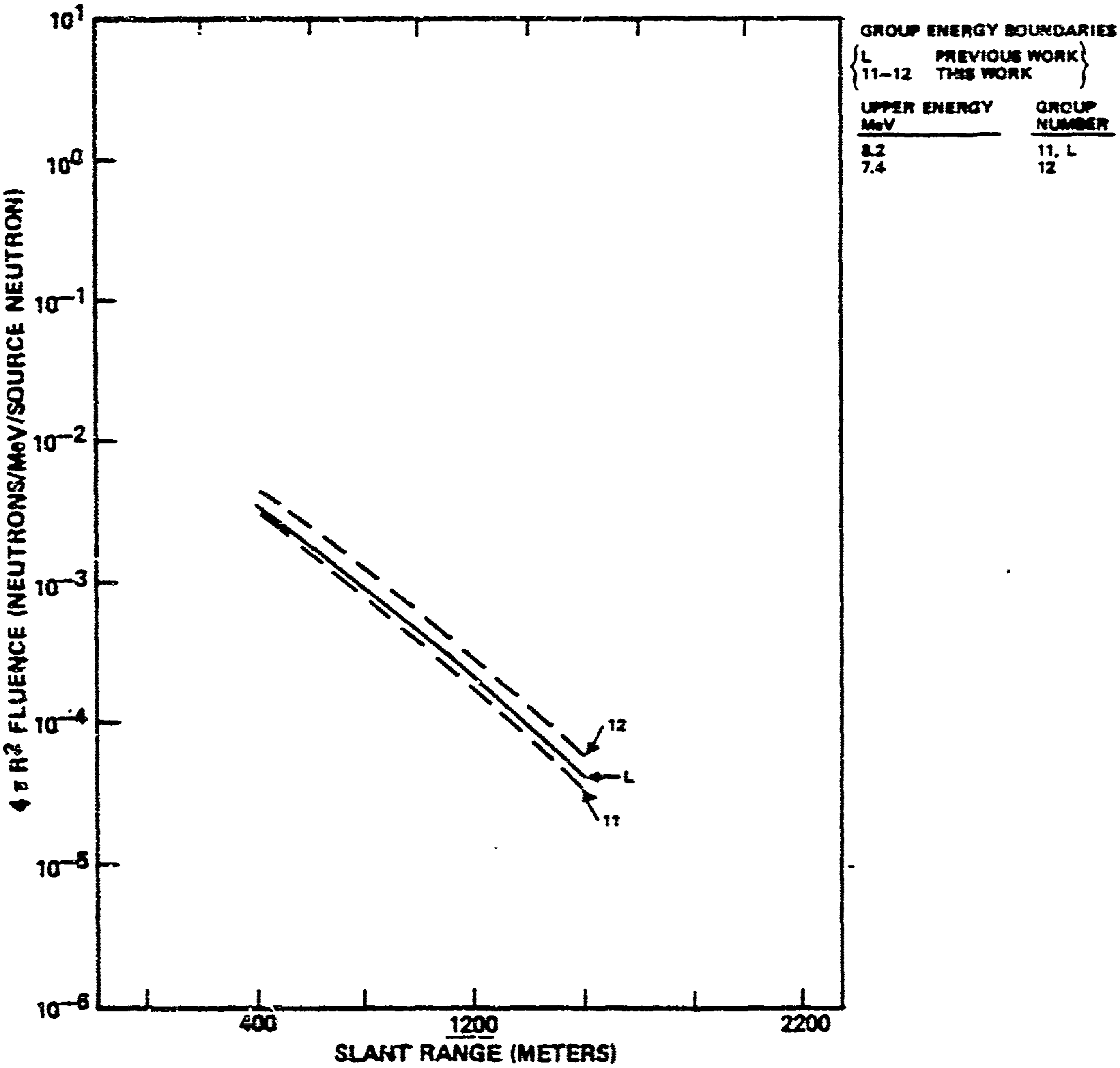

Figure 2m. Free Field Neutron Group Fluxes vs Range.

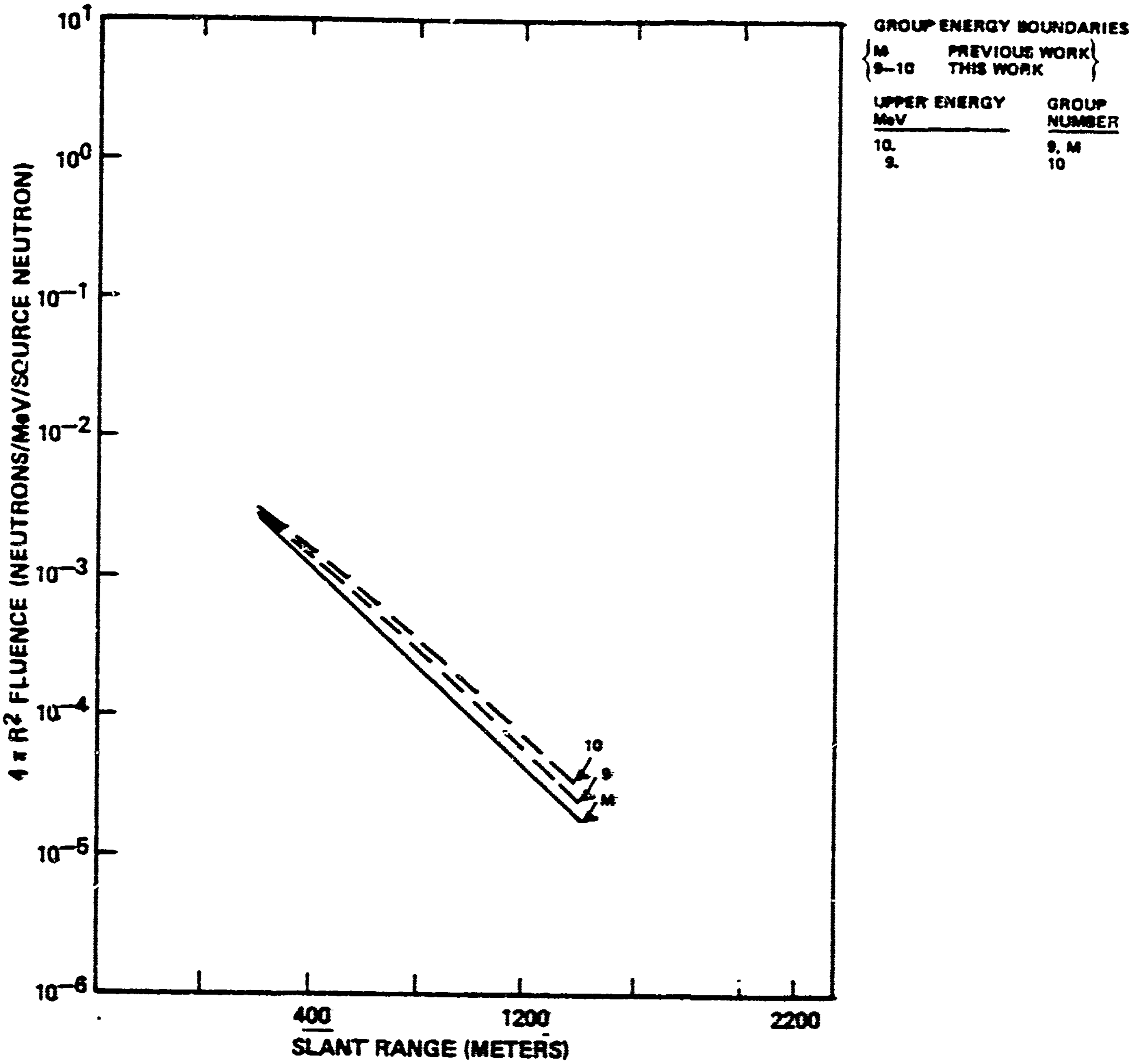

Figure 2n. Free Field Neutron Group Fluxes vs Range.

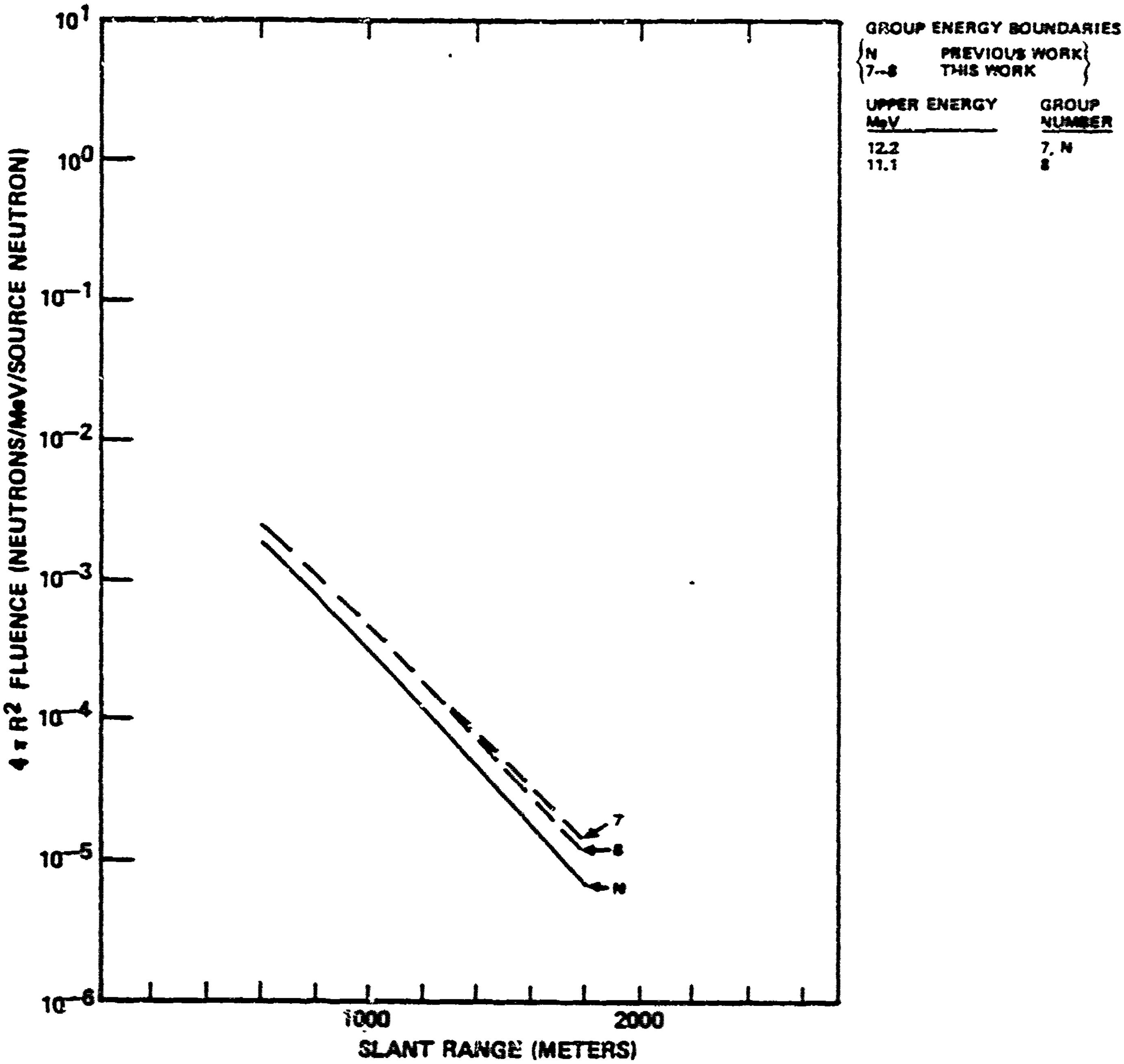

Figure 2o. Free Field Neutron Group Fluxes vs Range.

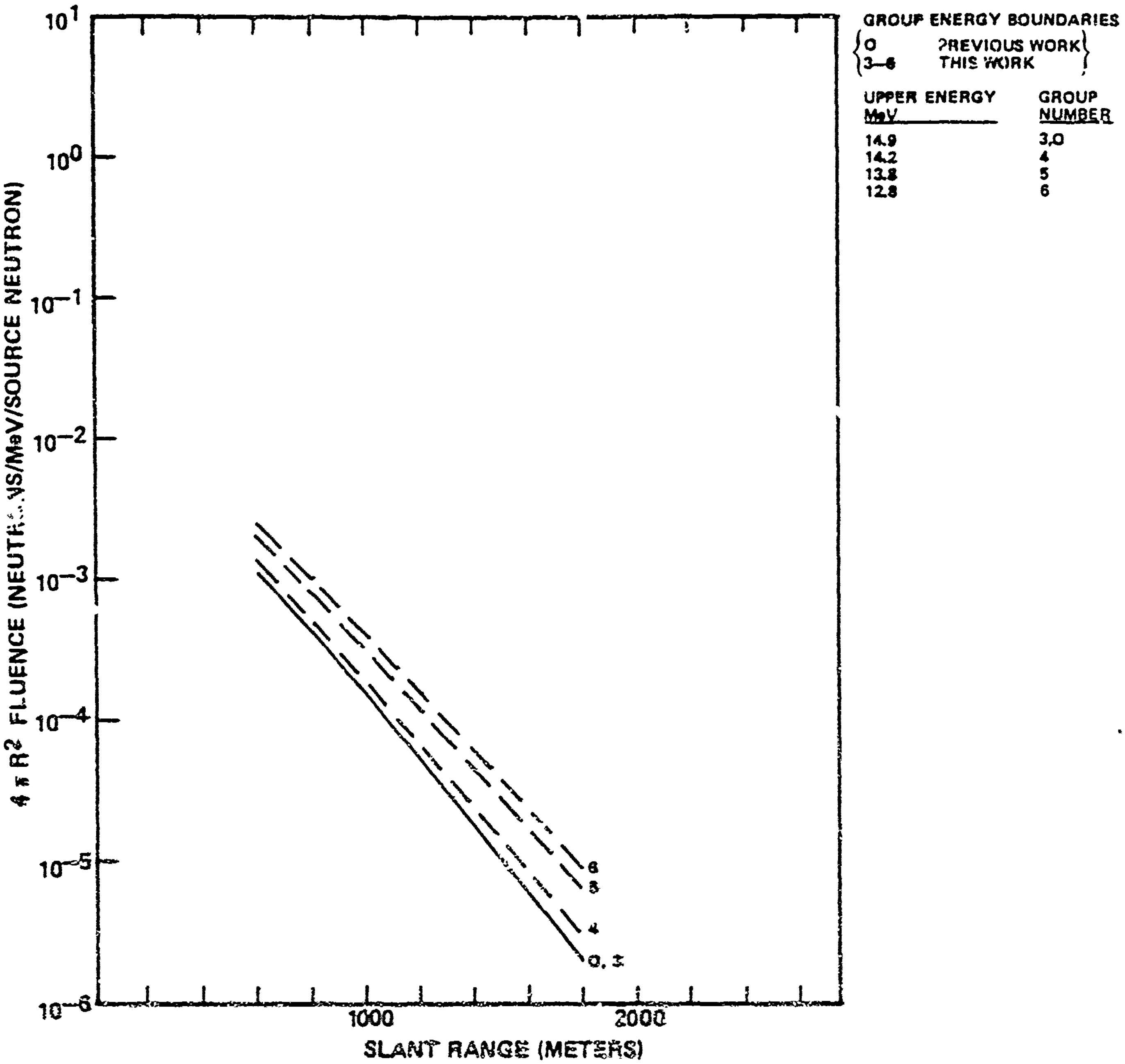

Figure 2p. Free Field Neutron Group Fluxes vs Range.

Table 4. Ratios of Expansion Coefficients of Dose Angular Distribution at Various Ranges (New Data/Old Data).

Range (m)	P_0	P_1	P_2	P_3
800	0.95	0.90	0.85	0.82
1200	0.91	0.87	0.83	0.80
1600	0.87	0.84	0.81	0.80
2000	0.83	0.82	0.80	0.79

Figure 3a-j shows the secondary gamma ray fluence per unit lethargy per source neutron for several ranges from 0.2 to 2 km. The spectra can be seen to be relatively insensitive to range. Figure 2f compares the secondary gamma ray fluence per unit lethargy of 1200 m with that reported in Reference 1. The spectra are also plotted as a function of range in Figure 4 in the format of Reference 1 to facilitate a comparison with previous work.

Figures 5a-c shows the Snyder Neufeld Tissue dose, the first moment of the dose, and the second moment of the dose as a function of range. Figures 6a-c shows the Henderson Tissue gamma ray dose, first and second moments of the dose, versus range. These plots are normalized to one source neutron.

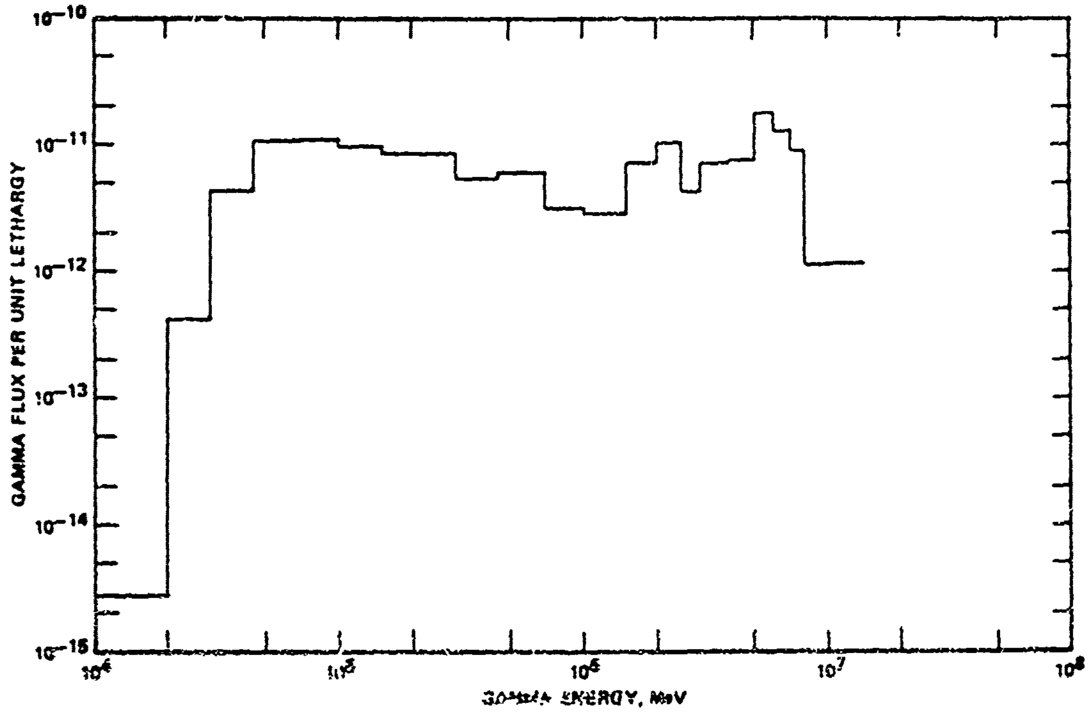

Figure 3a. Free Field Secondary Gamma Ray Fluence at 200 M.

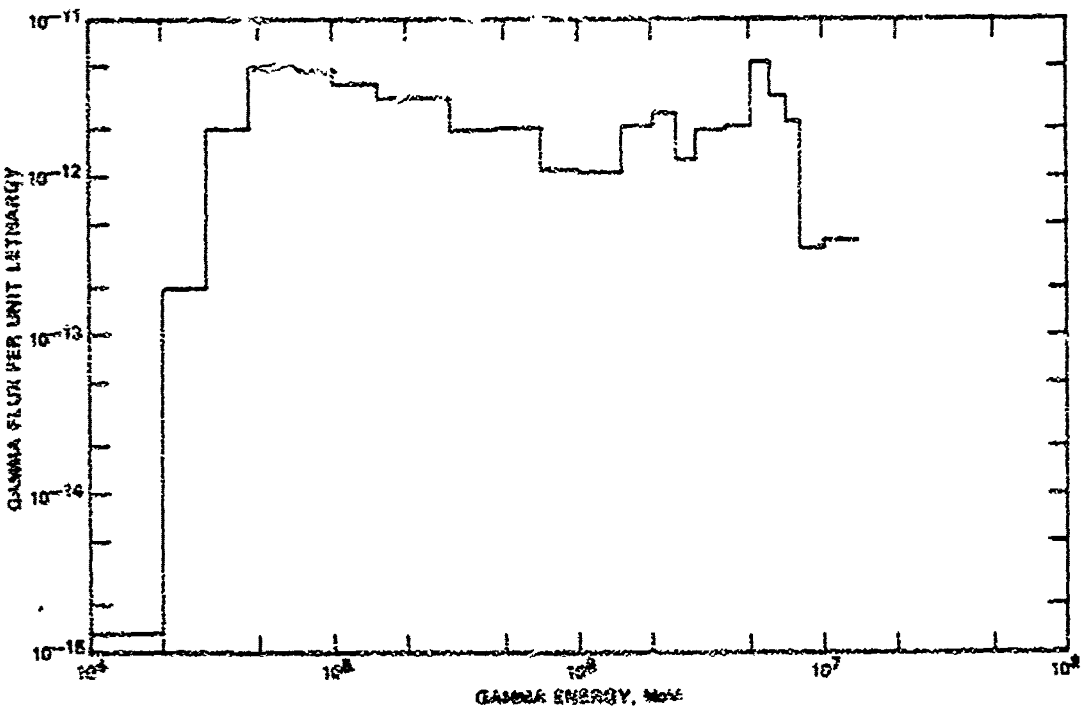

Figure 3b. Free Field Secondary Gamma Ray Fluence at 400 M.

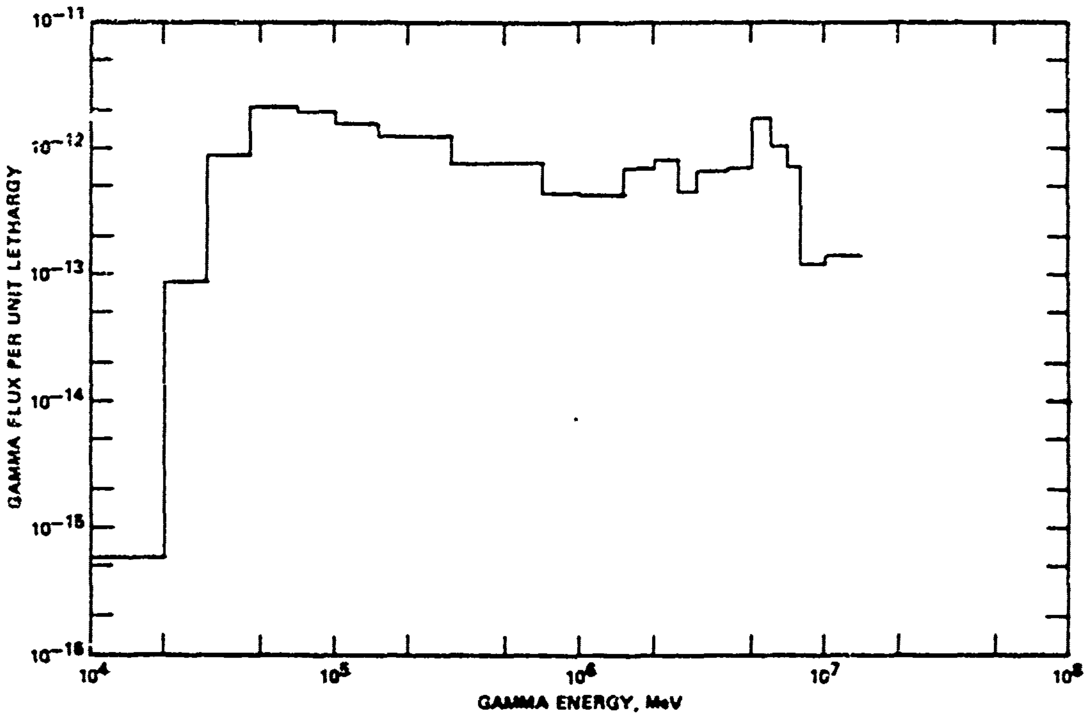

Figure 3c. Free Field Secondary Gamma Ray Fluence at 600 M.

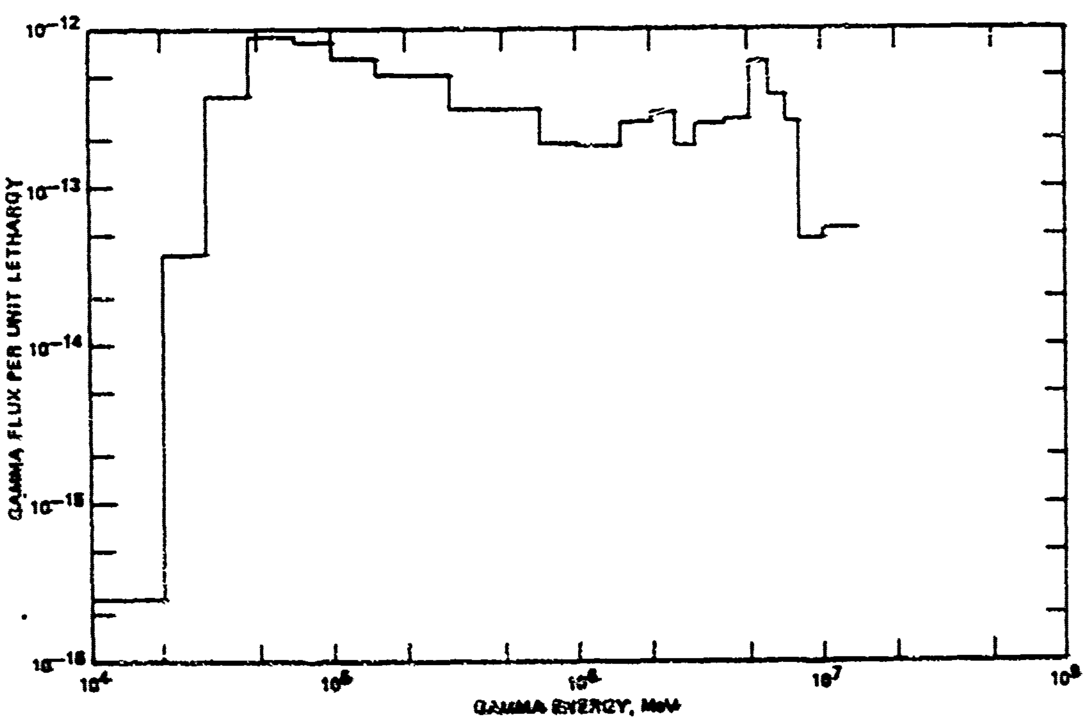

Figure 3d. Free Field Secondary Gamma Ray Fluence at 800 M.

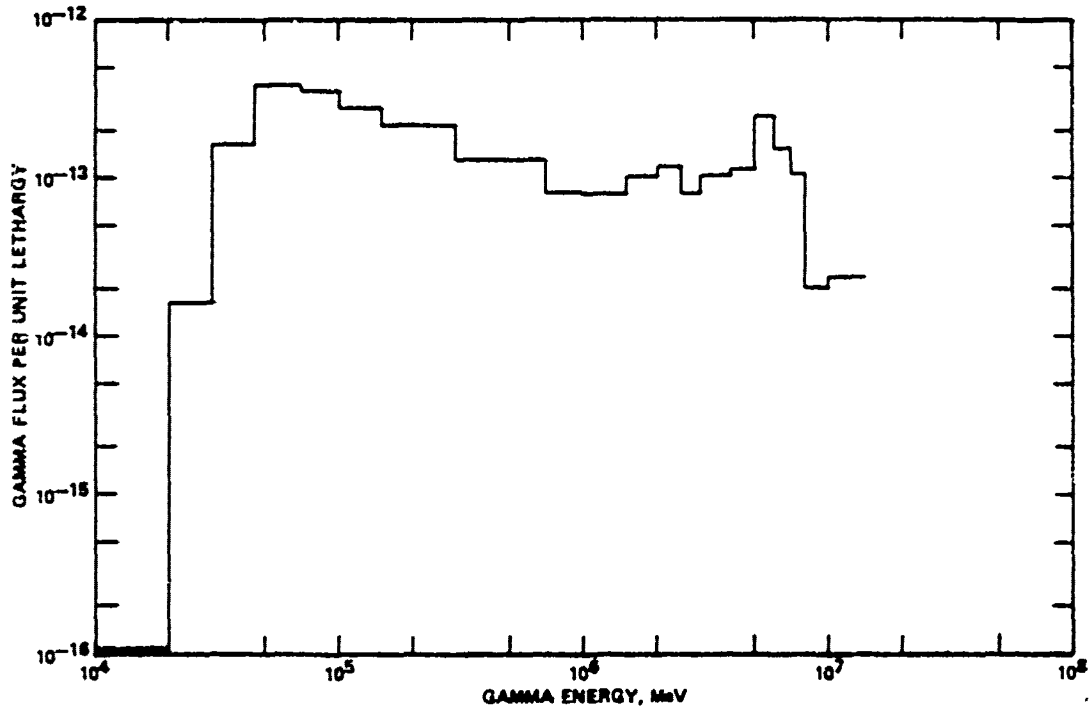

Figure 3e. Free Field Secondary Gamma Ray Fluence at 1000 M.

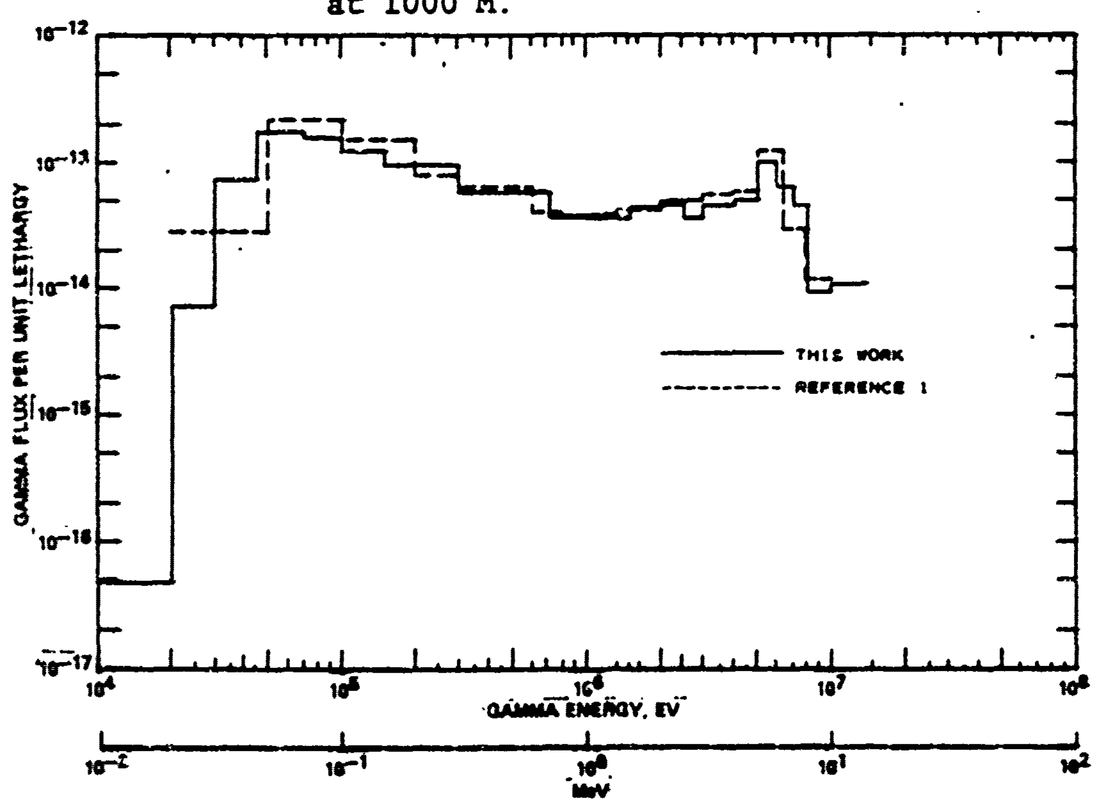

Figure 3f. Free Field Secondary Gamma Ray Fluence at 1200 M.

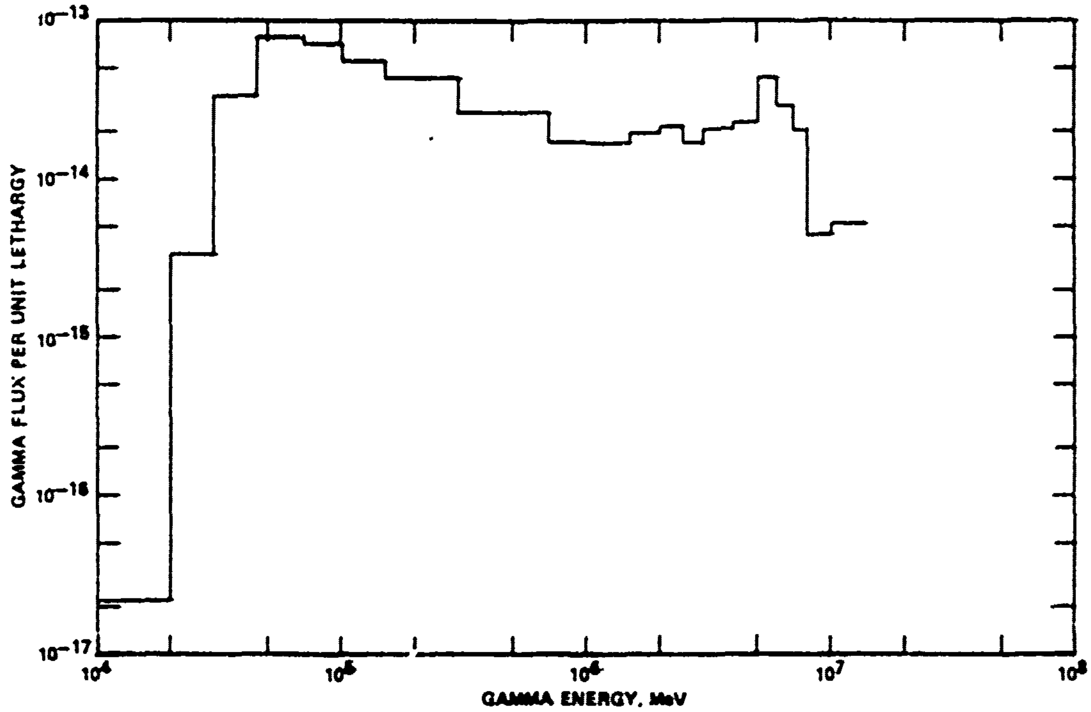

Figure 3g. Free Field Secondary Gamma Ray Fluence at 1400 M.

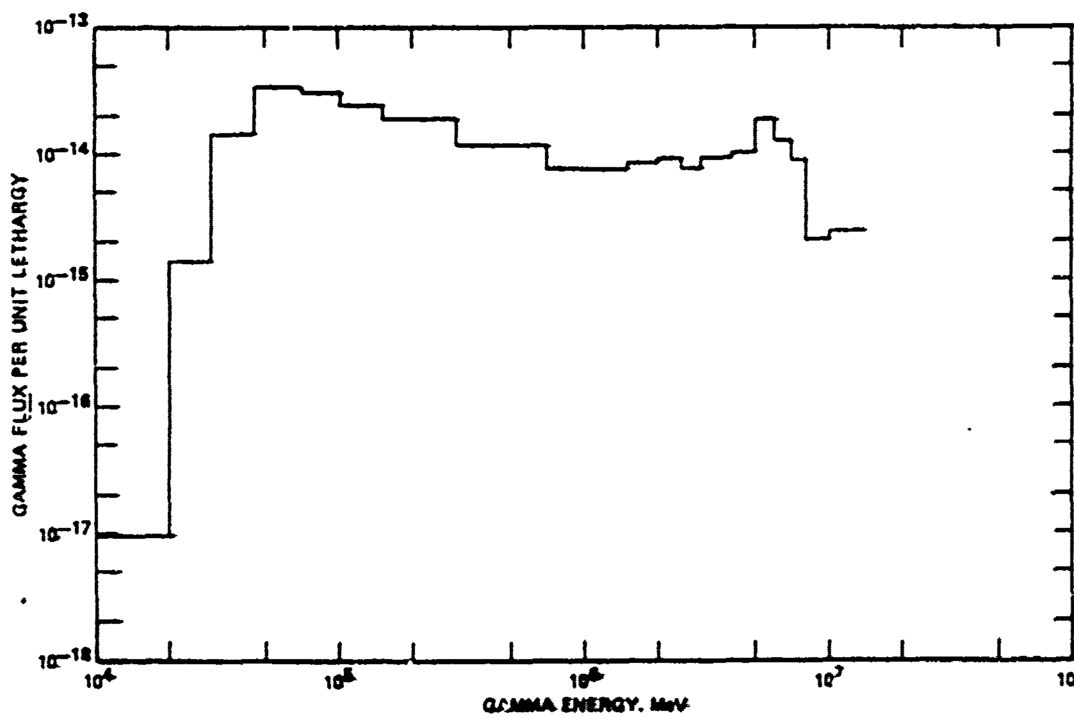

Figure 3h. Free Field Secondary Gamma Ray Fluence at 1600 M.

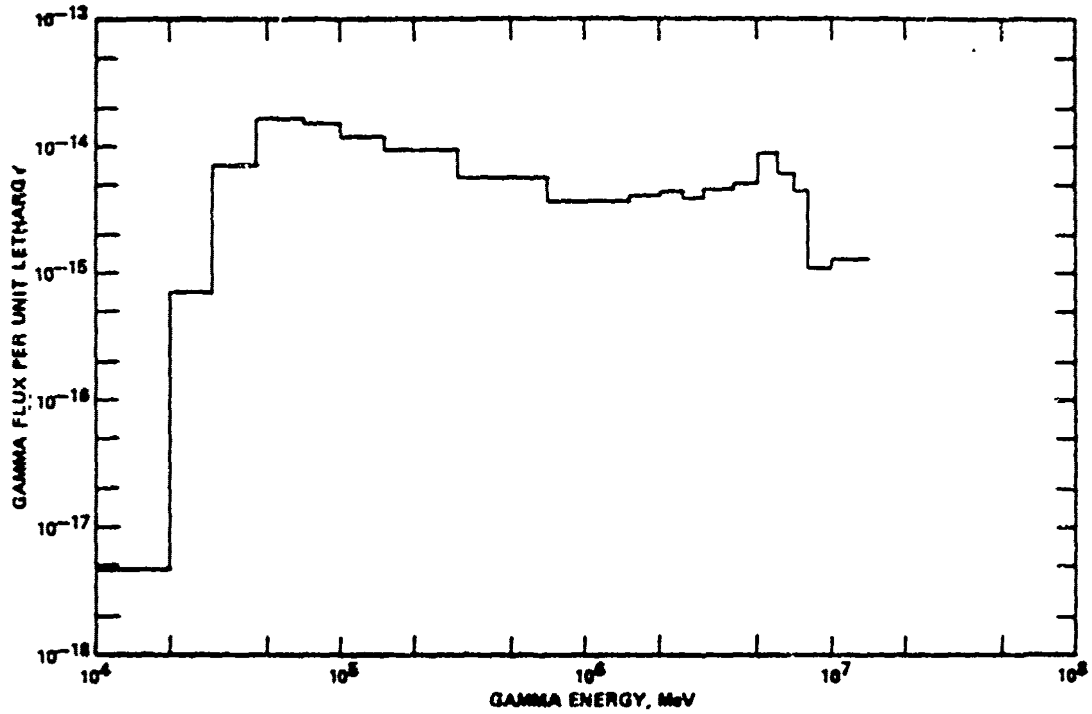

Figure 3i. Free Field Secondary Gamma Ray Fluence at 1800 M.

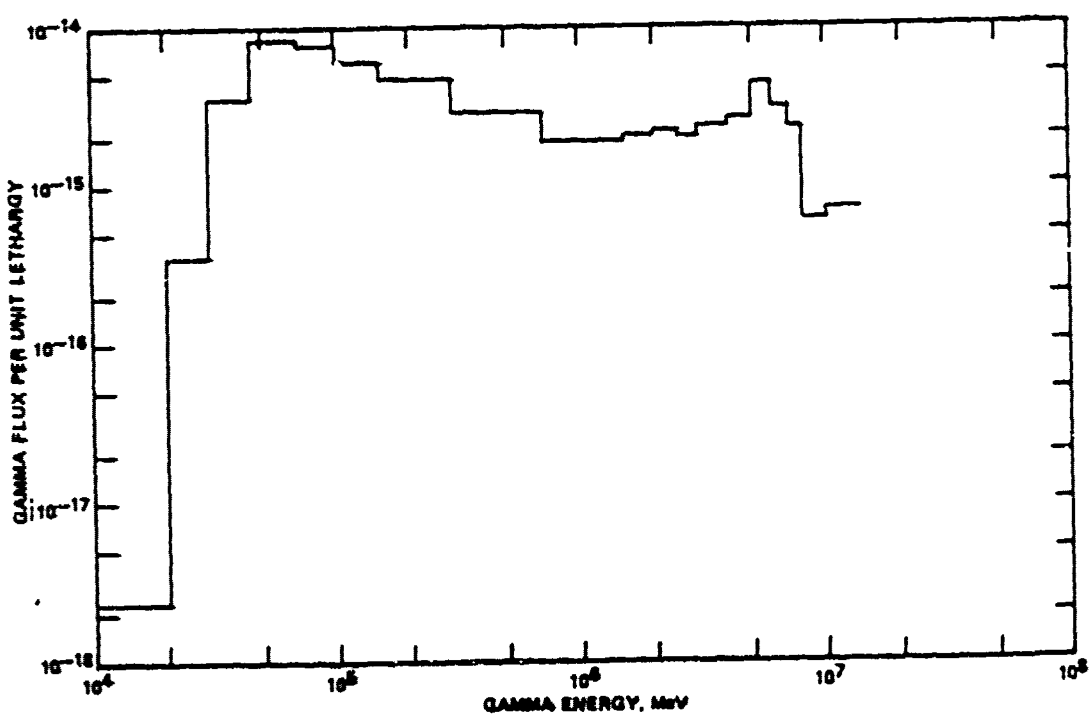

Figure 3j. Free Field Secondary Gamma Ray Fluence at 2000 M.

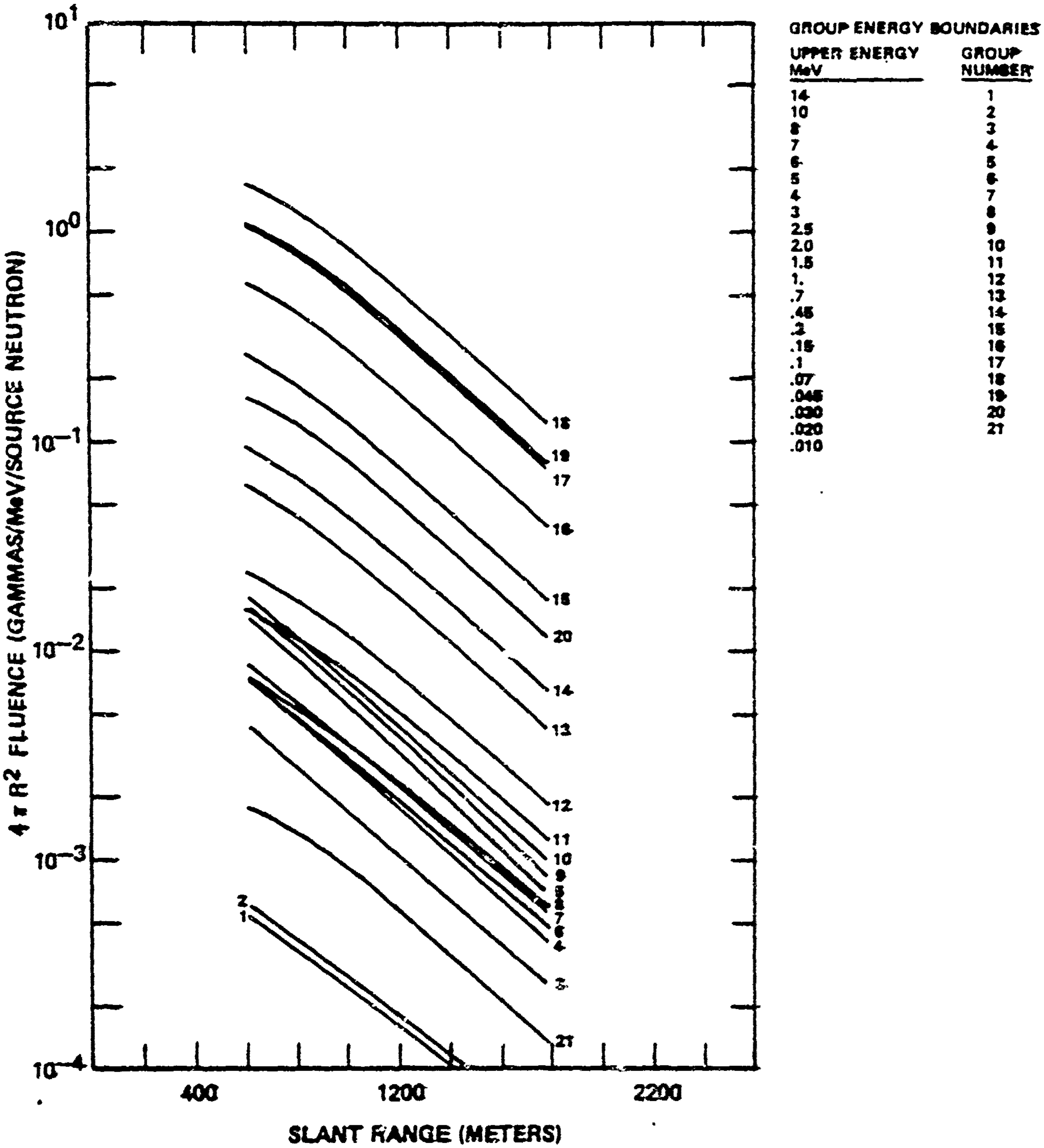

Figure 4. Free Field Secondary Gamma Ray Group Fluxes vs Range.

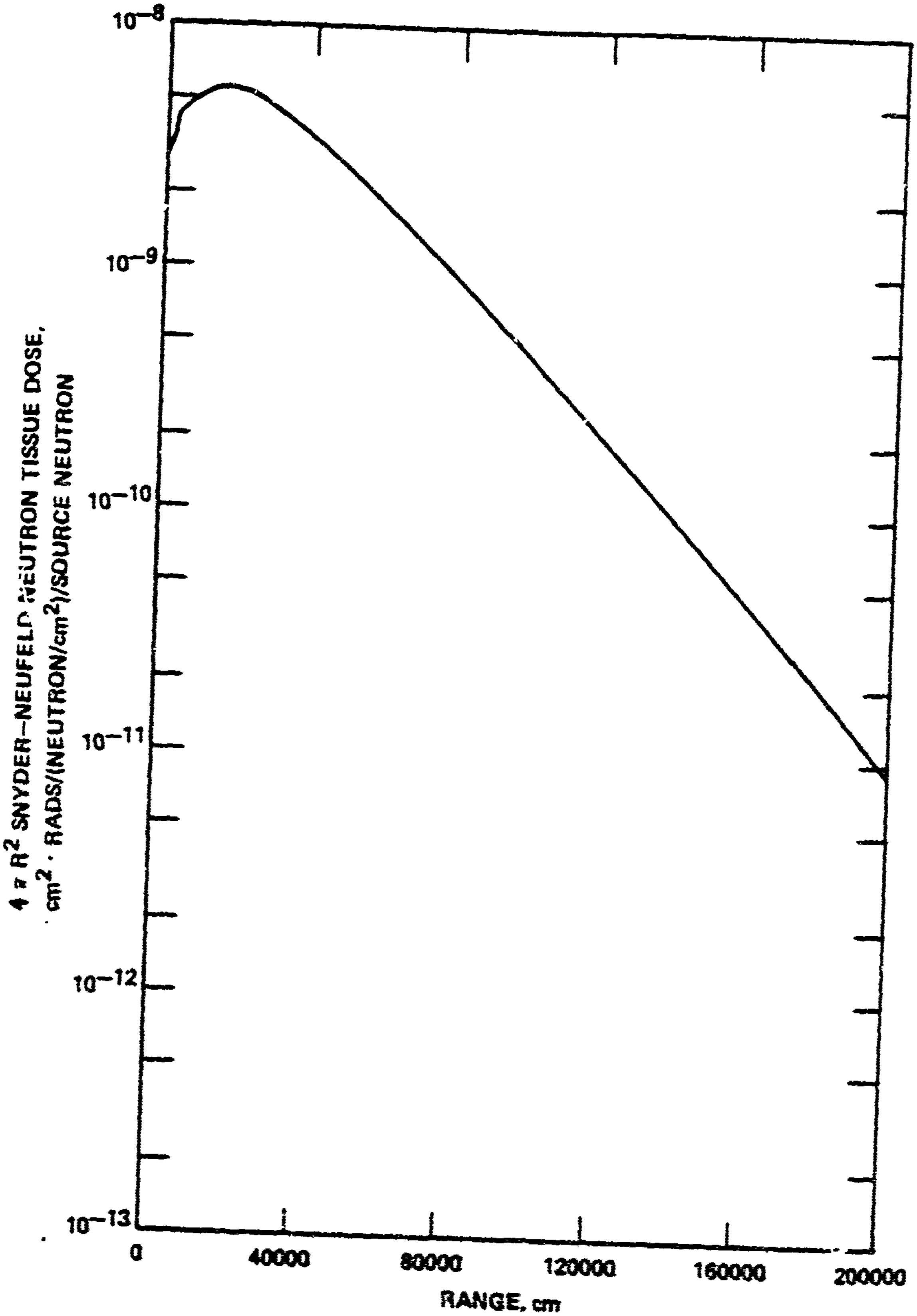

Figure 5a. Synder Neufeld Tissue Dose vs Range.

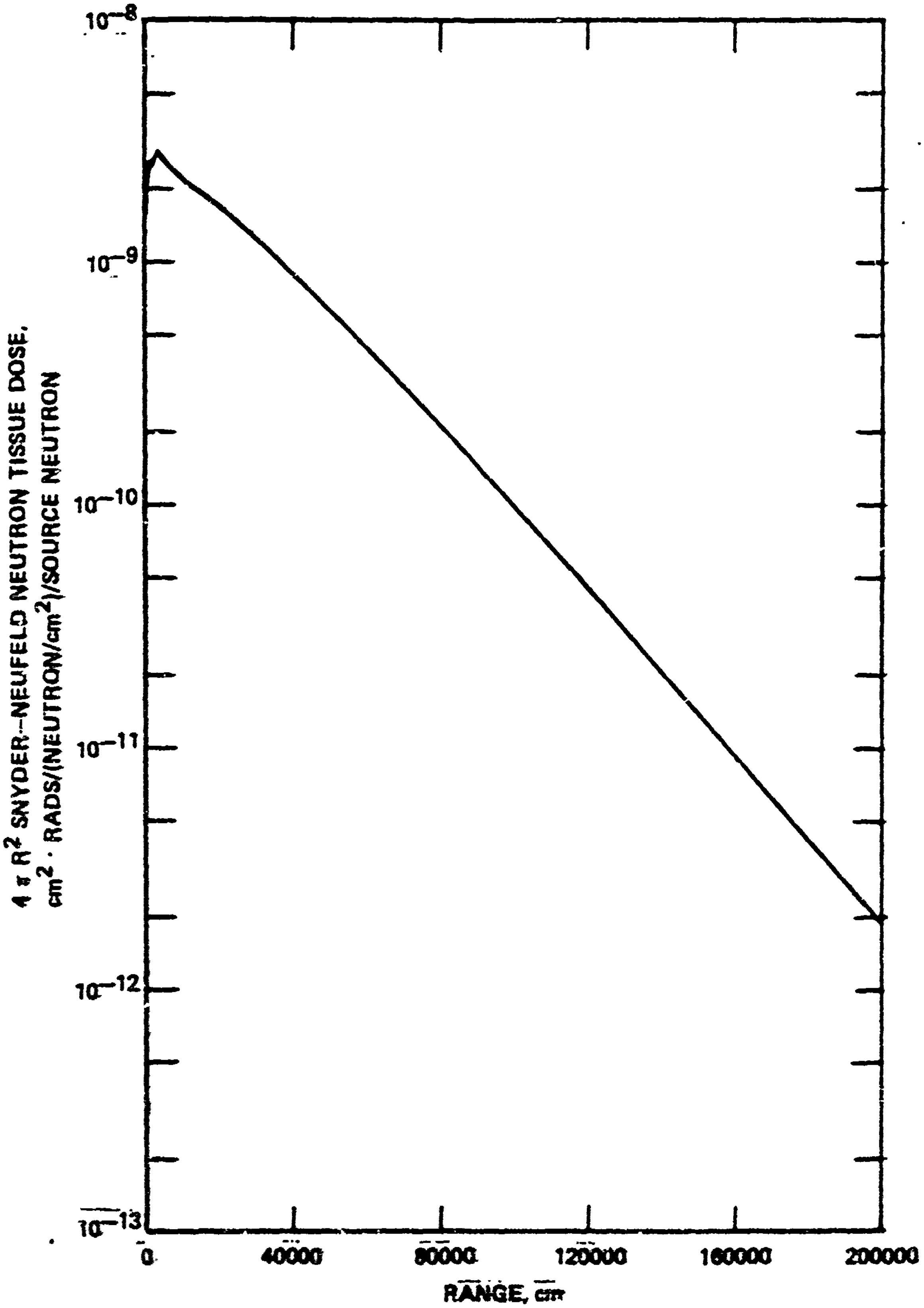

Figure 5b. First Angular Moment of Snyder Neufeld Tissue Dose vs Range.

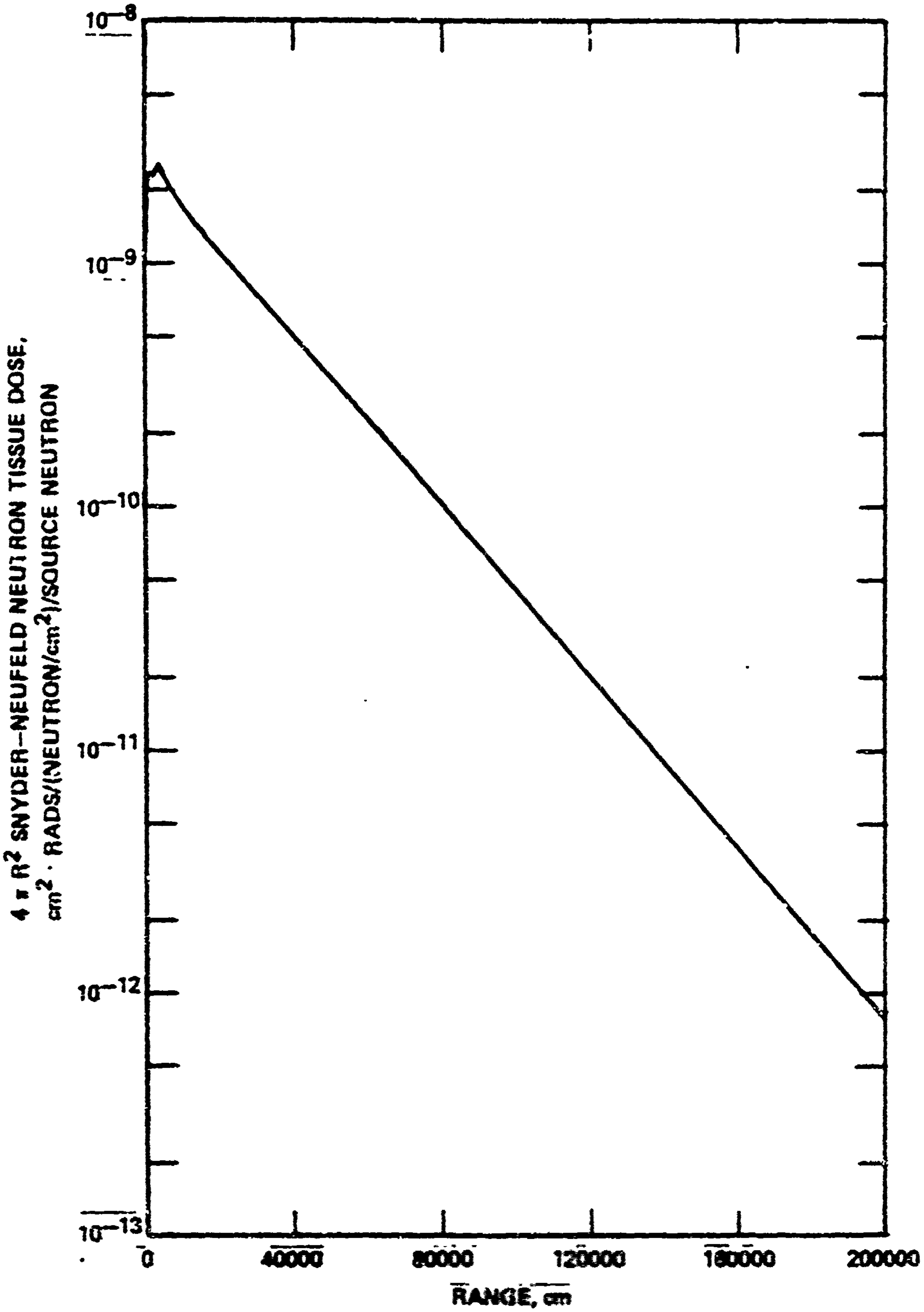

Figure 5c. Second Angular Moment of Snyder Neufeld Tissue Dose vs Range.

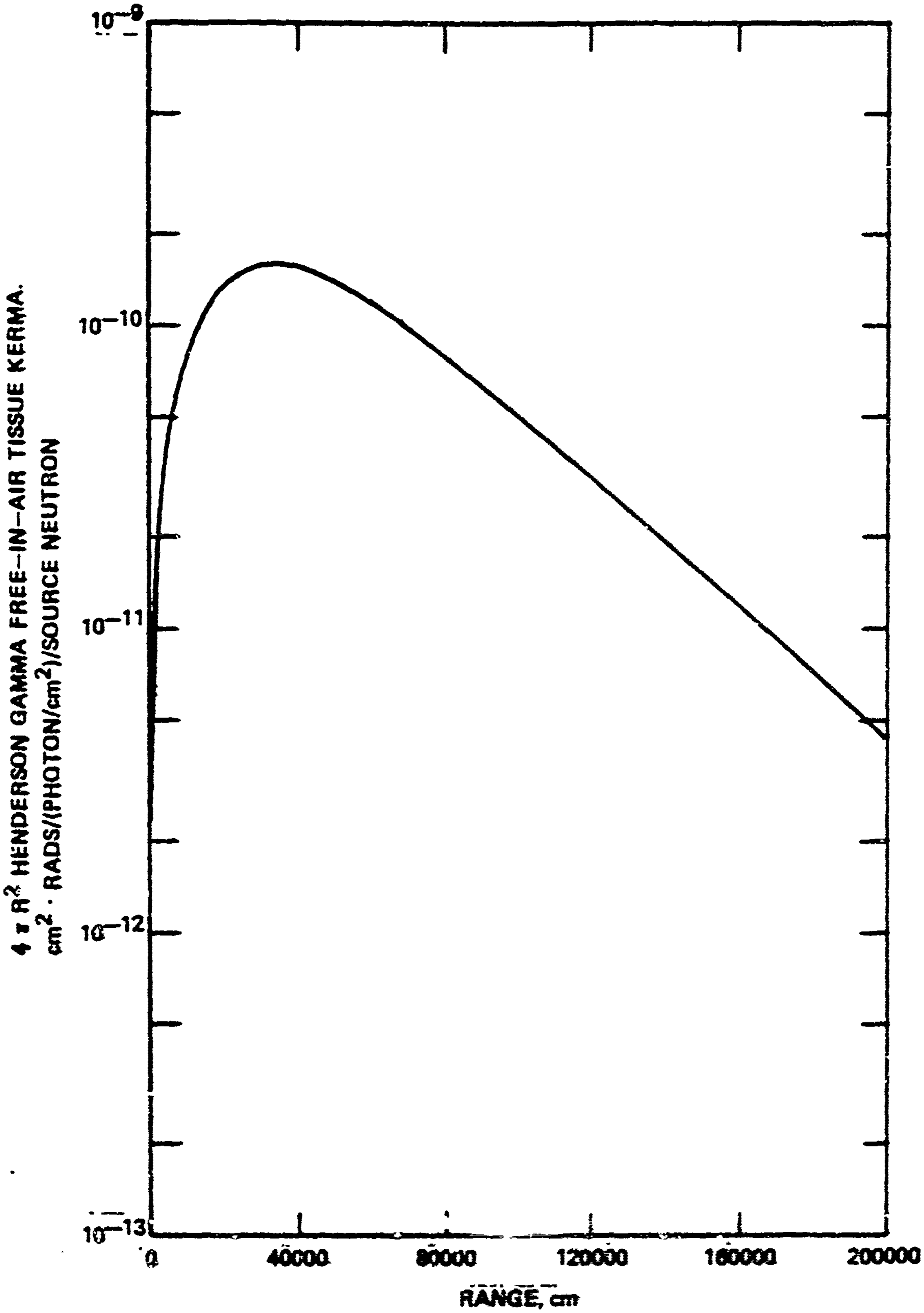

Figure 6a. Henderson Tissue Gamma Ray Dose vs Range in Air.

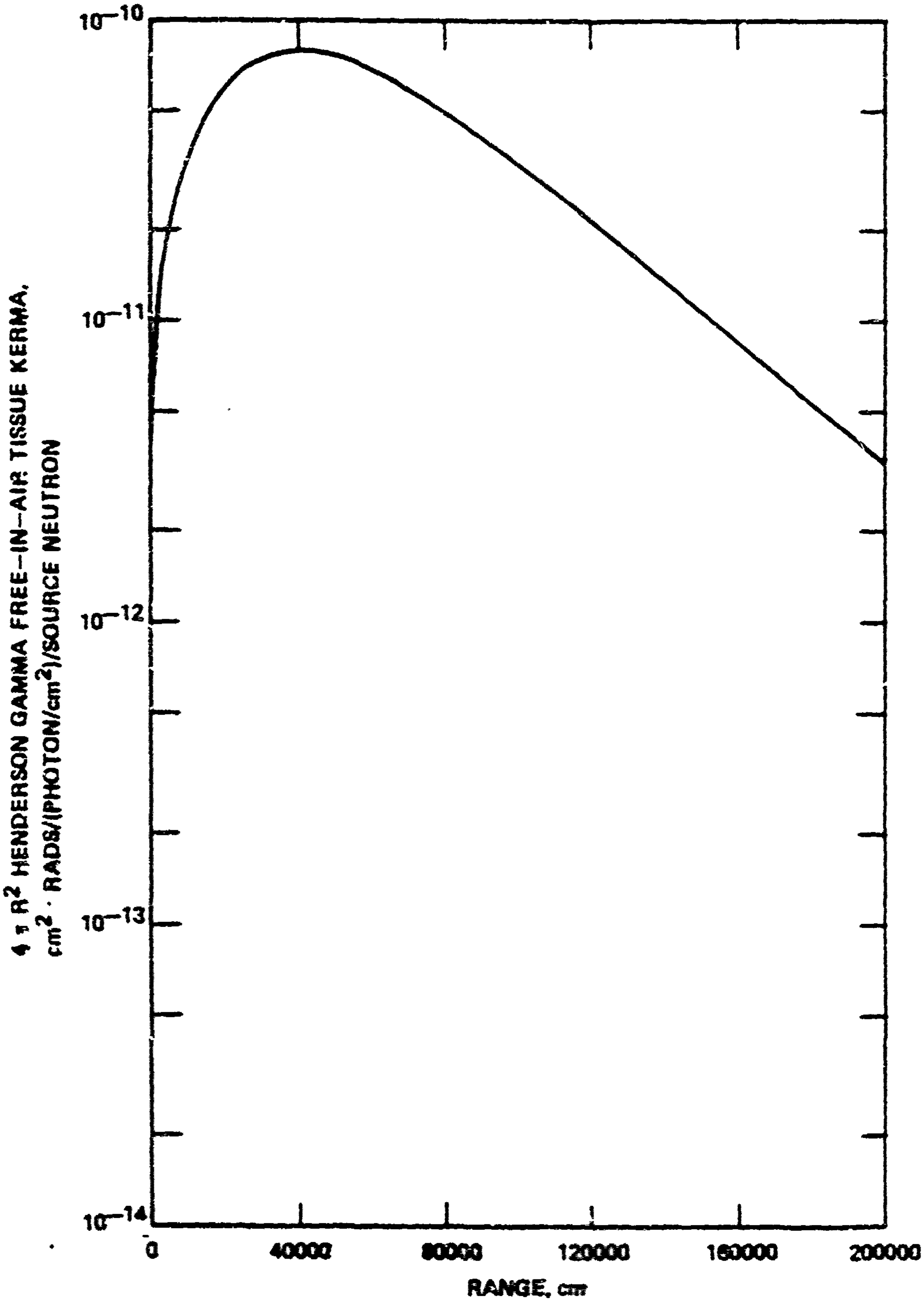

Figure 6b. First Angular Moment of Henderson Tissue Gamma Ray Dose vs Range.

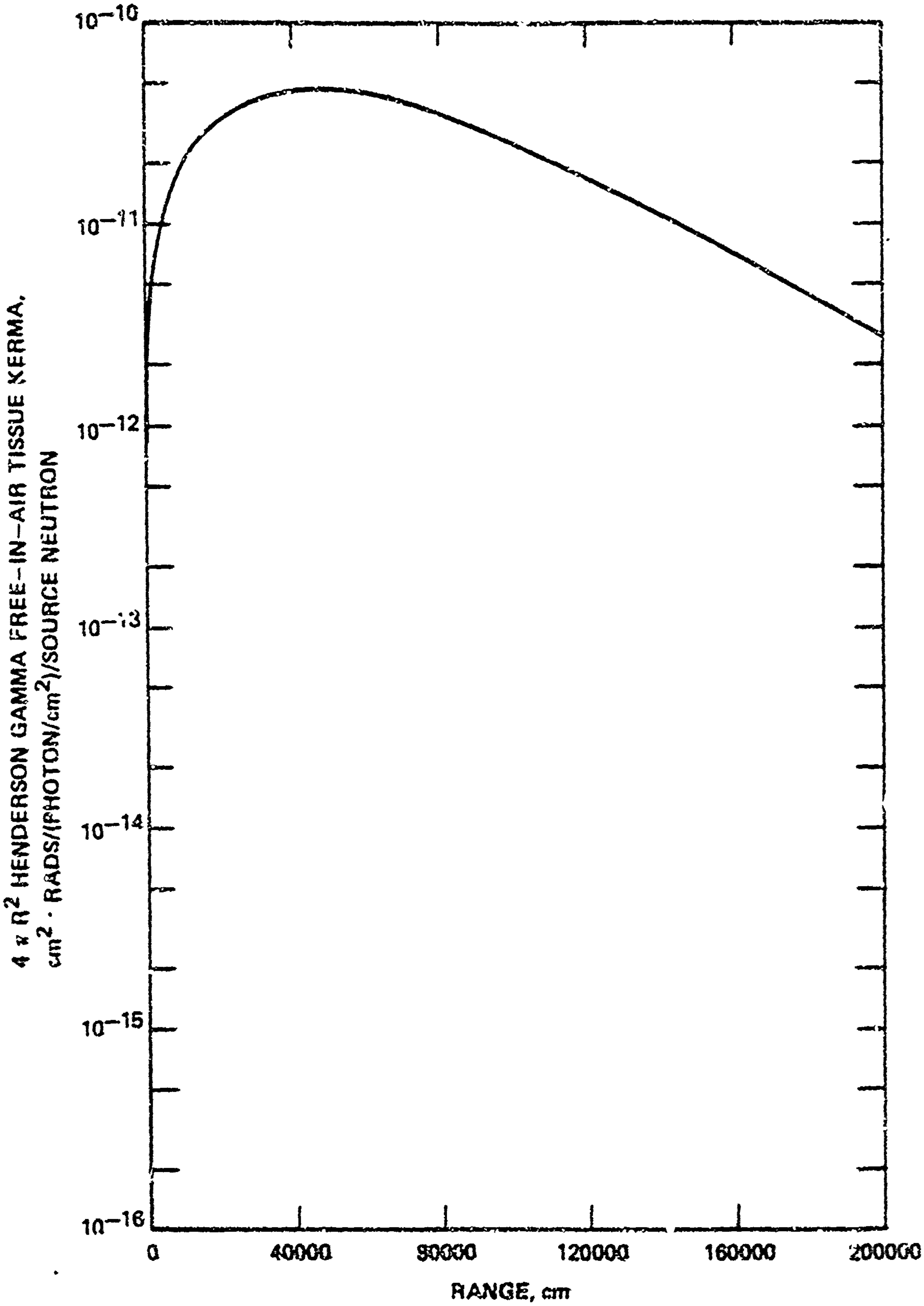

Figure 6c. Second Angular Moment of Henderson Tissue Gamma Ray Dose vs Range.

5. FREE FIELD ENVIRONMENT – DELAYED

BACKGROUND

The delayed radiation environment consists of neutrons and gamma rays emitted by the fission products from a nuclear weapon burst. The distinction between delayed radiation and fallout radiation is that delayed radiation is that radiation received while the fission products are contained in the fireball. Delayed radiation is defined to be part of the initial radiation environment which includes all radiation received during the first minute after the weapon burst. Even for yields on the order of 10 MT, 95% of the delayed radiation dose is received within 30 seconds from the weapon detonation.

In the past, the prediction of delayed radiation environments has been a less than satisfactory situation. The problem is a complex one, complicated by the fact that the radiation source is contained in a rising and expanding fireball and the transport of radiation is occurring in an atmosphere whose density distribution is changing due to the expanding shock front. For multiple bursts the problem is further complicated by interacting shock fronts and the possibility of interacting fireballs and is not well understood. Although, in principle, the problem could be solved using radiation hydrodynamics codes, the physical size of the problem precludes this as a practical means to a solution. Historically, empirical models based on test data have been developed and applied to the prediction of the delayed environments. Unfortunately, sufficient data are not available to construct an empirical model for the range of yields, burst heights, and weapon types of interest. More recently the problem

has been approached by phenomenology modeling as exemplified by the computer code, NUIDEA[6].

THE NUIDEA CODE

The development of the NUIDEA Code was sponsored by the Defense Nuclear Agency (DNA). The documentation and code should be available to users in the defense community in the near future.

The NUIDEA Code was developed as a systems-like code for the investigation of nuclear weapon environments from single or multiple bursts. The code includes phenomenology models of nuclear radiation, blast, and thermal radiation. The code incorporates portions of the Air Transport of Radiation (ATR)[7] Code and the Low Altitude Multiple Burst (LAMB)[8] Code.

5.1 CALCULATIONS

A matrix of calculations were performed using the NUIDEA Code for weapon yields from 1 KT to 10 MT and for three burst heights in meters, 1 meter, 60 $W^{1/3}$ m, and 225 $W^{1/3}$ m (where W is the yield in kilotons). The scaled burst heights were selected as those burst heights which preclude fallout and optimize blast effects (>10 psi), respectively. Several components of the delayed radiation environment were tabulated including tissue dose for delayed gamma rays, delayed neutrons, and secondary gamma rays from delayed neutrons. The prompt radiation dose, blast overpressure, and thermal exposure are also provided by the NUIDEA Code and have been tabulated as well. For each weapon yield considered, the fission yield was assumed to be 80% of the total yield. The ground elevations for these cases was 380 meters.

5.2 RESULTS

5.2.1 Radiation Environments

Figures 7, 8, and 9 show the radiation environments at 1500 m ground range versus yield for the three burst heights,

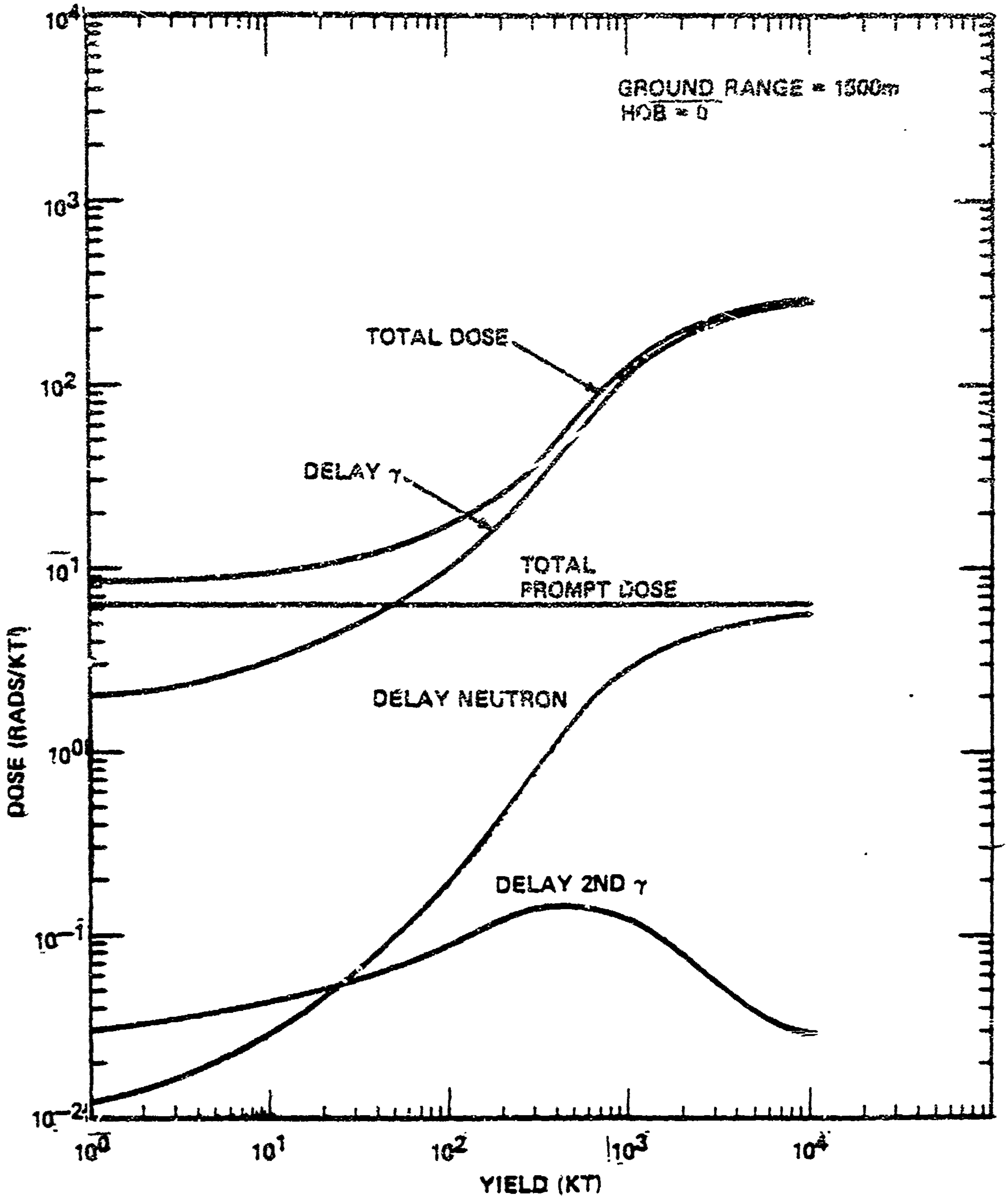

Figure 7. Radiation Dose Components vs Yield at 1500 M Ground Range for Ground Burst.

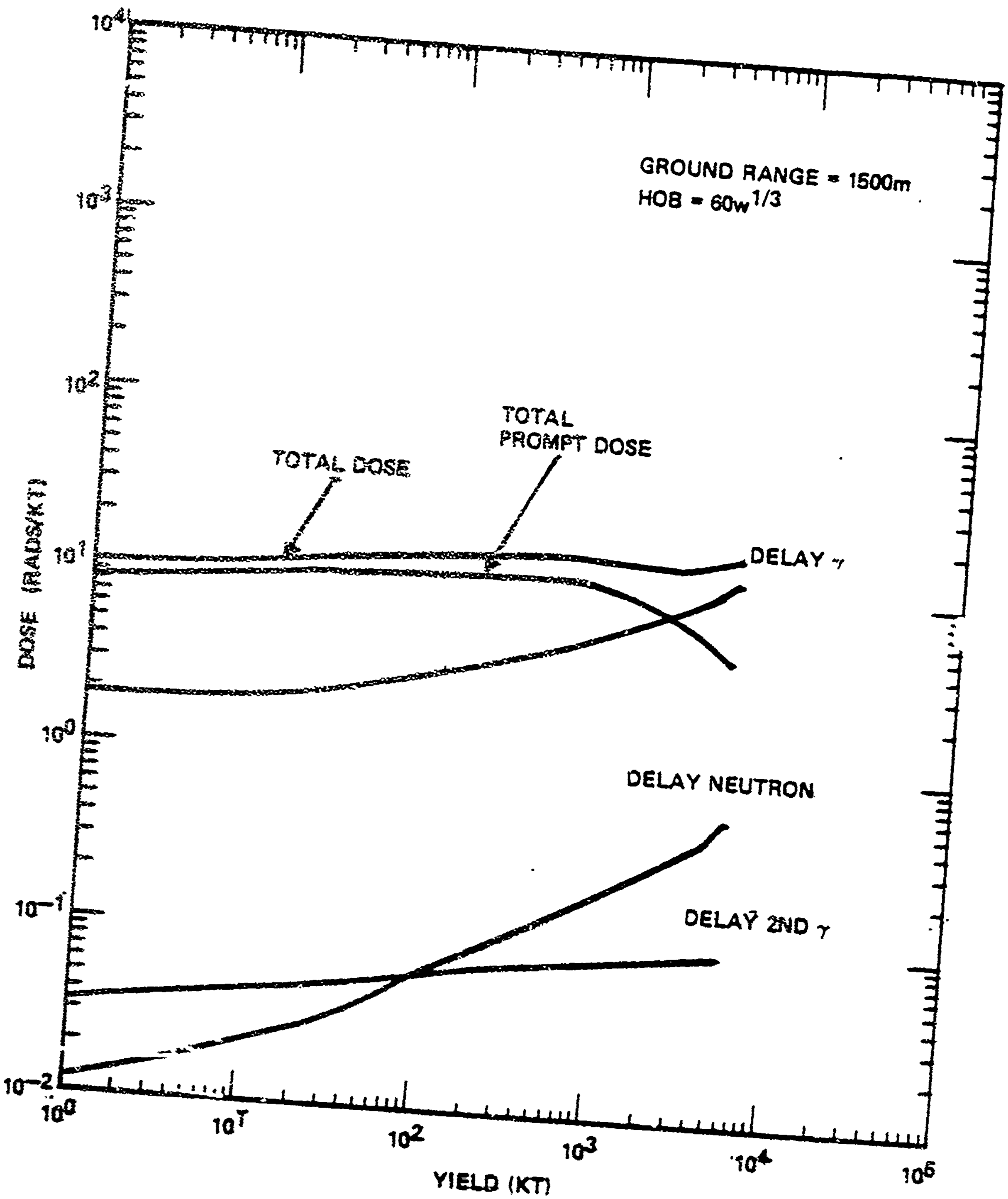

Figure 8. Radiation Dose Components vs Yield at 1500 M Ground Range for 60 W 1/3 Meter Burst Height.

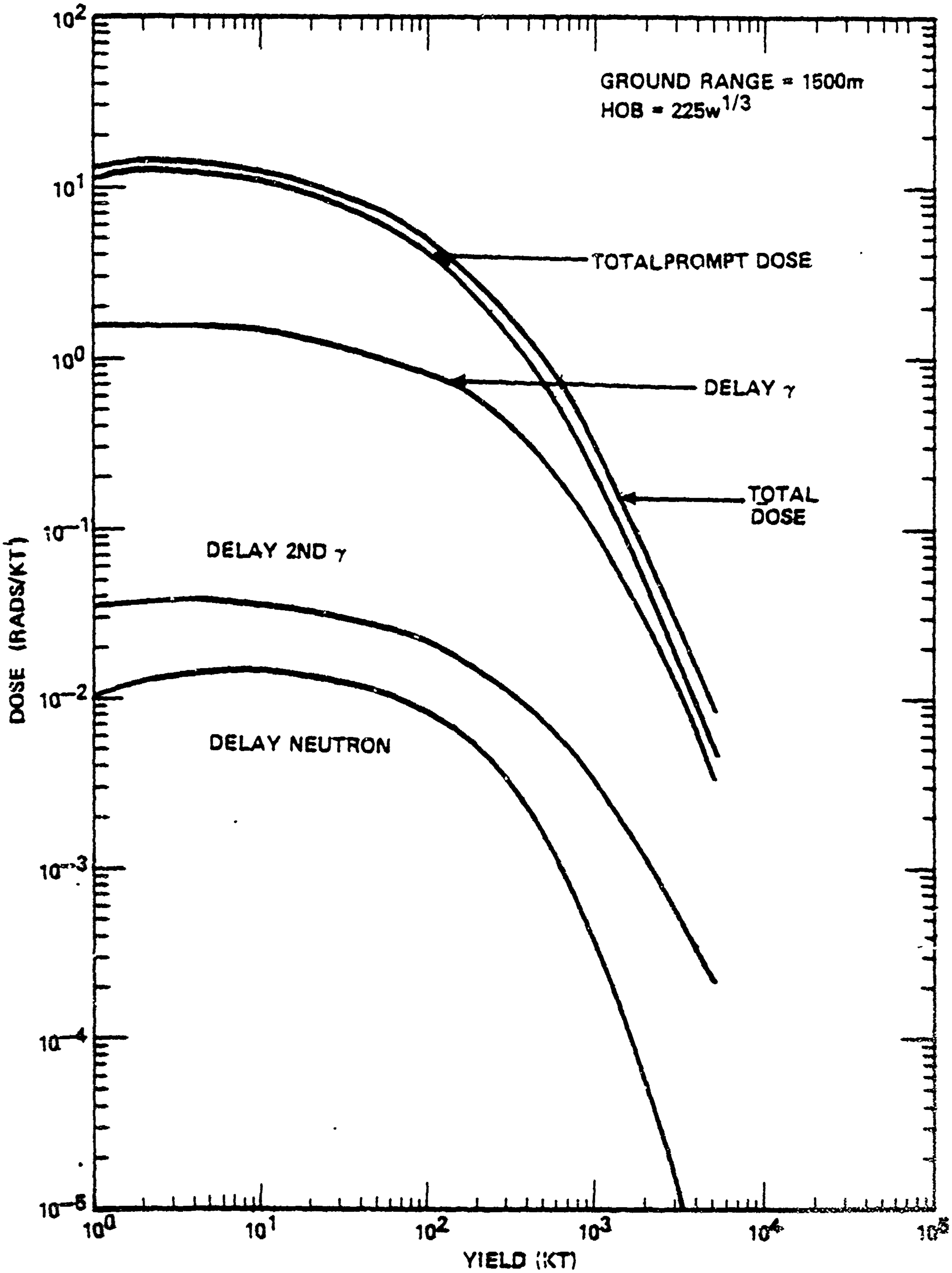

Figure 9. Radiation Dose Components vs Yield at 1500 M Ground Range for 225 M 1/3 Meter Burst Height.

respectively. The figures show all the components of the initial radiation dose including both prompt and delayed components. It is observed for the ground burst case that for yields greater than a few hundred kilotons the delayed gamma dose dominates the total dose. However, for the 60 $W^{1/3}$ case the delayed gamma dose exceeds the total prompt dose only for yields greater than 2 MT. For the 225 $W^{1/3}$ case, the prompt dose is always the predominate component of the total dose.

Figures 10, 11, and 12 show a similar set of curves for a ground range of 2500 meters. The same observations apply as in the 1500 meter ground range cases.

5.2.2 Blast Overpressure

Figure 13 shows the maximum overpressure from a 1 MT burst versus ground range for the three burst heights. The ground range for a given overpressure can be determined for other yields based on the standard cube root scaling laws

$$GR_1 = GR_0 \left(\frac{W_1}{W_0}\right)^{1/3}$$

where GR_1 is the ground range at yield W_1

GR_0 is the ground range at yield W_0 .

5.2.3 Thermal Exposure

Figures 14, 15, and 16 show the total thermal exposure versus ground range and weapon yield for the three respective burst heights.

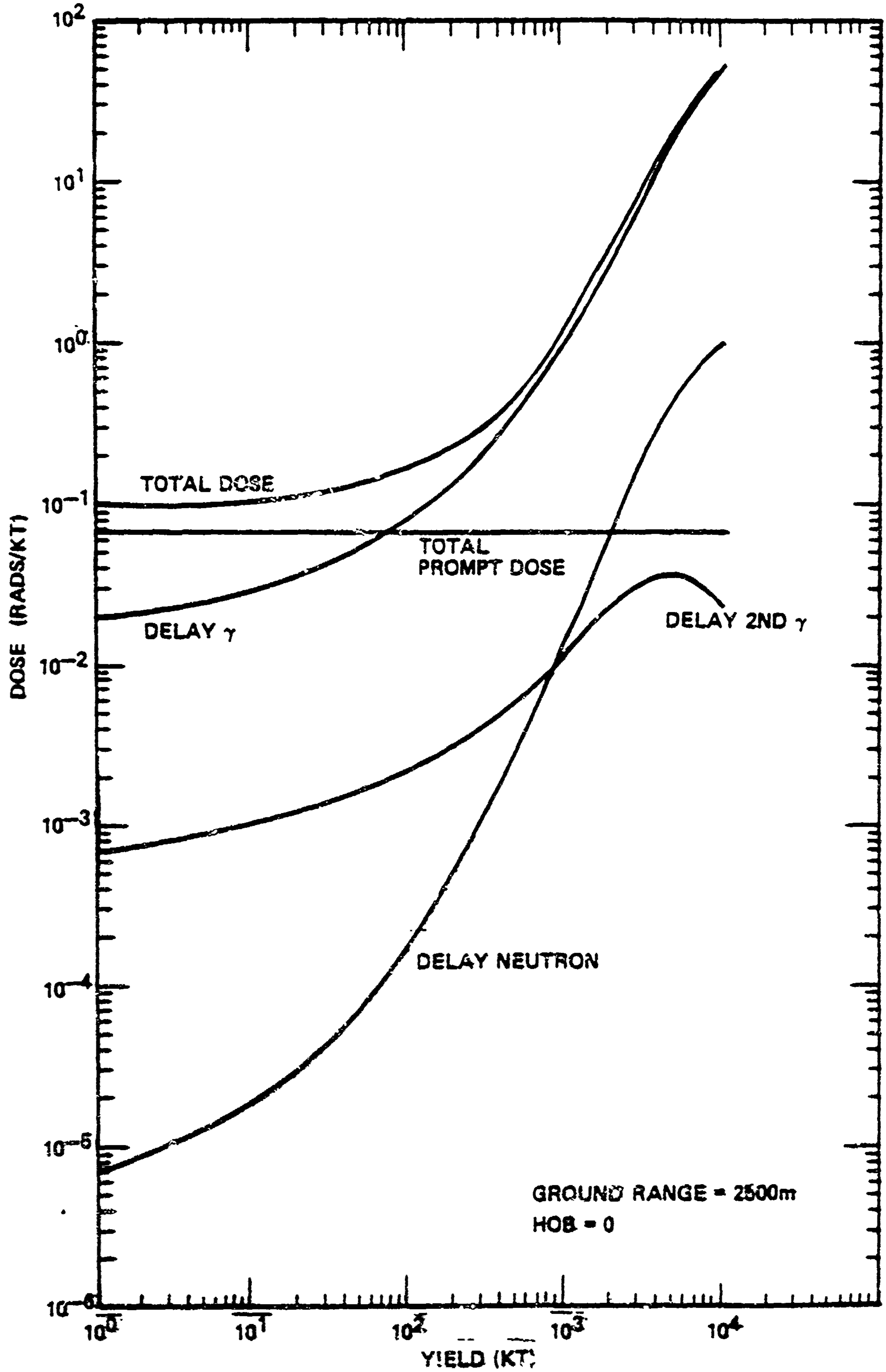

Figure 10. Radiation Dose Components vs Yield at 2500 M in Ground Range for Ground Burst.

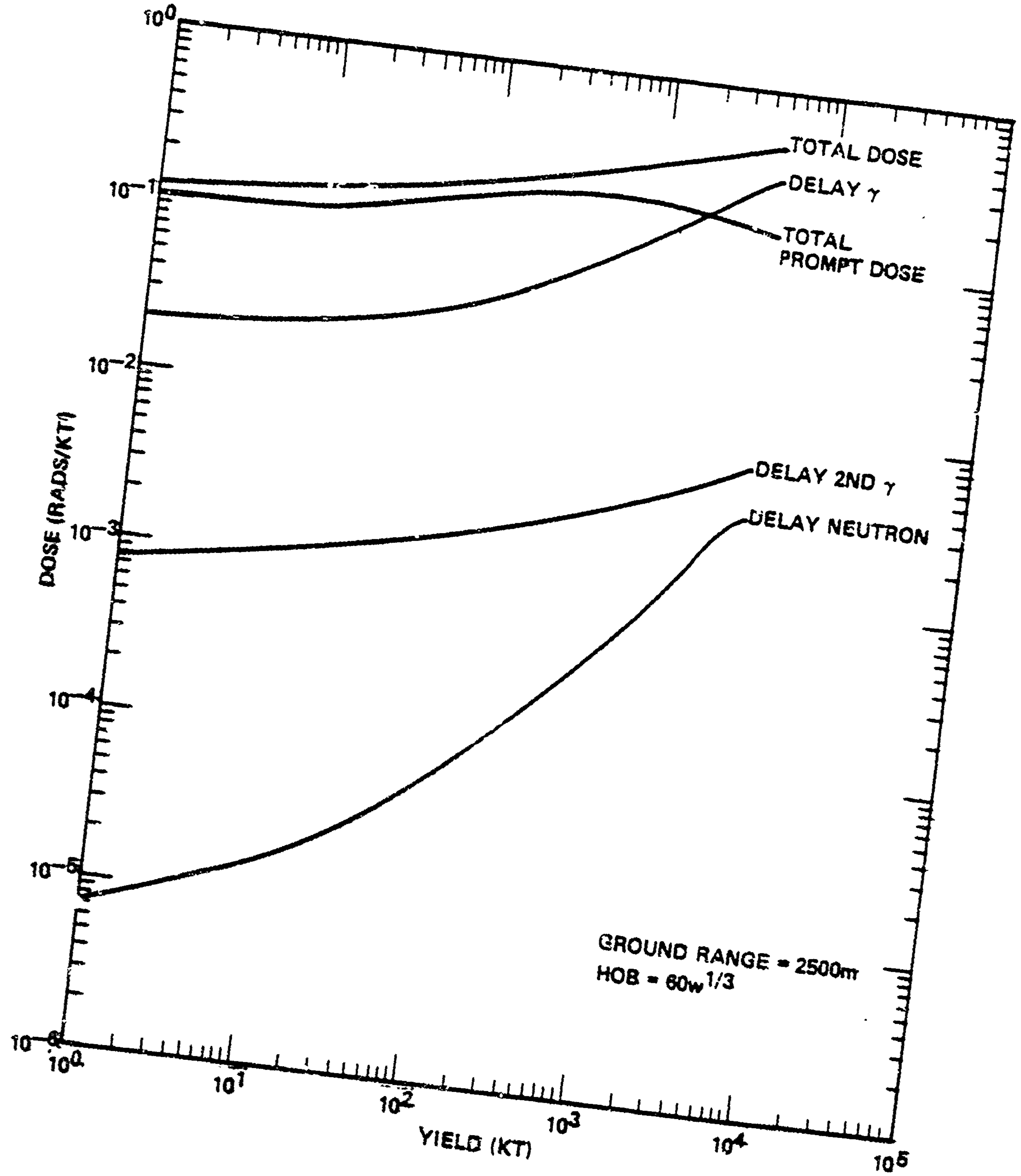

Figure 11. Radiation Dose Components vs Yield at 2500 M Ground Range for 60 W 1/3 Meter Burst Height.

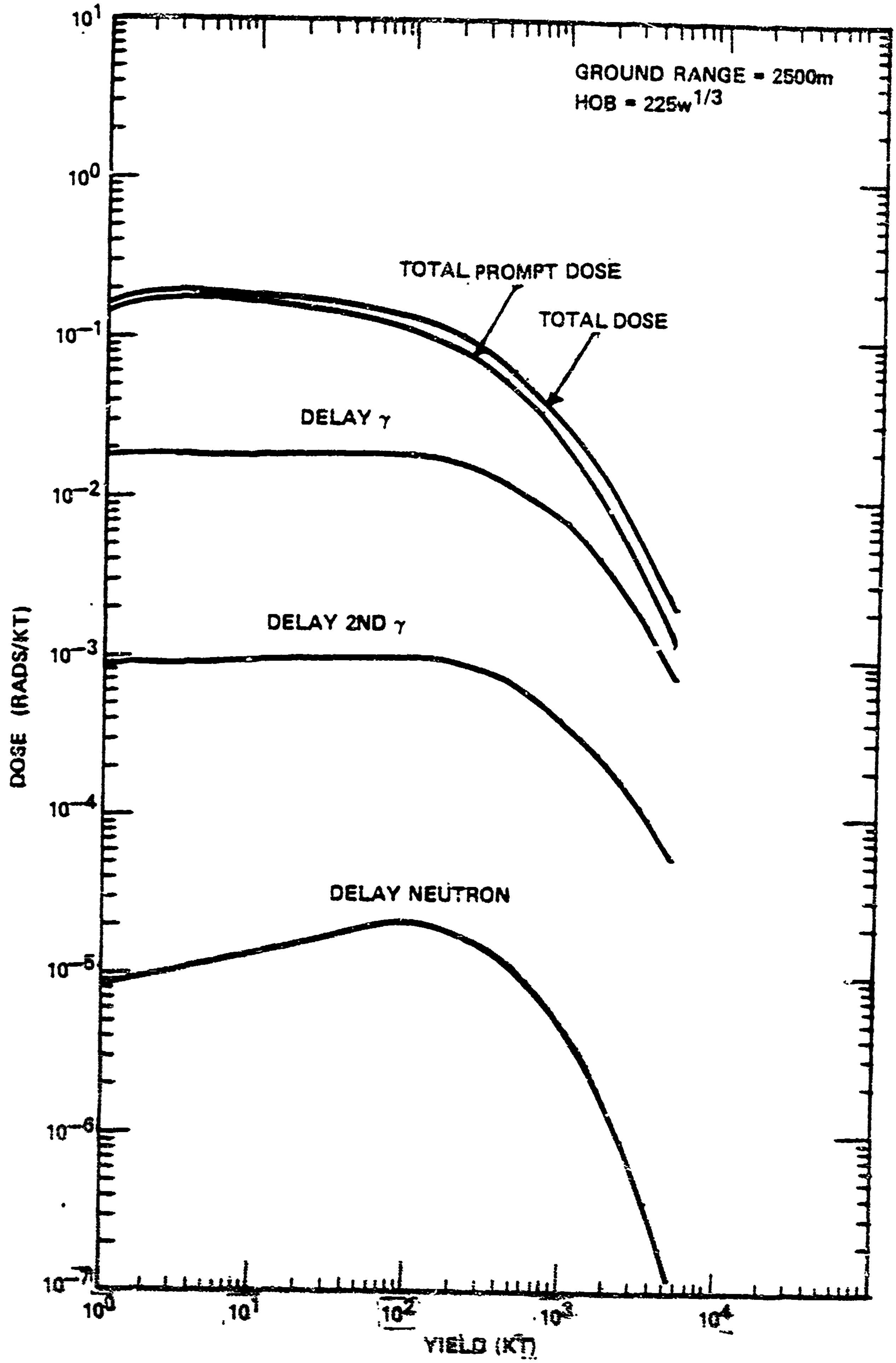

Figure 12. Radiation Dose Components vs Yield at 2500 M Ground Range for 225 W 1/3 Meter Burst Height.

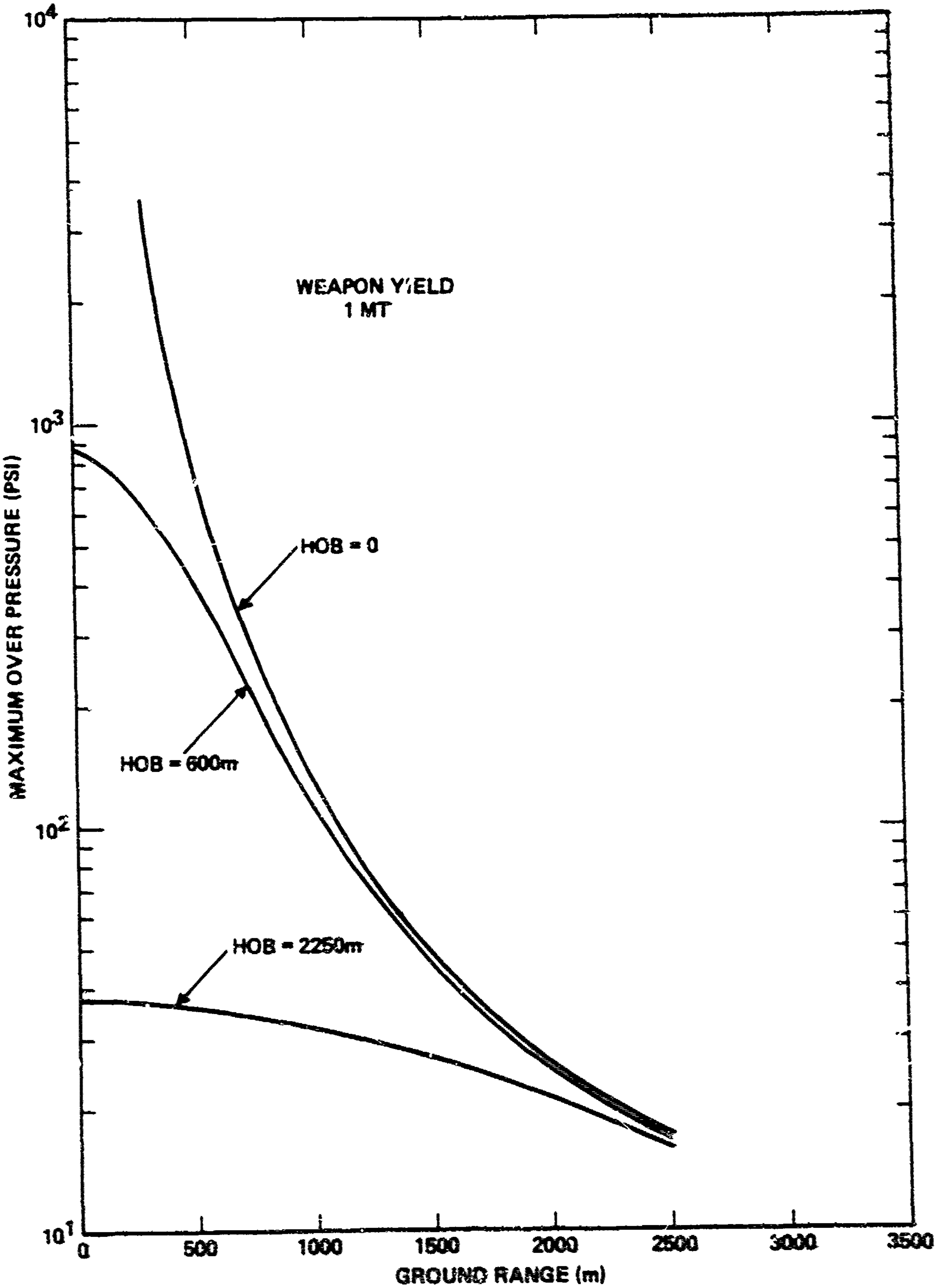

Figure 13. Maximum Overpressure vs Ground Range for 1 MT Burst.

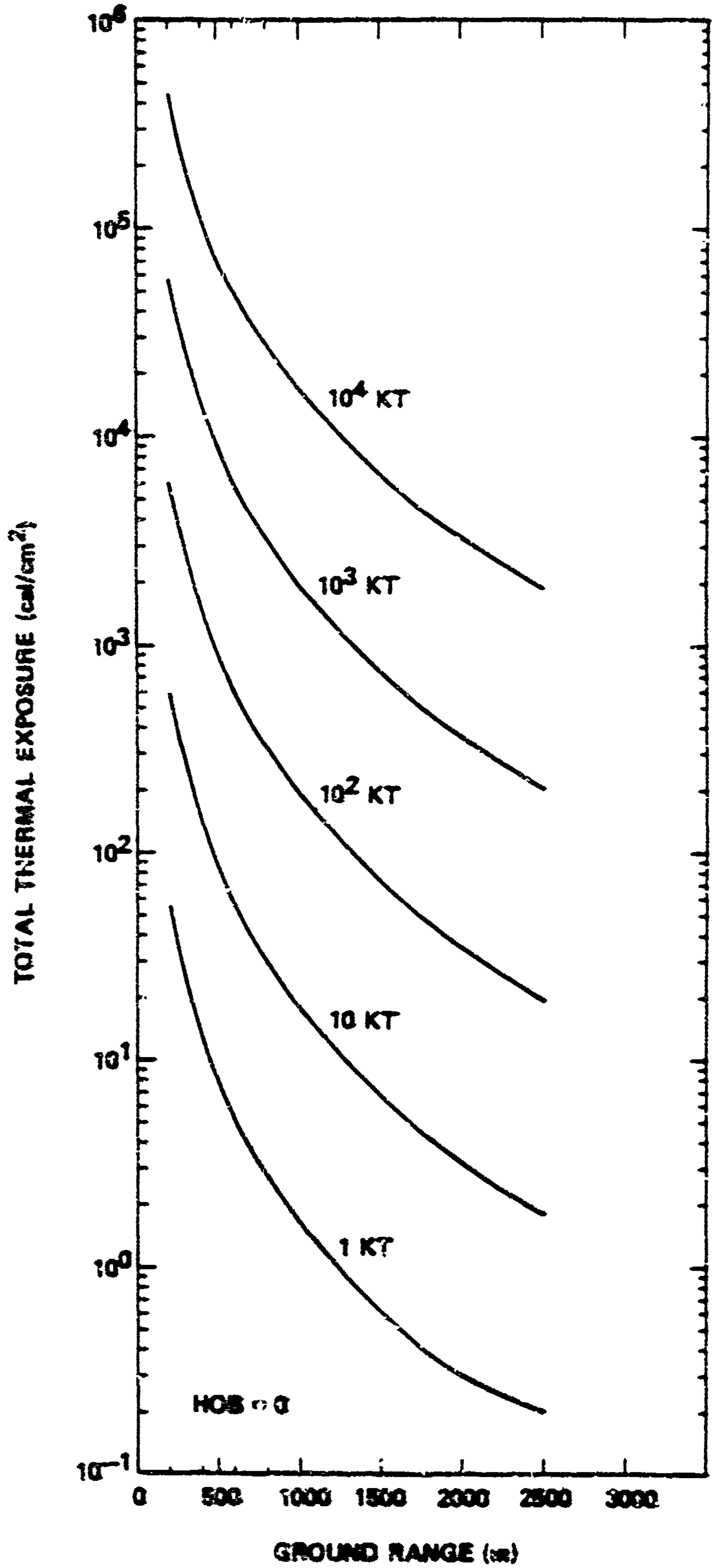

Figure 14. Thermal Exposure vs Ground Range and Yield for a Ground Burst.

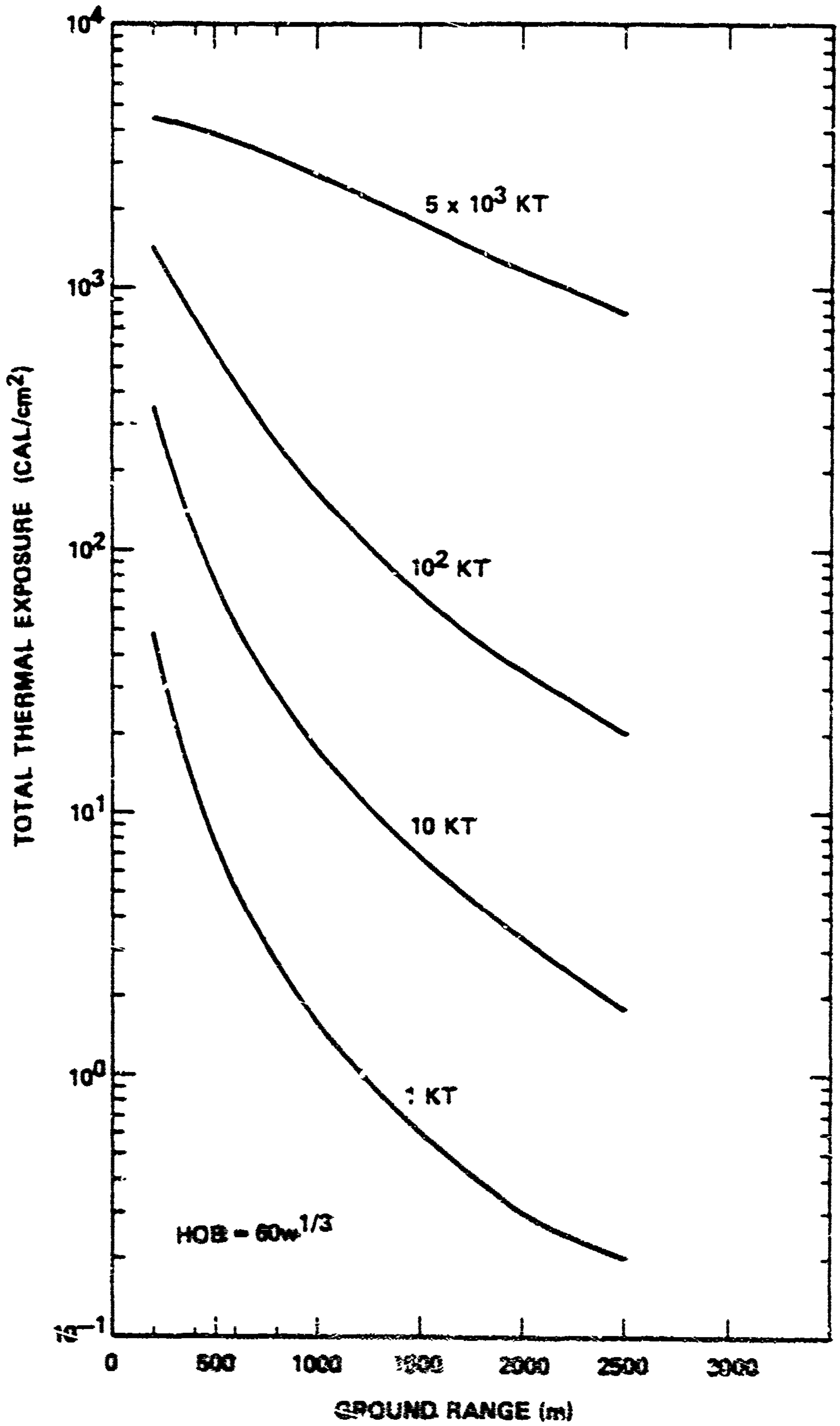

Figure 15. Thermal Exposure vs Ground Range and Yield for a 60 W 1/3 Meter Burst Height.

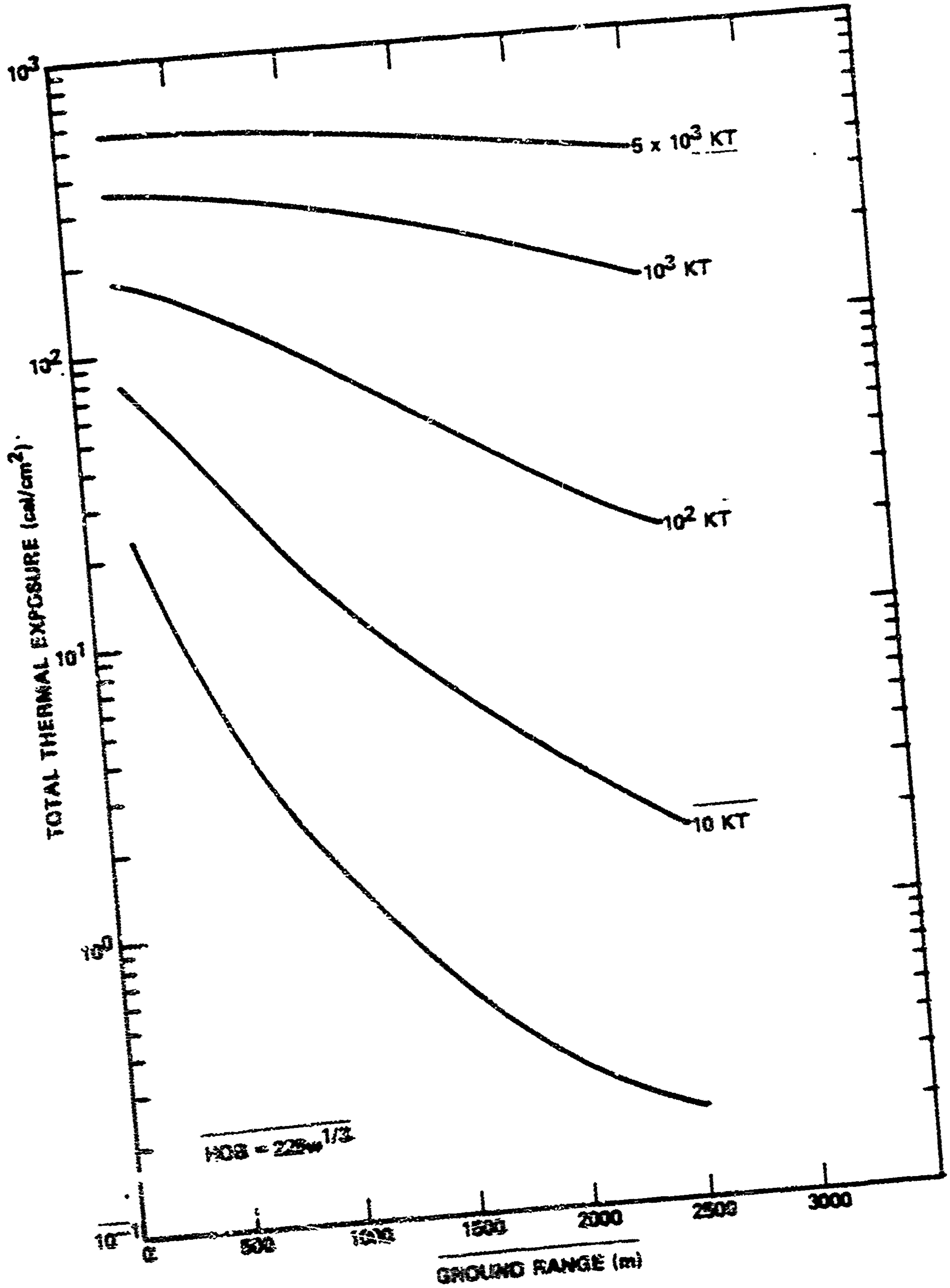

Figure 16. Thermal Exposure vs Ground Range and Yield for a 225 W 1/3 Meter Burst Height.

6. TRANSPORT THROUGH STRUCTURES

This chapter presents results of calculations of the transport of neutrons and gamma rays through structural materials. The transport of neutrons include the production of secondary gamma rays and their transport. Results for three types of calculations are presented

1. One-dimensional slab transport calculations,
2. Sensitivity calculations for transport through concrete, and
3. Ring source effects.

The structures considered in the calculations include

- Concrete slabs,
- Wood frame walls,
- Brick veneer walls,
- Shingle roofs, and
- Built up, asphalt roofs.

Forward and adjoint one-dimensional transport calculations were performed using the ANISN[3] discrete ordinates code. The forward calculations used a source distribution determined directly from the free field calculations reported in Chapter 4. All calculations used cross sections from the DNA few group library.

6.1 TRANSPORT THROUGH CONCRETE

6.1.1 Concrete Compositions

Concrete does not uniquely specify an elemental composition in the sense required for radiation transport analysis.

Variations in moisture content, regional variations in the constituents of concrete, and the basic type of concrete all will effect the shielding properties. Our approach, therefore, was to select several basic types of concrete for analysis and to account for variations within a particular type by perturbation methods.

The elemental composition for several important types of concrete are listed in Table 5.

6.1.2 Source and Response Functions

The source used for the forward one-dimensional slab transport calculations was a "shell source" taken directly from the air transport calculations reported in Chapter 4. The ANISN Code provides the capability of coupling calculations in this manner. The assumptions made in coupling the calculations in this manner is (1) the flux incident on the slab is not perturbed by the presence of the slab and (2) the radius of the coupling surface is sufficiently large and lateral transport sufficiently limited that the switch from spherical to slab geometry is appropriate.

The response function which was also used as the source distribution for the adjoint calculations was the Snyder Neufeld neutron response and the Henderson Tissue gamma ray response function (refer back to Chapter 4, Section 4.1.3 and Tables 2 and 3).

6.1.3 Forward Transport Results

The total dose transmission as a function of areal mass is plotted in Figure 17 for the seven types of concrete listed in Table 4. Figure 18 shows the ratio of the neutron dose to the gamma ray dose as a function of areal mass. Both the transmission and the n/γ ratio can be seen to vary substantially with concrete type even at the same areal mass.

Table 5. Concrete Compositions.

Element	Ordinary Type O3	Ordinary Type O4	Magnetite Type M	Magnetic and Steel Punchings Type MS2	Limonite and Steel Punchings Type LS	Serpentine Type S	Type TSF*
	Atomic Density, $\frac{\text{atoms}}{\text{barn}\cdot\text{cm}}$						
H	1.195(-2)	7.768(-3)	6.573(-3)	6.573(-3)	1.852(-2)	2.091(-2)	8.96(-3)
O	4.201(-2)	4.047(-2)	4.397(-2)	2.402(-2)	2.665(-2)	4.239(-2)	3.743(-2)
Si	7.333(-3)	1.580(-2)	1.951(-3)	1.565(-3)	1.437(-3)	9.863(-3)	1.79(-3)
Ca	8.746(-3)	2.915(-3)	3.772(-3)	3.877(-3)	3.922(-3)	2.254(-3)	1.192(-2)
C	5.917(-3)					1.003(-4)	2.13(-2)
Na		1.048(-3)				2.357(-4)	
Mg	1.412(-3)	1.486(-4)	8.173(-4)	4.210(-4)	1.734(-4)	7.355(-3)	
Al	1.898(-3)	2.389(-3)	1.833(-3)	1.072(-3)	6.474(-4)	9.376(-4)	
S	1.315(-4)	5.635(-5)	9.392(-5)				
K	6.162(-5)	6.932(-4)			6.162(-5)	1.386(-6)	
Fe	2.804(-4)	3.427(-4)	1.807(-2)	3.787(-2)	3.688(-2)	7.333(-4)	
Ti			2.414(-3)	9.305(-4)			
Cr			6.948(-5)			2.316(-5)	
V			1.300(-4)	3.546(-5)	4.729(-5)		
Mn			7.674(-5)				
Density gm/cm^3	2.39	2.35	2.53	4.64	4.54	2.1	2.31

*Tower Shielding Facility composition.

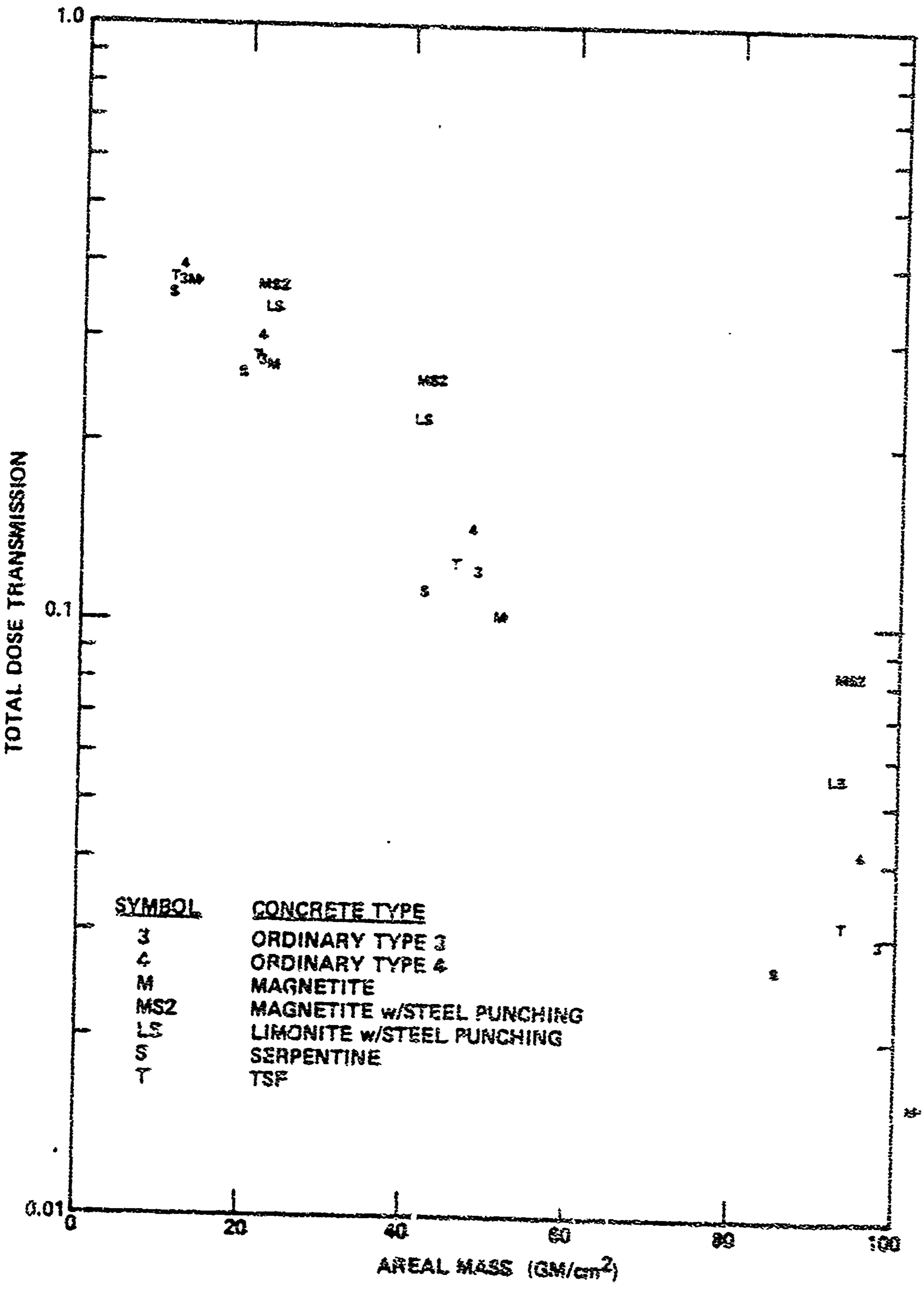

Figure 17. Transmission Factors through Various Concretes.

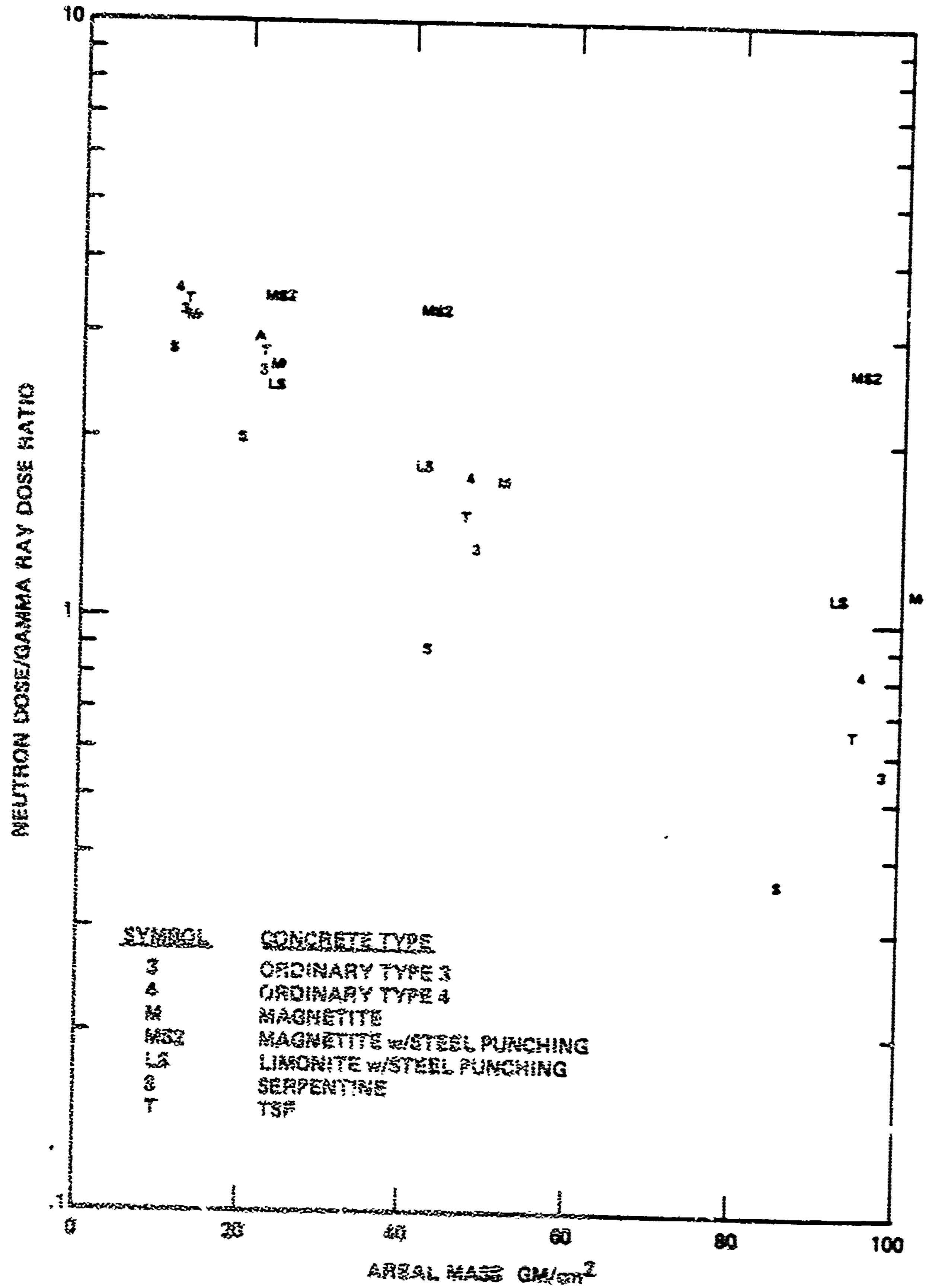

Figure 18. Transmitted Neutron Dose to Gamma Ray Dose Ratio through Various Concretes.

6.1.4 Perturbation Calculations

In order to investigate the sensitivity of the transmitted dose through concrete to the concrete composition, a series of perturbation calculations were performed using the SAIDOT Code[5]. The sensitivity calculation is based on the perturbation relationship

$$\frac{\Delta R}{R} = \frac{(\phi^{\dagger}, \Delta L\phi)}{R}$$

where
- R is the transmitted dose for a reference problem,
- ϕ is the flux for the reference problem,
- $\phi^{\dagger}$ is the adjoint flux for the reference problem,
- ΔL is the "perturbation" to the transport operator, and
- ΔR is the "perturbation" to the transmitted dose.

In the present calculations the perturbation to the transport operator, ΔL, has been considered to be a change in the concrete composition. By using the perturbation relationship and having calculated the forward and adjoint fluxes for a reference problem, the transmitted dose for any concrete composition can be estimated as long as the difference in the concrete composition is not too different from the composition of the reference problem. If we define the sensitivity function for a particular element to be

$$S_i \equiv (\phi^{\dagger}, \sigma_i \phi)$$

where σ_i is the microscopic cross section for element i,

then

$$R' = R + \Delta R = R\left[1 + \sum_{i=1}^{\#\,\text{elements}} (N_i' - N_i) S_i\right]$$

where
- N_i is the atomic density of element i in the reference concrete and
- N_i' is the atomic density of element i in the "perturbed" case.

Table 6 gives the sensitivity function S_i as a function of concrete thickness using type TSF concrete as a reference case.

The range of applicability for the perturbation can be tested by using the perturbation results to predict the transmission factors for the concrete compositions listed in Table 5 and comparing with the transport results. Table 7 shows the fractional error of the perturbation theory prediction when compared with the transport (ANISN) results. Using TSF concrete as a base case, perturbation theory can be seen to accurately predict the transmitted dose for ordinary concrete Type 03 and Type 04, as well as for Serpentine concrete. However, perturbation theory does not give an accurate prediction for the Magnetite concrete, and Limonite with steel punchings. Perturbation theory fails for these cases because the iron loading for these concretes is so high. However, it appears that perturbations from TSF concrete can be quite accurately predicted for concrete containing less than about 5 weight percent iron. In order to treat the more heavily iron loaded concretes with perturbation theory would require a reference fluxes for a more heavily loaded concrete. The results based on TSF concrete should be accurate for most concretes commonly encountered in the construction industry.

6.2 TRANSPORT THROUGH OTHER STRUCTURAL ELEMENTS

The transmission factors for other structural elements commonly found in the building industry have also been calculated. These structural elements include roof and wall constructions commonly found in residential homes. These include both wood and brick exterior walls, the shingle roof, and the built up asphalt and gravel roof. Figure 19 shows the materials and configuration of these structural elements. In order for these

Table 6. Sensitivity Functions for Various Elements in Concrete (Based on Type TSF Concrete).

	Sensitivity Function $(\frac{rad}{rad})$		
Element	12.14 gm/cm^2	46.94 gm/cm^2	93.88 gm/cm^2
H	-8.70	-17.9	-37.8
C	-3.92	-11.4	-21.6
O	-4.09	-12.4	-24.3
Na	-5.34	-14.9	-36.5
Mg	-4.33	-15.9	-34.3
Al	-3.68	-14.7	-33.9
Si	-3.88	-15.9	-36.4
S	-16.7	-67.8	-153.
K	-2.16	-10.8	-53.8
Ca	-4.43	-20.7	-52.6
Ti	0.497	27.1	0.049
V	-3.79	2.43	-55.1
Cr	-1.94	4.88	-20.6
Mn	0.179	55.1	-17.8
Fe	-4.03	-11.7	-56.8

Table 7. Error Analysis for Perturbation Results.

	Fractional Errors, $\frac{R_{Pert} - R_{Transport}}{R_{Transport}}$		
Concrete Type	5.80 cm	20.32 cm	40.64 cm
Ordinary Type 03	-0.0025	0.0081	0.010
Ordinary Type 04	-0.0075	-0.024	-0.060
Magnetite	0.035	0.46	0.39
Magnetite with Steel Punchings	0.071	0.77	-0.54
Liminite with Steel Punchings	0.046	1.13	-2.5
Serpentine	-0.010	-0.0031	-0.069
TSF	—	—	—

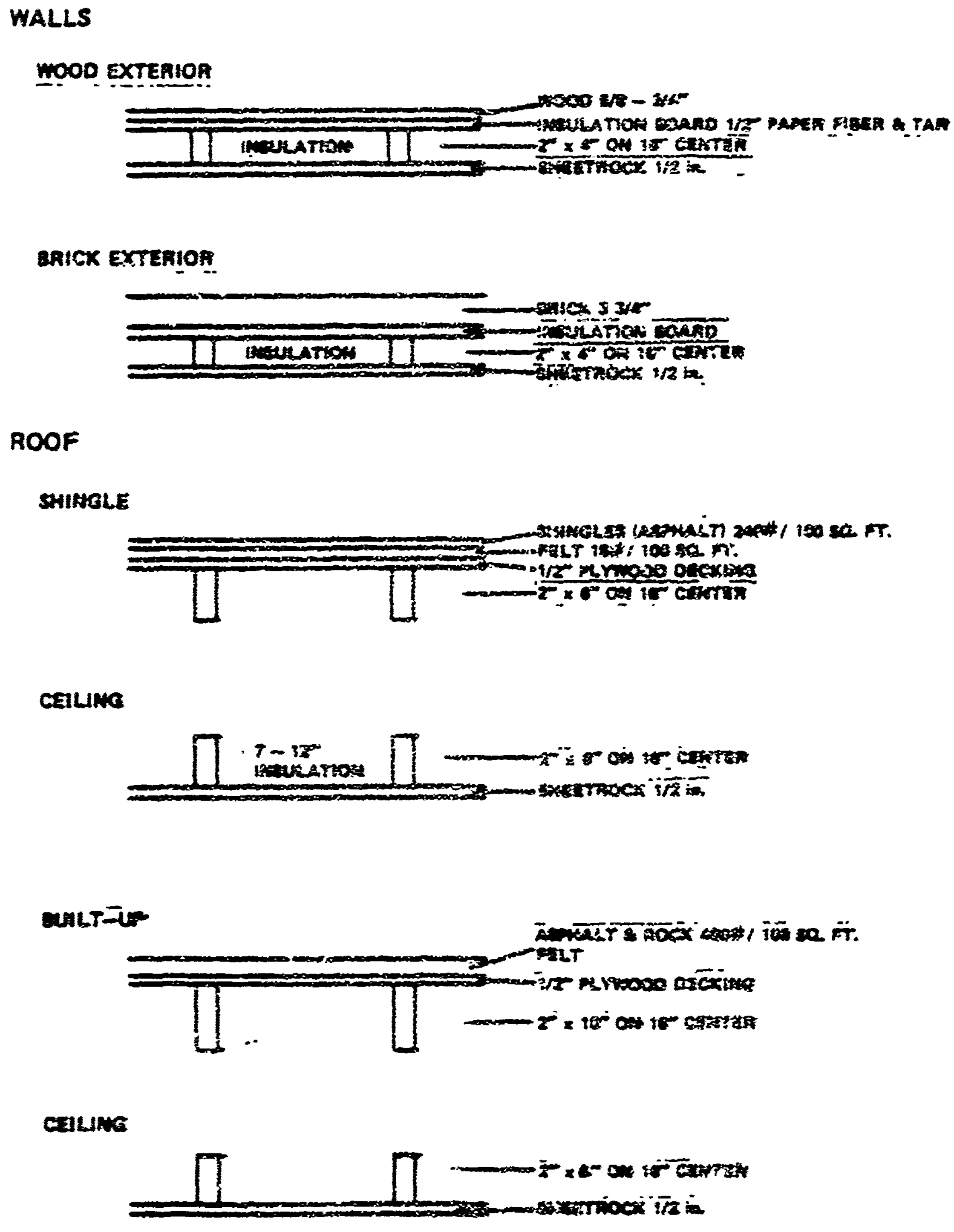

Figure 19. Configuration of Some Common Residential Home Structural Elements.

configurations to be amenable to one-dimensional transport analyses, the wood studs were approximated by a homogenous region of 1/8 the density of wood (the ratio 2:16). The results of the one-dimensional transport calculations for these configurations are summarized in Table 8.

6.3 RING SOURCE EFFECTS

The calculations reported in Sections 6.1 and 6.2 for dose transmission through concrete slabs and other building structural elements have been for a point source above an infinite slab. Since adjoint calculations were performed for the concrete slabs it is particularly convenient to fold these adjoint fluxes with the incident fluxes from other source configurations. The ring source is of particular interest since it has been the recommended source configuration for civil defense shielding analysis. The ring source results presented here are based on a rotation of the point source fluxes incident on the slab followed by a convolution with the slab response function.

6.3.1 Source Rotation and Lengendre Expansion

The problem is to calculate the flux on the axis of a ring source in air, given the flux from a point source in air. This can be determined by a straightforward rotation of coordinates. Let $[\phi]$ represent a vector whose elements are the flux moments for the point source,

$$[\phi] = \begin{bmatrix} \phi^0 \\ \phi^1 \\ \cdot \\ \cdot \\ \cdot \\ \phi^\ell \end{bmatrix} .$$

Table 8. Results of Walls and Roofs Calculation.

Configuration	Dose, $\frac{\text{rad}}{\text{source neutron}}$ Neutron	Gamma Ray	Total	Dose Transmission
Wall:				
Wood Exterior	3.68(-22)	1.46(-22)	5.14(-22)	0.37
Brick Exterior	2.46(-22)	1.01(-22)	3.48(-22)	0.25
Roof:				
Shingle	2.86(-22)	1.48(-22)	4.34(-22)	0.32
Built Up	2.28(-22)	1.50(-22)	3.78(-22)	0.28

where $$\phi^{\ell} \equiv \int_{-1}^{+1} \phi(\mu) P_{\ell}(\mu)\, d\mu \quad ,$$

μ = cosine of the angle measured from the line to the source

P_{ℓ} are the Legendre polynominals.

Also, let $[\tilde{\phi}]$ represent the corresponding Legendre expansion of the flux for the ring source, then

$$[\tilde{\phi}] = M[\phi]$$

where $$\tilde{\phi}^{\lambda} = M_{\lambda \ell}\, \phi^{\ell}$$

and

$$M_{\lambda \ell} = \sum_{\ell} \frac{2\ell+1}{2} \int_{-1}^{+1} P_{\lambda}(\mu)\, d\mu \int_{0}^{2\pi} P_{\ell}(\cos \tilde{\theta})\, d\tilde{\phi}$$

where $\tilde{\theta}$ and ϕ are illustrated below.

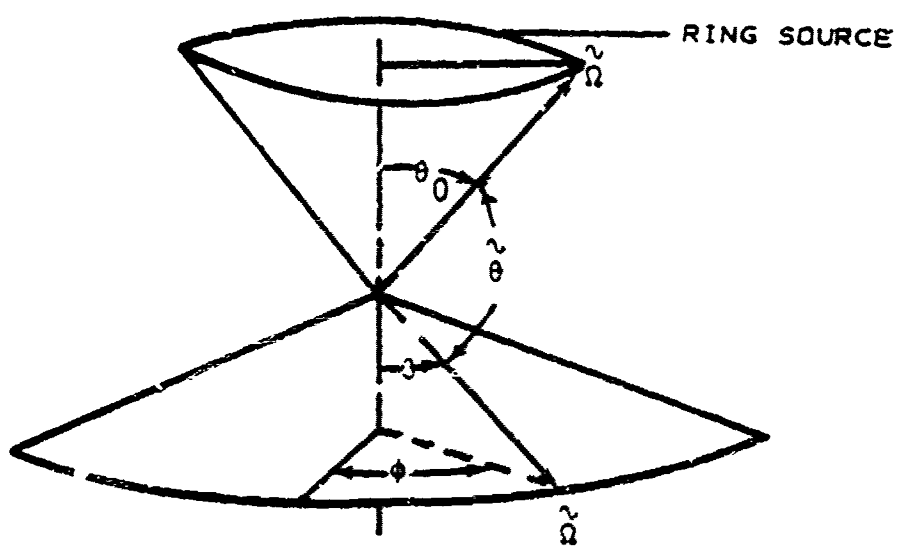

$\tilde{\theta}$ can be determined from θ_0, θ, and ϕ as follows.

$$\tilde{\mu} \equiv \cos \tilde{\theta}_0 \cos \theta + \sin \theta_0 \sin \theta \cos \phi \ .$$

6.3.2 Ring Source Results

The source rotation and folding with the adjoint flux was performed for three thicknesses of TSF concrete and for ring source delimation angles, θ_0, from 0 to 90° (0° corresponds to the point source). The ratio of the transmitted dose from the ring source to the transmitted dose from the point source are plotted in Figure 20 as a function of the cosine of the declination angle. In general, the transmitted dose decreases with increasing declination angle due to the effectively increased average path length through the slab. It is interesting to note, however, that for the thinner slabs, build up effects cause a small increase in the transmitted dose over the first few degrees of declination. These results used the infinite air angular fluxes at 1200 m.

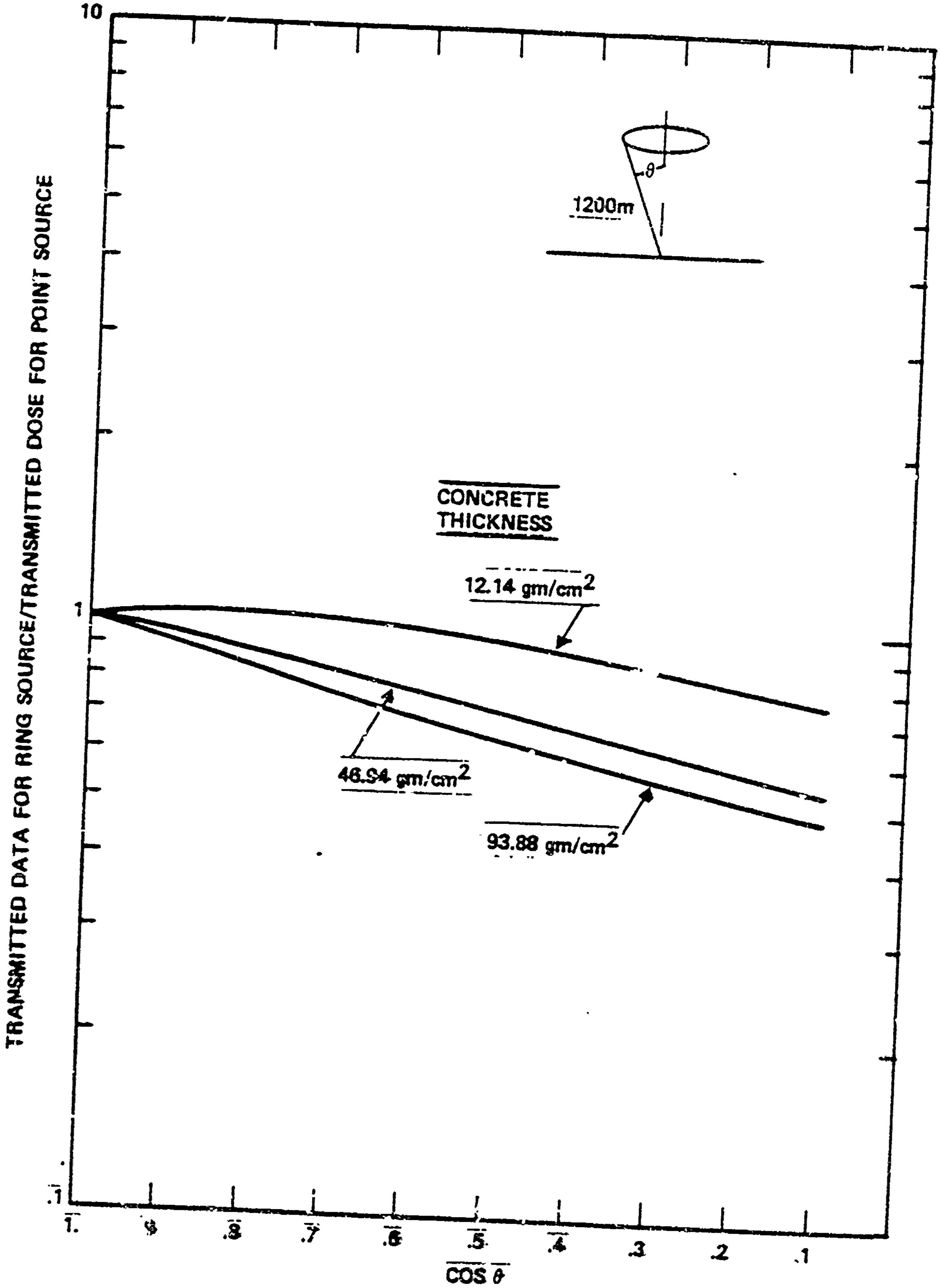

Figure 20. Ring Source Effects for a Thermonuclear Source at 1200 M in Air.

7. CONCLUSIONS AND RECOMMENDATIONS

The relative importance of delayed radiation for civil defense applications for high yield weapons has been demonstrated. These data are presented in Chapter 5. The angular dependence of the delayed radiation have not been studied in detail, however, preliminary indications are that the angular distributions tend to be more forward peaked then the prompt radiation and, therefore, could have some impact on the wall and roof barrier factors for INR. These effects should be evaluated.

The use of newer cross section data to determine the free field environments from prompt radiation indicates some differences relative to the ENDF/B-II data. These differences should be indicated in the final methodology which is to be used for INR applications.

It appears that the selective use of perturbation techniques is more than sufficient to determine that variation (either an increase or decrease) in the initial protection factor for changes in material compositions based on elemental differences. It is recommended that provisions be made in the INR methodology for inclusion of procedures to estimate the effects of both elemental composition and construction techniques on predicted values of IPF. These techniques could quite easily be developed by using the data in Chapter 6, along with some supplementary calculations.

8. REFERENCES

1. J. A. Auxier, Z. G. Burton, R. L. French. F. F. Haywood, L. G. Mooney, and E. A. Straker, "Nuclear Weapons Free-Field Environment Recommended for Initial Radiation Shielding Calculations," ORNL-TM-3396, February 1972.

2. D. E. Bartine, J. R. Knight, J. V. Pace III, R. Rousin, "Production and Testing of the DNA Few-Group Coupled Neutron-Gamma Cross Section Library," ORNL-TM-4840, March 1977.

3. W. W. Engle, Jr., "A User's Manual for ANISN, A One-Dimensional Discrete Ordinates Transport Code with Anisotropic Scattering," X-1693, Computing Technology Center, 1967.

4. E. A. Straker and M. L. Gritzner, "Neutron and Secondary Gamma Ray Transport in Infinite Homogeneous Air," ORNL-TM-4464, 1969.

5. T. E. Albert and G. L. Simmons, "A Two-Dimensional Cross Section Sensitivty Analysis in a Concrete Shield," Nuclear Cross Sections and Technology, NBS-SP-425, pp 459-463, October 1975.

6. E. A. Straker and L. Huszar, "NUIDEA – A Computer Code for the Prediction of Radiation, Blast, and Thermal Environments from Nuclear Weapons," Science Applications, Inc., Unpublished Report, November 1976.

7. L. Huszar, W. Woolson, and E. A. Straker, "Version 4 of ATR (Air Transport of Radiation)," Science Applications, Inc., SAI-76-561-LJ, 1976.

8. C. E. Needham and L. A. Wittwer, "The Air Force Weapons Laboratory Low Altitude Multiple Burst (LAMB) Models," Air Force Weapons Laboratory, AFWL-DYT-TN-75-2, 1975.

August 1976

REVISED MANDATORY STANDARD DISTRIBUTION LIST FOR RESEARCH REPORTS
(ALL PROJECTS)

(Number of Copies - One unless otherwise indicated)

Defense Civil Preparedness Agency
Research
ATTN: Administrative Officer
Washington, D.C. 20301 (50)

Assistant Secretary of the Army (R&D)
ATTN: Assistant for Research
Washington, D.C. 20301

Chief of Naval Research
Washington, D.C. 20360

Commander, Naval Supply Systems
Command (0421G)
Department of the Navy
Washington, D.C. 20376

Commander
Naval Facilities Engineering Command
Research and Development (Code 0322C)
Department of the Navy
Washington, D.C. 20390

Defense Documentation Center
Cameron Station
Alexandria, Virginia 22314 (12)

Civil Defense Research Project
Oak Ridge National Laboratory
ATTN: Librarian
P.O. Box X
Oak Ridge, Tennessee 37830

Chief
Joint Civil Defense Support Group
Office of Chief of Engineers
Department of the Army
Forrestal Building, 1F035
Washington, D.C. 20314

Ballistic Research Laboratory
Attn: Librarian
Aberdeen Proving Ground, MD 21005

National War College
Attn: Librarian
Fort Leslie J. McNair
Washington, D.C. 20315

Commander CCTC
Pentagon, Room 3E-685
Washington, D.C. 20310

Weapons Systems Evaluation Group
Attn: Dr. Harold Knapp
400 Army-Navy Drive
Arlington, VA 22202

Er[illegible] Research & Development Adm.
H[illegible]ers Library, G049
Wa[illegible]ngton, D.C. 20545

Civil Defense Technical Services Center
College of Engineering
Department of Engineering
University of Florida
Gainesville, FL 32601

Mr. Burke Stannard
Defense Research Board
Defense Research Analysis Establishment
National Defense Headquarters
Ottawa 4, Ontario, Canada

Dr. Carl F. Miller
Center for Planning and Research, Inc.
Post Office Box 553
Moriarty, NM 87035

Oak Ridge National Laboratory
Civil Defense Research Project
Attn: Dr. Eugene Wigner
Oak Ridge, TN 37831

Project Director
Engineer Strategic Studies Group
Office of Chief of Engineers
6500 Brooks Lane, N.W.
Washington, D.C. 20315

Technical Library
USA-MERDC
Building 315
Fort Belvoir, VA 22060

Defense Nuclear Agency
Attn: Librarian
Washington, D.C. 20305

Defense Intelligence Agency
Attn: DS-4A
Washington, D.C. 20301

Defense Nuclear Agency
Commander Field Command
Sandia Base
Albuquerque, NM 87115

Director Disaster and Defense Services Staff
Agricultural Stabilization and Conservation Service
U.S. Department of Agriculture
Washington, D.C. 20250

Dikewood Corporation
1009 Bradbury Drive, S.E.
University Research Park
Albuquerque, NM 87106

Institute for Defense Analysis
Attn: Leo Schmidt
400 Army-Navy Drive
Arlington, VA 22202

National Academy of Sciences
Advisory Committee on Emergency Planning
Attn: Dr. Lauriston Taylor
2101 Constitution Avenue, N. W.
Washington, D.C. 20418

Oak Ridge National Laboratory
Attn: Dr. Conrad Chester
Oak Ridge, TN 37831

Stanford Research Institute
Attn: Mr. Robert M. Rodden
Menlo Park, CA 94025

Mr. Bert Greenglass
Director, Office of Administration
Program Planning and Control
Department of Housing and Urban Development
Washington, D. C. 20410

Dr. Daniel Willard
Office of Operations Research
Office of Under Secretary of Army
Room 2E729, Pentagon
Washington, D. C. 20310

Center for Naval Analysis
Attn: Head Studies Mgmt Group
1401 Wilson Boulevard
Arlington, VA 22209

AFOSR Library
1400 Wilson Boulevard
Arlington, VA 22209

Human Sciences Research
Attn: Dr. Peter G. Nordlie
Westgate Industrial Park
P. O. Box 370
McLean, VA 22101

Peter K. Dai, R1/2170
TRW Defense & Space Systems
1 Space Park
Redondo Beach, CA 90278

Dr. Stanley I. Auerback
Director, Environmental Sciences Division
Building 2001
Oak Ridge National Laboratory
Oak Ridge, TN 37831

Disaster Research Center
Ohio State University
404B West 17th Avenue
Columbus, OH 43210

American Technical Assistance Corporation
Attn: Mr. Elwyn Bull
7655 Old Springhouse Road
McLean, VA 22101

University of California
Department of Economics
Attn: Professor Jack Hirschleifer
Los Angeles, CA 90024

Center for Planning & Research, Inc.
Stanford Professional Center
Attn: Mr. Richard K. Laurino
750 Welch Road
Palo Alto, CA 94304

University of Pittsburgh
Department of Sociology
Attn: Dr. Jiri Nehnevajsa
Pittsburgh, PA 15213

Government Services Adm.
Office of Preparedness
Attn: Dr. James Pettee
Main Building, Room 3235
Washington, D. C. 20405

Dr. Martin O. Cohen
Mathematical Applications Group, Inc.
3 Westchester Plaza
Elmsford, N. Y. 10523

Dr. Charles Eisenhauer
National Bureau of Standards
Center for Radiation Research
Washington, D. C. 20234

Science Applications, Inc.
Attn: Dr George L. Simmons
1200 Prospect Street
P. O. Box 2351
La Jolla, CA 92038

Sensitivity of INR Shielding Analyses to Source and Structural Variations, Unclassified, SAI-77-867-LJ, Science Applications, Inc., December 31, 1977, 82 pages, DCPA01-76-C-0326, Work Unit 1118E.

Results of a study of three specific items of interest to the development of procedures for estimating initial radiation protection factors for buildings are presented. These include (1) the effects of new cross section data for nitrogen and oxygen on initial radiation environments are presented, (2) calculations of delayed radiation environments for large yield weapons are presented; the calculations are based on the NUIDEA code, and (3) sensitivity analyses of the effects of composition, thickness, and design characteristics of wall constructions are presented.

Sensitivity of INR Shielding Analyses to Source and Structural Variations, Unclassified, SAI-77-867-LJ, Science Applications, Inc., December 31, 1977, 82 pages, DCPA01-76-C-0326, Work Unit 1118E.

Results of a study of three specific items of interest to the development of procedures for estimating initial radiation protection factors for buildings are presented. These include (1) the effects of new cross section data for nitrogen and oxygen on initial radiation environments are presented, (2) calculations of delayed radiation environments for large yield weapons are presented; the calculations are based on the NUIDEA code, and (3) sensitivity analyses of the effects of composition, thickness, and design characteristics of wall constructions are presented.

Sensitivity of INR Shielding Analyses to Source and Structural Variations, Unclassified, SAI-77-867-LJ, Science Applications, Inc., December 31, 1977, 82 pages, DCPA01-76-C-0326, Work Unit 1118E.

Results of a study of three specific items of interest to the development of procedures for estimating initial radiation protection factors for buildings are presented. These include (1) the effects of new cross section data for nitrogen and oxygen on initial radiation environments are presented, (2) calculations of delayed radiation environments for large yield weapons are presented; the calculations are based on the NUIDEA code, and (3) sensitivity analyses of the effects of composition, thicknesu, and design characteristics of wall constructions are presented.

Sensitivity of INR Shielding Analyses to Source and Structural Variations, Unclassified, SAI-77-867-LJ, Science Applications, Inc., December 31, 1977, 82 pages, DCPA01-76-C-0326, Work Unit 1118E.

Results of a study of three specific items of interest to the development of procedures for estimating initial radiation protection factors for buildings are presented. These include (1) the effects of new cross section data for nitrogen and oxygen on initial radiation environments are presented, (2) calculations of delayed radiation environments for large yield weapons are presented; the calculations are based on the NUIDEA code, and (3) sensitivity analyses of the effects of composition, thickness, and design characteristics of wall constructions are presented.